Ferromagnetism and electron-phonon coupling in the manganites

D M Edwards
Department of Mathematics
Imperial College
London SW7 2BZ, UK
d.edwards@ic.ac.uk

February 1, 2008

Abstract

The physics of ferromagnetic doped manganites, such as $La_{1-x}Ca_xMnO_3$ with $x \approx 0.2$–0.4, is reviewed. The concept of double exchange is discussed within the general framework of itinerant electron magnetism. The new feature in this context is the coupling of electrons to local phonon modes. Emphasis is placed on the quantum nature of the phonons and the link with polaron physics. However it is stressed that the manganites fall in an intermediate coupling regime where standard small-polaron theory does not apply. The recently-developed many-body coherent potential approximation is able to deal with this situation and Green's recent application to the Holstein double-exchange model is described. Issues addressed include the nature of the basic electronic structure, the metal-insulator transition, a unification of colossal magnetoresistance, pressure effects and the isotope effect, pseudogaps in spectroscopy and the effect of electron-phonon coupling on spin waves.

Contents

1 Introduction

Since the discovery of high temperature superconductivity about fifteen years ago it has become clear that a metallic state obtained by doping an antiferromagnetic insulating oxide is substantially different from that of ordinary metals. Despite enormous experimental and theoretical effort neither the superconductivity nor the normal state of this unusual type of metal is at all well understood. There is no generally accepted view about the mechanism of superconductivity in the cuprates. To gain a wider perspective it is clearly important to study other oxides which become metallic upon doping. In fact interest has recently revived in the manganites $A_{1-x}A'_xMnO_3$ (A=trivalent rare-earth ion, A′=divalent alkaline earth ion), which were first studied fifty years ago. An excellent history of this early work is given in the introduction of an extensive review of mixed-valence manganites by Coey et. al. [1]. These compounds are ferromagnetic in the metallic state, typically for $x \approx 0.2$–0.4, and the origin of this metallic ferromagnetism is much less problematic than that of superconductivity in the cuprates. However above the Curie temperature T_C many of the manganites become insulating, and this metal-insulator transition is unlike anything that occurs in ordinary ferromagnetic metals such as Fe, Co, Ni or Gd. There are competing theories of this behaviour, and of the detailed exchange mechanism responsible for the ferromagnetism. Also the importance of electron-phonon coupling, and the possible existence of small polarons, is hotly debated. These are some of the issues which are focussed upon in this review.

Two of the most-studied manganites are $La_{1-x}Sr_xMnO_3$ (LSMO) and $La_{1-x}Ca_xMnO_3$ (LCMO). The parent compound $LaMnO_3$, with nominal valence $La^{3+}Mn^{3+}O_3^{2-}$, is an antiferromagnetic insulator. Mn^{3+} ions have four d electrons and in the cubic environment the t_{2g} states, with d wavefunctions of the xy, yz, zx type, lie lower in energy than the e_g (x^2-y^2, $3z^2-r^2$) ones. The spins of the four d electrons are aligned, by Hund's rule, so the Mn^{3+} ion adopts a $t_{2g}^3e_g^1$ configuration with spin 2. The effect of doping, which removes x electrons per Mn atom, depends on whether $LaMnO_3$ is a Mott-Hubbard or charge-transfer insulator, in the terminology of Zaanen et. al. [2]. In the latter case holes are created in the oxygen 2p band and, since the observed ferromagnetic saturation moment is less than $4\mu_B$ per Mn atom, their spins must be antiparallel to the $S = 2$ Mn ions. In the former case electrons are removed from a narrow e_g band and the three t_{2g} electrons may be regarded as forming a local spin with $S = 3/2$. This is the traditional view [3] which is still most widely held. The e_g band contains $n = 1-x$ electrons per atom with the possibility of metallic behaviour. The electrons are strongly correlated, avoiding double occupation of a Mn site, so that for $n = 1$ ($x = 0$) the system is a Mott insulator. The itinerant e_g electrons are completely spin-polarized and align the local spins via Zener's [3] double-exchange mechanism. The validity of this general picture is thoroughly discussed in sections 2 and 3.

The structure of manganites such as $LaMnO_3$ is based on the ideal cubic perovskite ($CaTiO_3$) structure shown in figure 1. However the oxygen octahedra surrounding each Mn atom undergo two types of distortion. One is a rotation and tilting due to the La^{3+} ion being smaller than the O^{2-} and the other is a tetragonal distortion due to the Jahn-Teller

(JT) effect. Since the octahedra are connected the rotations and tilting alternate in sense so that the final orthorombic structure has a unit cell whose volume corresponds to four perovskite unit cells. The JT distortion is predominantly of the Q_2 type (see figure 1) in which each octahedron is stretched along one of the axes in the basal plane. Clearly, the locally stretched axis alternates in direction by 90°. The JT distortion arises from the degenerate e_g^1 configuration; it splits the e_g level so as to lower the energy of the Mn $3z^2-r^2$ orbital, with local z axis along the long Mn–O bonds. The JT distortion in $LaMnO_3$ is a large effect, with an octahedral aspect ratio of 1.12 compared with 1.004 in $CaTiO_3$ [4]. It encourages orbital ordering in the basal plane with local $3z^2 - r^2$ orbitals pointing in alternate directions. This has been observed [5]. The magnetic ordering of $LaMnO_3$, as indicated in figure 1, is A-type antiferromagnetic, with ferromagnetic basal planes arranged antiferromagnetically. In a doped system such as $La_{0.7}Sr_{0.3}MnO_3$, which is a ferromagnetic metal, the crystal structure is much more nearly cubic [6]. The slight distortion seems to be predominantly due to octahedral rotation and there is no evidence of a static JT effect [4]. However a dynamic JT effect may occur as the e_g electron moves from site to site and this constitutes a JT polaron. An important parameter in all manganites is the Mn–O–Mn bond angle which is less than 180° in a distorted structure. This reduced angle leads to reduced Mn–Mn hopping and hence to a narrowing of the e_g band.

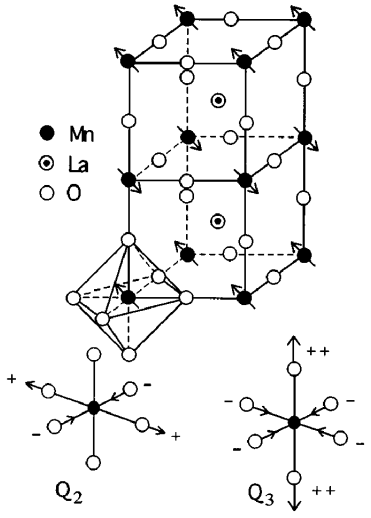

Figure 1: The ideal cubic perovskite structure, showing the AF type A order for $LaMnO_3$. Also shown are the breathing mode (Q_1), the basal-plane distortion mode (Q_2), and the octahedral stretching mode (Q_3) which are present in the actual structure. (from reference [4])

Phase diagrams in the x-T plane of LSMO and LCMO are shown in figure 2. For $x < 0.5$ the two diagrams appear to be quite similar with a maximum Curie temperature T_C at $x \approx 0.33$. However the maximum T_C in LCMO is considerably lower than in LSMO and the paramagnetic state above T_C is insulating in LCMO and a poor metal in LSMO. In LCMO charge-ordering sets in at $x \approx 0.5$ and in the ferromagnetic insulator regimes

at $x \lesssim 0.2$, in both LSMO and LCMO, substitutional disorder must play an important role. Much of the theoretical work reviewed here is concentrated on $x \approx 0.3$, where neither charge order nor orbital order is expected, and it is assumed that the system is homogeneous. However, it has been argued by Moreo et. al. [7] and Nagaev [8] that charge inhomogeneity is widespread in the manganites with a tendency for holes, produced by doping, to segregate in ferromagnetic clusters. Unfortunately most quantitative work along these lines has employed models in which long range Coulomb forces are neglected. This leads to unrealistic predictions of macroscopic phase separation [7].

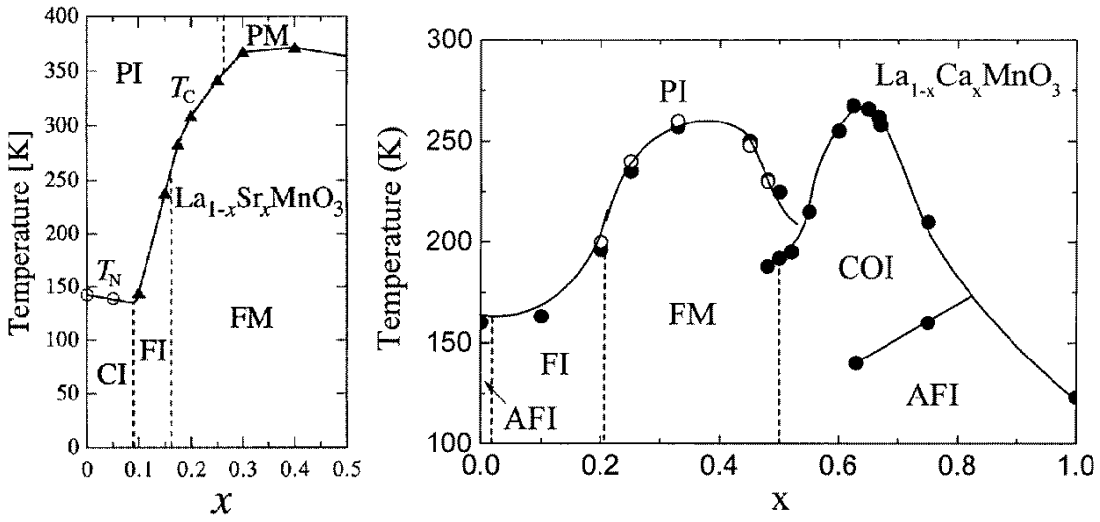

(a) (from reference [9]) (b) (from reference [10])

Figure 2: Phase diagram for $La_{1-x}Sr_xMnO_3$ (a) and $La_{1-x}Ca_xMnO_3$ (b). The various states are: paramagnetic insulating (PI), paramagnetic metal (PM), canted insulating (CI), ferromagnetic insulating (FI), ferromagnetic metal (FM), antiferromagnetic insulating (AFI) and charge-ordered insulating (COI). T_C and T_N are Curie and Neél temperatures, respectively.

The importance of the Mn–O–Mn bond angle was mentioned above. This can be varied in the system $A_{0.7}A'_{0.3}MnO_3$, with a fixed number of electrons $n = 0.7$ in the e_g conduction band, by varying either the average A-site ionic radius $\langle r_A \rangle$ or by applied pressure. Rodriguez-Martinez and Attfield [11] have also stressed the role of the variance in r_A. An increase of either $\langle r_A \rangle$ or applied pressure tends to push the Mn–O–Mn bond angle closer to 180°, thereby increasing the Mn–Mn hopping parameter and consequently the width of the e_g band. The sensitivity of the Curie temperature T_C to such changes is shown in figure 3. The effect on the transport properties is even more striking. The contrast between the temperature-dependence of the resistivity $\rho(T)$ for LSMO and LCMO, with $x \approx 0.3$, is seen in figures 4 and 5. In LSMO the resistivity above T_C (~ 370 K) continues to rise, as in a poor metal, whereas in LCMO the resistivity peaks at T_C (~ 260 K) and

decreases as the temperature is raised above T_C. This indicates a metal-insulator transition at T_C. Furthermore in LSMO, above T_C, $\rho \sim 4$ mΩcm whereas the resistivity of LCMO peaks at about 40 mΩcm . A satisfactory theory of the manganites must be able to account for this huge difference in behaviour between two apparently very similar materials. The effect of applied magnetic fields of magnitude 0–5.5 T on $\rho(T)$ in LCMO is shown in figure 5. The large change in resistance near T_C is termed 'colossal magnetoresistance' (CMR) and it is this phenomenon which has inspired much of the recent research on the manganites. However the large fields required make it unlikely that this intrinsic property will be used in a sophisticated device for sensing magnetic fields. Low-field magnetoresistance observed in polycrystalline $La_{2/3}Sr_{1/3}MnO_3$ is attributed to spin-polarized tunneling between 'half-metallic' grains [12, 13]. The half-metallic property of manganites is discussed in the next section on electronic structure.

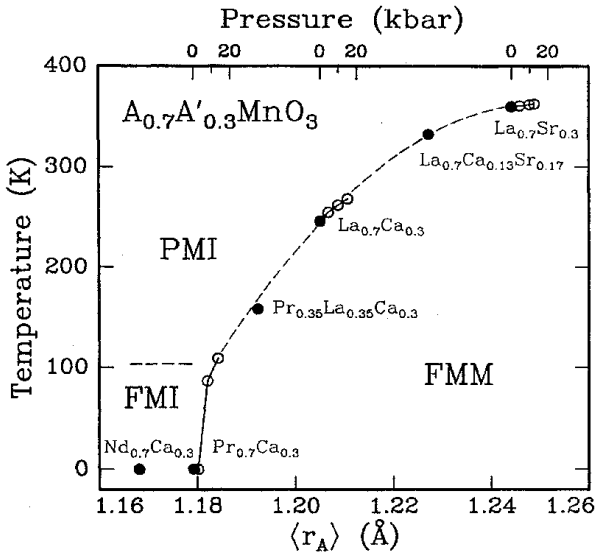

Figure 3: The phase diagram of $A_{0.7}A'_{0.3}MnO_3$ as a function of the bandwidth. Closed circles represent variations of the bandwidth due to internal pressure (variations of the average A-site ionic radius $\langle r_A \rangle$), and open circles indicate variations due to externally applied pressure. (from reference [14])

2 Electronic structure

Before discussing the origin of metallic ferromagnetism in the doped manganites it is necessary to understand their electronic structure. The most important question is whether doping $LaMnO_3$ introduces holes predominantly into a Mn d band or into an O p band. This depends of course on which occupied band lies higher in energy. The question must be answered by a combination of theory and experiment. The usual starting-point is a

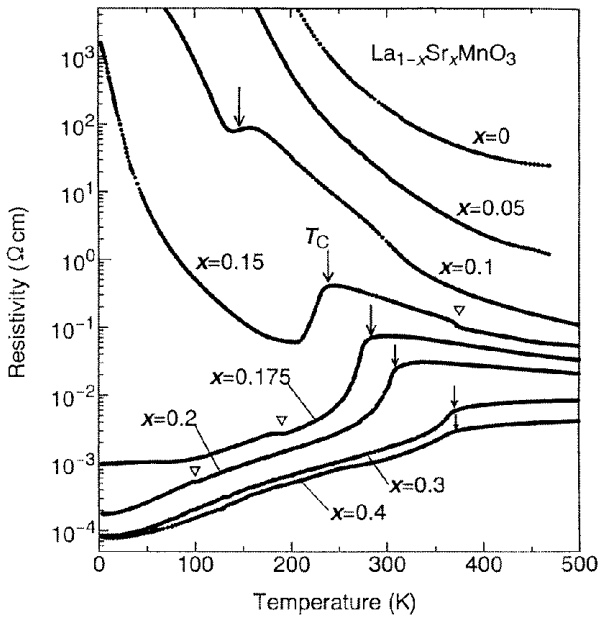

Figure 4: Resistivity versus temperature for $La_{1-x}Sr_xMnO_3$ crystals. Arrows indicate the Curie temperature T_C for the ferromagnetic phase transition. (from reference [15])

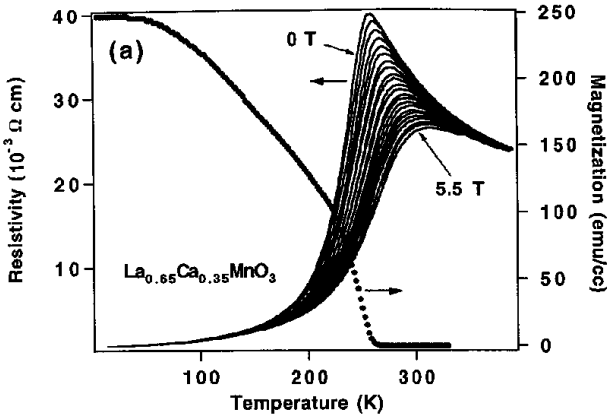

Figure 5: Resistivity (solid lines) of $La_{0.65}Ca_{0.35}MnO_3$, acquired in applied fields ranging from 0 to 5.5 T, and the bulk magnetization in an in-plane applied field of 50 G (•), both as a function of temperature. (from reference [16])

band calculation based on the local spin-density approximation (LSDA). In this approximation all electrons of a given spin experience the same crystal potential and therefore all d orbitals of that spin, apart from a modest crystal field splitting between t_{2g} and e_g, have the same on-site energy. In order to obtain a d^n configuration, with $n \neq 0$, 5 or 10, it is inevitable that the d band must overlap the Fermi level. Consequently in LSDA calculations for $LaMnO_3$, with a Mn d^4 configuration, the d band lies above the filled O p band [17, 4, 18]. The JT lattice distortion of Q_2 type is required to open a small gap in the e_g band so that the system becomes an insulator with orbital ordering. Also, the JT distortion stabilizes the observed antiferromagnetic structure over the ferromagnetic one [4]. The calculated Mn magnetic moment is $3.4\mu_B$ compared with $3.7\mu_B$ found by neutron scattering [18]. Thus the LSDA calculations are compatible with the observed magnetic and structural details in $LaMnO_3$.

However it is well-known that in some oxides, like NiO [19], the p band lies above the d band and the LSDA fails [20]. This is the case of a charge-transfer insulator where excitations across the gap are O p $\rightarrow$ Ni d. To describe such a system within band theory one must use extensions of the LSDA, such as LDA+U or the self-interaction correction (SIC), or a Hartree-Fock method. In these approaches different d orbitals may see different potentials. For example one $\uparrow$ spin e_g orbital could lie well below the Fermi energy and the other $\uparrow$ spin e_g orbital could lie above it. Since a particular e_g orbital must be picked out for occupation on a given site cubic symmetry is broken and orbital ordering occurs. The splitting between the e_g levels would be the Hubbard on-site Coulomb interaction U. The p band can then lie above the occupied e_g band. The density of states (DOS) obtained by Su et. al. [21] in a Hartree-Fock calculation for $LaMnO_3$ is shown in figure 6. Here the occupied majority spin d states ($t_{2g}^3 e_g^1$) lie well below the oxygen band and the Mn moment is close to $4\mu_B$. The DOS sketched by Satpathy et. al. [4] to illustrate the results of a LDA+U calculation for $LaMnO_3$ is slightly less extreme. The majority spin d band lies just within the bottom of the oxygen p band. $LaMnO_3$ orders magnetically as an A-type antiferromagnet (AAF) with ferromagnetic ordering within the basal planes. In figure 6 it is seen that the projected $O_{II} - p$ DOS, corresponding to oxygen in the basal planes (see figure 1), has an exchange splitting of about 0.75 eV at the top of the band. If the system were ferromagnetically ordered one would expect a similar, or slightly greater, exchange splitting. Thus, according to this picture, the ferromagnetic metal obtained by doping $LaMnO_3$ sufficiently with Sr, for example, would contain $S = 2$ Mn ions aligned by itinerant p holes of opposite spin.

Both of the very different theoretical pictures presented above can explain the magnetic and structural properties of $LaMnO_3$. To distinguish between them we must examine some spectroscopic data. Barman et. al. [22] give a very clear picture of the situation in the related material $LaNiO_3$. This is a non-magnetic metal with the Ni^{3+} ion in a nominal $t_{2g}^6 e_g^1$ configuration, that is $t_{2g}^3 e_g^{0.5}$ for each spin. Thus the band structure should be very similar to the majority spin band in ferromagnetic $La_{0.5}Sr_{0.5}MnO_3$. Indeed the calculated DOS in reference [22], shown in figure 7, resembles in detail majority spin bands found in LSDA calculations for $LaMnO_3$ [4], $La_{2/3}Ca_{1/3}MnO_3$ [17] and $La_{2/3}Ba_{1/3}MnO_3$ [23]. Comparison should be made with the total DOS in figure 8, due to Pickett and Singh

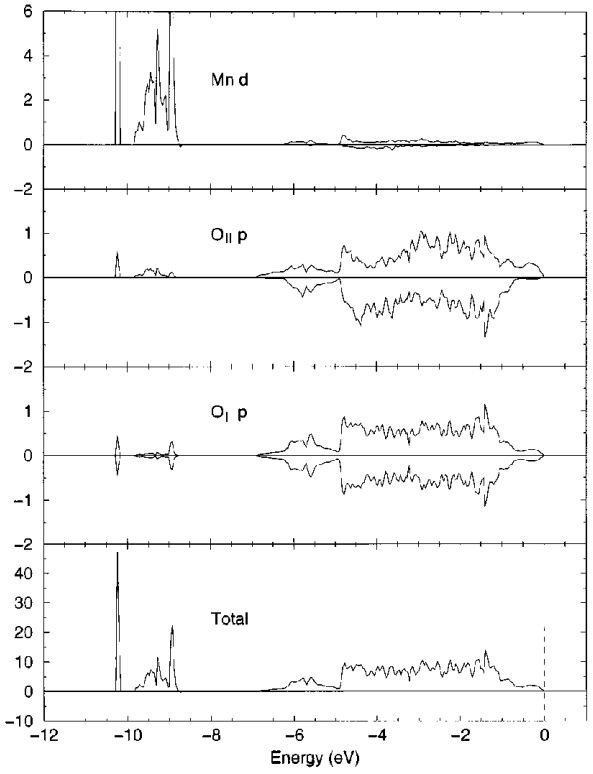

Figure 6: The (projected) DOS of $LaMnO_3$, with AAF ordering. Positive and negative DOS are for up- and down-spin states, respectively. Energies are relative to the top of the valence band. The projected Mn-d and O_{II}-p DOS are for Mn and O on an up-spin basal plane. (from reference [21])

[17]. Their calculation is for ordered $La_{2/3}Ca_{1/3}MnO_3$ with planes of La and Ca in a regular sequence. The feature of the DOS marked A in figure 7(b) is an e_g band and B corresponds to the t_{2g} band. C and D are two features of the broad oxygen p band. In the inset of figure 7(a) a calculated x-ray photoemission (XP) spectrum, including the effects of matrix elements as well as resolution and lifetime broadenings, is compared with the experimental spectrum. The peak near the Fermi energy E_F arises from the d band features A and B. The shoulder on the left of this peak and the second peak arise from the p band features C and D respectively. Sarma et. al. [18] showed that this good agreement between theory based on LSDA band calculations and the observed XP spectrum extends to $LaCoO_3$, $LaFeO_3$ and $LaMnO_3$. In the Fe and Mn compounds, both insulators, the calculated valence band had to be shifted by 2.0 and 1.3 eV, respectively, to enlarge the band-gap. The LDA invariably underestimates band-gaps in semi-conductors and insulators (maybe LDA + small U should be considered, as discussed at the end of section 3.1). In the ultraviolet photoemission (UP) spectrum of $LaNiO_3$ shown in figure 7(a) features A and B appear much more weakly than C and D, in contrast to the XP spectrum, and this is consistent with the assigned d and p angular momentum character [22]. The UP spectrum of $LaMnO_3$, both doped and undoped, is quite similar to that of $LaNiO_3$ with clear p band features C and D [24, 25]. However features A and B are not visible and seem only to contribute to a tail in the spectrum which extends to E_F in metallic samples such as $La_{1-x}Sr_xMnO_3$ [25]. It seems even more difficult to photo-excite d electrons near E_F, with ultraviolet photon energies, in doped $LaMnO_3$ than in $LaNiO_3$. Furthermore only a weak shoulder corresponding to features A and B is seen in the XP spectrum of $La_{0.7}Sr_{0.3}MnO_3$, unlike the large peak in $LaNiO_3$ [24]. However Park et. al. [26], in high resolution spectra, see clear Fermi edges at 80 K in $La_{0.67}Ca_{0.33}MnO_3$ and $La_{0.7}Pb_{0.3}MnO_3$. A contributory factor to low density of states at E_F may be the effect of electron-phonon coupling, which tends to open a pseudo-gap in the one-electron spectrum as discussed in sections 6 and 8.3. Surface preparation is clearly also very important since the probing depth in photoemission may be as small as 5 Å [27].

According to LSDA calculations, for example that shown in figure 8, a doped manganite like $La_{2/3}Ca_{1/3}MnO_3$ is almost 'half-metallic'. This term applies to a ferromagnetic metal in which the Fermi level lies in a gap in the DOS for states of one spin. In figure 8 the Fermi level lies just above a gap in the minority spin DOS. According to this calculation states from just below E_F to about 1.4 eV below it should be 100% spin polarized. Spin polarization at E_F can be measured directly by Andreev reflection and values of up to 80% have been found in $La_{0.7}Sr_{0.3}MnO_3$ at 4.2 K by Soulen et. al. [28] and Osofsky et. al. [29]. Large spin polarization in $La_{0.67}Sr_{0.33}MnO_3$ is also deduced from spin-polarized tunneling measurements [30, 31]. Spin-polarized photoemission can probe below E_F and Park et. al. [32] find 100% polarization in thin films of $La_{0.7}Sr_{0.3}MnO_3$ down to 0.6 eV below E_F. This suggests a smaller gap in the minority spin DOS than predicted theoretically. In early work on spin-polarized photoemission from $La_{0.7}Pb_{0.3}MnO_3$ Alvarado et. al. [33] attributed their failure to see more than 20% polarization to a broad band of unpolarized Pb 6s states extending almost up to E_F.

A stringent test of a proposed electronic structure of a metal is whether it gives the

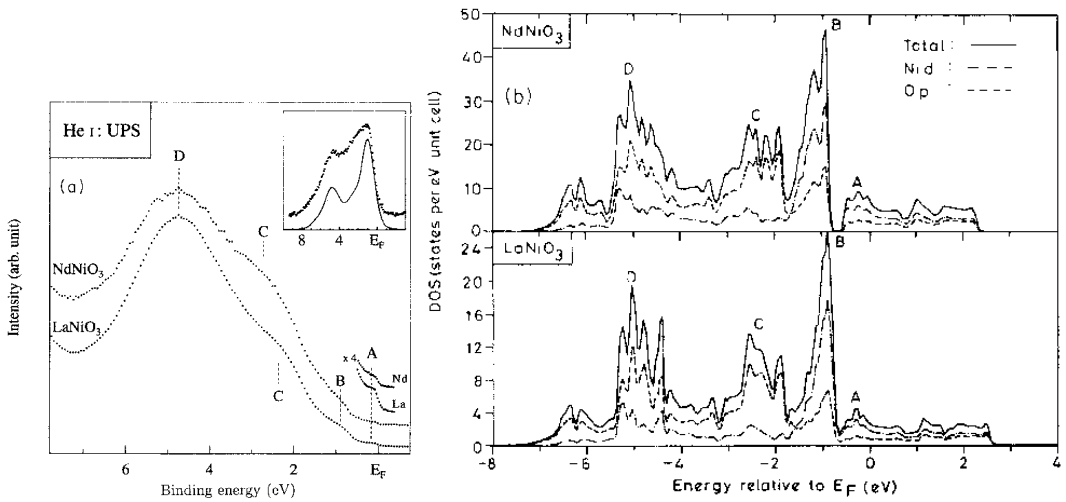

(a) (b)

Figure 7: (a) He I UP spectra of $LaNiO_3$ and $NdNiO_3$. The experimental (dotted line) and calculated (solid line) XP spectra of $LaNiO_3$ are shown in the inset. (b) The total DOS (solid line), Ni d (dot-dashed line), and O p (dashed line) partial DOS for $LaNiO_3$ and $NdNiO_3$ calculated within LMTO-ASA [22].

observed Fermi surface. In a disordered system like $La_{0.7}Sr_{0.3}MnO_3$ the Fermi surface is not sharp as in a pure metal. Even at $T = 0$ there is no actual discontinuity in occupation number between states inside and outside a perfectly-defined surface in $\boldsymbol{k}$-space. Standard methods of determining the Fermi surface, like the de Haas–van Alphen method, can generally not be applied, except for the case of weak scattering in dilute alloys. However if scattering is not too strong the transition between occupied and unoccupied states in $\boldsymbol{k}$-space is sufficiently rapid to show up in the electron momentum distribution as a fairly clear Fermi surface. The momentum distribution can be measured by Compton scattering or positron annihilation. Livesay et. al. [34] have used positron annihilation to investigate the Fermi surface of $La_{0.7}Sr_{0.3}MnO_3$ and compare it with a LSDA band calculation. They used a cubic perovskite structure and a virtual crystal approximation, which makes the Fermi surface sharp, to find the band structure shown in figure 9. The system is almost half-metallic and the two majority spin Fermi surface sheets are shown in figure 10. These comprise hole cuboids at the R $(\pm\pi/a, \pm\pi/a, \pm\pi/a)$ points that touch an electron spheroid, centred at the Γ $(0, 0, 0)$ point, along the (111) directions. Similar Fermi surface sheets are described by Pickett and Singh [35]. The analysis of the positron annihilation data is not simple, but Livesay et. al. conclude that their results agree well with the theory and establish the existence of the cuboid hole sheets. The virtual crystal approach is reasonable since Pickett and Singh [17, 23, 35] have shown that scattering due to random A-site occupation has little effect on the majority-spin bands around E_{F}. However the

disorder localizes states at the bottom of the minority-spin band near $E_{\rm F}$. Even if the bottom of the band falls just below $E_{\rm F}$ the system will still behave as half-metallic in transport [35].

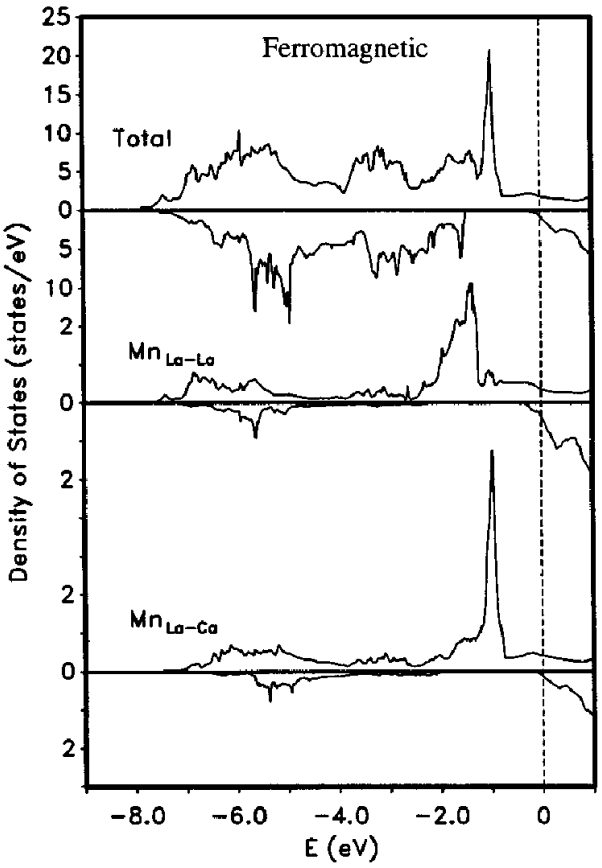

Figure 8: The total DOS and local DOS on each inequivalent Mn ion for ordered $La_{2/3}Ca_{1/3}MnO_3$ with FM spin ordering [17]. The subscripts denote the types of cation planes sandwiching that layer of Mn ions.

The standard method of investigating band structure experimentally, away from the Fermi level, is angle resolved photoemission (ARPES). McIlroy et. al. [16] have investigated $La_xCa_{1-x}MnO_3$ and $La_xBa_{1-x}MnO_3$ with $x = 0.35$ using this technique. As pointed out above, the e_g states close to the Fermi energy are hardly visible in photoemission, so one is looking at the dense ensemble of bands between 2 and 8 eV below $E_{\rm F}$ (see figure 9). It is hardly to be expected that any clear dispersion curves will emerge and McIlroy et. al. deduce that in the Ca-doped compound there are a lot of very flat bands. They conclude that all the occupied states are extremely localized, but this seems an improbable assessment of the broad p bands. Some dispersion is found in the Ba compound, possibly associated with the steeply dropping bands in the ΓX direction at around 4 eV below $E_{\rm F}$. A discussion of ARPES measurements by Dessau et. al. [36] on a bilayer manganite is deferred to section 8.3.1.

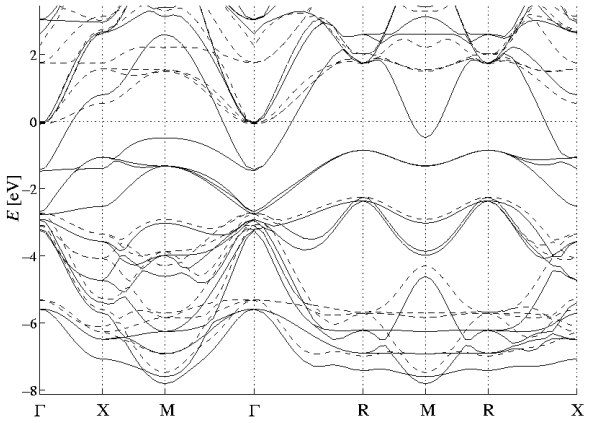

Figure 9: Spin-polarized band structure of $La_{0.7}Sr_{0.3}MnO_3$. The majority spin bands are shown as solid lines, and the minority as dashed lines [34].

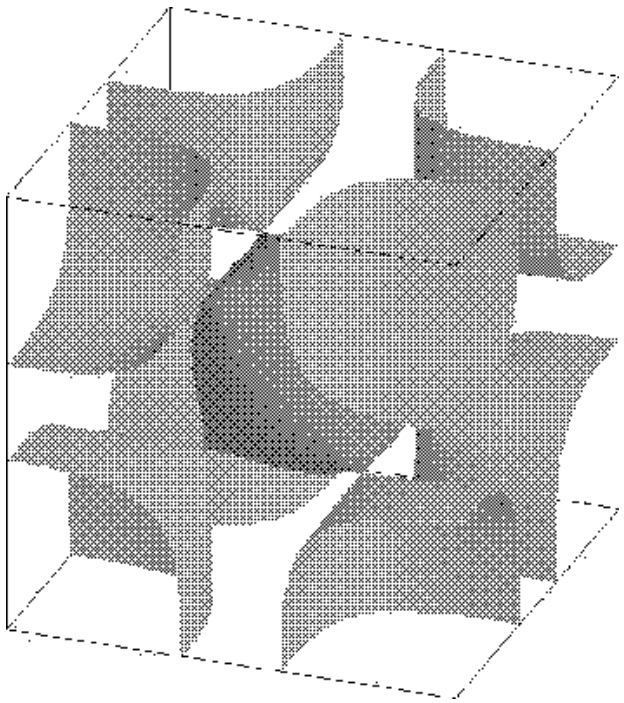

Figure 10: Two sheets of the Fermi surface of $La_{0.7}Sr_{0.3}MnO_3$. Hole cuboids at the R points, coined 'woolsacks'. Electron spheroid centred at the Γ point [34].

Clearly there is a lot of evidence that the electronic structure of the manganites is well described by LSDA calculations and that states near the Fermi level have predominantly Mn d character with e_g symmetry. However hybridization with O 2p states is by no means negligible. Sarma et. al. [18] find that at the valence-band top and conduction-band bottom in $LaMnO_3$ the d component is 58% and 73% respectively. Simple one-band or two-band models must be thought of as hopping between orbitals of e_g symmetry centred on Mn but extending onto neighbouring O atoms. The simple nature of the bands crossing the Fermi level, and the simple Fermi surface, suggest that a suitably parameterized two-band model, as used by many authors, may be quite realistic. Sarma et. al. [18] discuss the reasons for the success of LSDA in the $LaMO_3$ compounds with M=Mn, Fe, Co and Ni. In these perovskites the M–O bond is shorter than in the rocksalt MO compounds, so that the M–O hopping parameter is larger. Also the effective Coulomb interaction U on the M site is smaller due to better screening by the closer O ions and to larger effective d–d hopping.

We now briefly discuss some work which is often quoted in support of the hypothesis that $LaMnO_3$ is an insulator with a charge-transfer (O p $\rightarrow$ Mn d) gap. Instead of a band calculation for the crystal Saitoh et. al. [25] performed configuration-interaction calculations for an isolated MnO_6 cluster. The parameters of the model are the d–d Coulomb interaction U, the p $\rightarrow$ d charge-transfer energy Δ and p $\rightarrow$ d hopping parameter. They varied the parameters to obtain the best fit to the observed Mn 2p core-level photoemission spectrum, O 1s x-ray absorption spectrum and valence-band photoemission. They conclude that for $LaMnO_3$ $U = 7.8$ eV and $\Delta = 4.5$ eV so that the condition $U > \Delta$ for a charge-transfer insulator is satisfied. On the other hand Chainani et. al. [24] in a similar, but slightly different, analysis find $\Delta = 5.0$ eV, $U = 4.0$ eV which makes $LaMnO_3$ more Mott-Hubbard-like than charge-transfer-like. Even for spectroscopic properties the results of cluster calculations seem inconclusive. Energy loss spectroscopy (EELS) on $La_{1-x}Sr_xMnO_3$ in which electrons are excited from O 1s states to empty p-like states, has been presented [37] as confirmation of the hypothesis that $LaMnO_3$ is a charge-transfer-type insulator. A peak at the Fermi level grows with increasing x and this is interpreted as proof that doping produces holes in the oxygen p band. However it seems that the scenario extensively discussed in this section, where the charge carriers have Mn e_g character, although significantly hybridized with O 2p states, is not excluded.

In the next section we discuss the exchange mechanism responsible for ferromagnetism in the doped manganites from the general viewpoint of itinerant electron magnetism. It is clearly related to the nature of the underlying electronic structure.

3 Itinerant electron ferromagnetism and double exchange

3.1 The double-exchange (DE) model

All work on the electronic structure of the manganites is in agreement on one point. The three majority spin t_{2g} orbitals are all occupied and the minority spin ones are unoccupied.

This suggests that t_{2g} electrons play no part in transport and may be considered as localized. Consequently the system may be considered as consisting of local spins $S = 3/2$ on each Mn site coupled to electrons in a predominantly e_g conduction band by local exchange interactions. According to the alternative view of the electronic structure, discussed in section 2, one e_g electron per Mn site is also localized and local spins $S = 2$ are coupled to holes in the oxygen p band. Although we mention this alternative view again later we shall primarily adapt the former view for which strong evidence has been given in section 1.

Metallic rare-earth materials can also be considered as systems of local moments coupled to electrons in a conduction band by local exchange interactions. We now discuss the distinction between these and the manganites. The Hamiltonian for such a system is

$$H = \sum_{ij\sigma} t_{ij} c^\dagger_{i\sigma} c_{j\sigma} - J \sum_i \boldsymbol{S}_i \cdot \boldsymbol{\sigma}_i - h \sum_i (S^z_i + \sigma^z_i) \ , \tag{3.1}$$

where $c^\dagger_{i\sigma}$ creates an electron of spin σ on lattice site i, $\boldsymbol{S}_i$ is a local spin operator and $\boldsymbol{\sigma}_i = (\sigma^x_i, \sigma^y_i, \sigma^z_i)$ is a conduction electron spin operator defined by

$$\sigma^+_i = \sigma^x_i + i\sigma^y_i = c^\dagger_{i\uparrow} c_{i\downarrow} \ , \ \sigma^-_i = \sigma^x_i - i\sigma^y_i = c^\dagger_{i\downarrow} c_{i\uparrow} \ , \ \sigma^z_i = \frac{1}{2}(n_{i\uparrow} - n_{i\downarrow}) \tag{3.2}$$

with $n_{i\sigma} = c^\dagger_{i\sigma} c_{i\sigma}$. The three terms of equation (3.1) describe hopping of the conduction electrons, exchange coupling between local and itinerant spins and coupling to an external magnetic field. If the local exchange coupling arises from hybridization between the localized and itinerant electrons, as in anomalous rare earth systems exhibiting heavy fermion behaviour, the exchange parameter J is negative. The Hamiltonian (3.1) is then often called the Kondo lattice model in view of its connection with the Kondo impurity model which has a local spin on one site only [38]. When Hund's rule coupling is dominant $J > 0$ and the system is sometimes called a ferromagnetic Kondo lattice. This is misleading since for $J > 0$ there is no connection with the Kondo effect.

For $J > 0$ it is useful to distinguish two distinct physical regimes, depending on the magnitude of J compared with the width $2W$ of the conduction band. If $J \ll W$, as in a normal rare earth metal, the exchange coupling can be treated as a perturbation which gives rise to the Ruderman-Kittel-Kasuya-Yosida (RKKY) interaction between local moments. In most rare earth metals this interaction, which oscillates in space, leads to oscillatory or spiral configurations of the localized f electron moments. The uniform ferromagnet Gd is an exception. In this weak coupling regime the Hamiltonian (3.1) is usually referred to as the $s - f$ or $s - d$ model.

If $J \gg W$ the exchange coupling can no longer be treated as a perturbation. A conduction electron can only hop onto a site with its spin parallel to the local moment at that site. Furthermore if the number of conduction electrons per atom $n \leq 1$ double occupation of a site is strongly suppressed. A single electron at a site, with its spin parallel to the local spin $\boldsymbol{S}$, enjoys an exchange energy $-JS/2$ which is lost if a second electron hops on. The system is therefore a *strongly correlated electron system*, just like the Hubbard model in the regime of strong on-site Coulomb interaction U, and for $n = 1$

the system is a Mott insulator. In much of the theoretical work on the present model the local spins are treated as classical vectors, corresponding to $S \to \infty$. Since for $J \gg W$ the itinerant spin must always be parallel to the local spin on each site, the effective hopping integral for hopping between sites i and j becomes $t_{ij} \cos(\theta_{ij}/2)$, where θ_{ij} is the angle between the classical spins $\boldsymbol{S}_i$, $\boldsymbol{S}_j$. The cosine factor arises from the scalar product of two spin 1/2 eigenstates with different axes of quantization. The resultant band narrowing in the paramagnetic state favours ferromagnetism in order to lower the kinetic energy. This mechanism for ferromagnetism was first introduced by Zener [3] and developed by others [39, 40, 41]. Since it involves strong exchange coupling on two adjacent atoms it is known as double-exchange. Consequently the Hamiltonian (3.1) in the strong-coupling regime $J \gg W$ is called the double-exchange (DE) model. We note that the p-hole picture is not in the DE regime since the antiferromagnetic coupling between the Mn local spins and the O p-holes is weak compared with the large oxygen band-width. This review is largely concerned with the DE model, with quantum and classical local spins, and with its extension to include coupling of the electrons to local phonons. We call this extended model the Holstein-DE model [42]. We now proceed to place the DE model in the wider context of itinerant electron ferromagnetism.

3.2 A wider view

The macroscopic exchange energy in a ferromagnet takes the form

$$A \int \sum_i \left(\nabla n_i(\boldsymbol{r})\right)^2 \mathrm{d}^3 r \tag{3.3}$$

where n_1, n_2, n_3 are the direction cosines of the magnetization direction at position $\boldsymbol{r}$. Here A is the Bloch wall stiffness constant. A long wavelength spin-wave is a macroscopic oscillation in which the magnetization precesses around the equilibrium z direction. The transverse components of magnetization vary in space and time as

$$M^+ = M_x + \mathrm{i}M_y \propto \exp\left[\mathrm{i}(\boldsymbol{q} \cdot \boldsymbol{r} - \omega t)\right] . \tag{3.4}$$

The dispersion relation is

$$\hbar\omega = Dq^2 \tag{3.5}$$

and the spin-wave stiffness constant $D \propto A/M_s$ where M_s is the saturation moment. This macroscopic picture is valid for any ferromagnet, at zero or finite T ($< T_\mathrm{C}$) and with an ordered or disordered crystal structure. In exciting a spin-wave quantum (magnon), for example by neutron scattering, a single spin is flipped down. For ferromagnets with a substantial moment per atom, of a Bohr magneton or two, long wavelength spin-waves make an important, and often dominant, contribution to the temperature dependence of the magnetization for $T \lesssim T_\mathrm{C}/2$, through the well-known Bloch $T^{3/2}$ law. In manganites with $T_\mathrm{C} \gtrsim 350$ K the ratio $\delta = D/(k_\mathrm{B} T_\mathrm{C} a^2)$, where a is the lattice constant, is close to

the value 0.286 for the spin 3/2 nearest neighbour simple cubic Heisenberg model. For manganites with lower $T_{\rm C}$, δ can be larger by up to a factor 2 and this is attributed to strong electron-phonon coupling [43]. However in general D provides a good measure of $T_{\rm C}$. This is not the case, however, in very weak itinerant ferromagnets such as $ZrZn_2$, with small saturation moment, where longitudinal spin fluctuations are a determining influence on $T_{\rm C}$.

A very useful feature of D is that it is in effect a ground state property. It is directly related to the Bloch wall stiffness constant A, which can be determined from the ground state energy of the system in a non-uniform transverse magnetic field. Thus in principle D can be calculated exactly in spin density functional theory, even though the band structure used in the course of the calculations has no such rigorous validity. In practice one obtains good values for D in Fe and Ni, and their alloys, on the basis of LSDA band calculations [44, 45]. We are aware of only one calculation along these lines for any manganite material. Solovyev and Terakura [46] find $D \approx 300$ meVÅ^2 for $La_{0.7}Ba_{0.3}MnO_3$ which is comparable to experimental values of somewhat less than 200 meVÅ^2 for similar manganites with $x = 0.3$. We discuss the general approach below since it gives insight into the exchange mechanism in ferromagnetic metals and makes clear the basis of the double-exchange model.

Edwards and Muniz [44] showed how D can be evaluated directly from a multi-band tight-binding parameterization of a LSDA band calculation for the ferromagnetic ground state. No input about the underlying electron-electron interaction is required. However at a more microscopic level one may consider the band structure to arise from a Hartree-Fock approximation (HFA) to a Hamiltonian of the form

$$H = \sum_{\boldsymbol{k}} \sum_{\mu\mu'\sigma} V_{\mu\mu'}(\boldsymbol{k}) c^{\dagger}_{\mu\boldsymbol{k}\sigma} c_{\mu'\boldsymbol{k}\sigma} + H_{\rm int} \equiv H_0 + H_{\rm int}\,, \tag{3.6}$$

where $c^{\dagger}_{\mu\boldsymbol{k}\sigma}$ creates an electron of spin σ in a Bloch state of wave-vector $\boldsymbol{k}$ formed from orbitals μ. Here the first term H_0 represents the electron 'kinetic energy', actually the kinetic energy plus a spin-independent local potential, and $H_{\rm int}$ is a local (intraatomic) interaction term. Off-diagonal elements $V_{\mu\mu'}$ describe hybridization between different orbitals. In general $H_{\rm int}$ contains screened Coulomb interactions and exchange interactions of the Hund-rule type between the various orbitals. It can also include an additional one-electron term representing spin-independent diagonal disorder and may be generalized to include interaction with local phonons, as we shall discuss later. The Hamiltonian may be considered at two levels; either with effective interactions designed to reproduce the LSDA band structure within the HFA, or as a true many-body Hamiltonian in which correlation effects must be treated explicitly, for example by dynamical mean field theory [47, 48]. In both approaches one may start with an exact expression for D [49]:

$$D = \frac{\hbar^2}{N_\uparrow - N_\downarrow} \left(\lim_{q\to 0} (\hbar q)^{-1} \langle [J^-_{\boldsymbol{q}}, S^+_{-\boldsymbol{q}}] \rangle - \lim_{\omega\to 0} \chi_J(0,\omega) \right) . \tag{3.7}$$

Here $S^-_{\boldsymbol{q}} = \sum_{\boldsymbol{k}\mu} c^{\dagger}_{\mu\boldsymbol{k}+\boldsymbol{q}\downarrow} c_{\mu\boldsymbol{k}\uparrow}$ is a spin-flipping operator representing a transverse component

of spin density and $J_{\boldsymbol{q}}^-$ is the spin current operator defined by

$$\hbar q J_{\boldsymbol{q}}^- = [S_{\boldsymbol{q}}^-, H] = \sum_{\boldsymbol{k}} \sum_{\mu\mu'} \left(V_{\mu\mu'}(\boldsymbol{k}) - V_{\mu\mu'}(\boldsymbol{k}+\boldsymbol{q}) \right) c^\dagger_{\mu \boldsymbol{k}+\boldsymbol{q}\downarrow} c_{\mu' \boldsymbol{k}\uparrow} \,. \tag{3.8}$$

$N_\uparrow$ and $N_\downarrow$ are the total number of electrons of $\uparrow$ and $\downarrow$ spin and $\chi_J(\boldsymbol{q},\omega)$, the spin current-spin current response function, is given by the Fourier transform of a retarded Green function in the form

$$\chi_J(\boldsymbol{q},\omega) = \int \mathrm{d}t \langle\langle J_{\boldsymbol{q}}^-(t), J_{-\boldsymbol{q}}^+ \rangle\rangle \mathrm{e}^{-\mathrm{i}\omega t} \,. \tag{3.9}$$

The expression in brackets in equation (3.7) is proportional to the Bloch wall stiffness constant A ($\propto D(N_\uparrow - N_\downarrow)$) and the second term is a generalized superexchange term which always makes a negative contribution to D. The first term therefore yields an upper bound to D and corresponds to the variational ansatz $S_{\boldsymbol{q}}^- |F\rangle$ for the state with a spin-wave of wave-vector $\boldsymbol{q}$ excited, where $|F\rangle$ is the ferromagnetic ground state. This zeroth approximation D_0 is often the dominant term in itinerant electron ferromagnets with maximum spin alignment such as the doped manganites. It is therefore worth examining in detail and for a cubic crystal may be written in the form

$$D_0 = \frac{1}{6(N_\uparrow - N_\downarrow)} \sum_{\boldsymbol{k}} \sum_{\mu\mu'\sigma} \nabla^2 V_{\mu\mu'}(\boldsymbol{k}) \langle c^\dagger_{\mu\boldsymbol{k}\sigma} c_{\mu'\boldsymbol{k}\sigma} \rangle \,, \tag{3.10}$$

where the expectation value is evaluated in the ferromagnetic ground state and differentiation in ∇^2 is with respect to $\boldsymbol{k}$. If a particular orbital $\mu\sigma$ is completely full or completely empty in the ground state it makes no contribution to D_0. This follows because under these circumstances $\langle c^\dagger_{\mu\boldsymbol{k}\sigma} c_{\mu'\boldsymbol{k}\sigma} \rangle$ and $\langle c^\dagger_{\mu'\boldsymbol{k}\sigma} c_{\mu\boldsymbol{k}\sigma} \rangle$ are both zero for $\mu \neq \mu'$ and the integral of $\nabla^2 V_{\mu\mu}(\boldsymbol{k})$ over the whole zone may be written as a surface integral over the zone boundary which clearly vanishes. Thus in the manganites the $\mathrm{t_{2g}}$ orbitals do not contribute to the first term in the Bloch wall stiffness constant A, as long as their mixing into $\uparrow$ spin states above E_F and into $\downarrow$ spin states below E_F is negligible. Of course the $\mathrm{t_{2g}}$ electrons make the largest contribution to the factor $N_\uparrow - N_\downarrow$ in D, and without their exchange coupling to the $\mathrm{e_g}$ electrons there would be no ferromagnetism. The considerations above provide a justification for treating the $\mathrm{t_{2g}}$ electrons as local spins, despite the substantial width of the $\mathrm{t_{2g}}$ bands, and for the model DE Hamiltonian of equation (3.1). We shall see that recent calculations of D in this model are special cases of the general formalism presented here.

Quijada et. al. [50] have considered a two-band generalization of equation (3.1) and calculate D in an approximation equivalent to the random phase approximation (RPA). Nearest-neighbour hopping integrals on a simple cubic lattice are parameterized appropriately for $\mathrm{e_g}$ orbitals, assuming only one non-zero Slater-Koster parameter ($\mathrm{dd}\sigma$). For $J \to \infty$ the result is just D_0 given by equation (3.10), with $N_\uparrow - N_\downarrow = (2S+n)N$ where $n = 1 - x$ is the total number of electrons per atom in the conduction bands and N is the

number of atoms in the crystal. For nearest-neighbour hopping $\nabla^2 V_{\mu\mu'}(\boldsymbol{k}) = -a^2 V_{\mu\mu'}(\boldsymbol{k})$, where a is the lattice constant and the on-site orbital energy taken as zero. Thus

$$D_0 = -\frac{Ka^2}{6(2S+n)}\,, \tag{3.11}$$

where $K = N^{-1}\langle H_0 \rangle$ is the expectation value of the 'kinetic energy' per atom. The K defined in reference [50] is one-third of that defined here and has the opposite sign. In general our $K \leq 0$ and equation (3.11) emphasizes that exchange stiffness is driven by one-electron ('kinetic') energy in the DE model.

It is important to notice that equations (3.10) and (3.11) are still valid if terms corresponding to spin-independent diagonal disorder and local coupling to phonons are included in the Hamiltonian. This last point has been exploited to investigate the effect of electron-phonon coupling on D [43], as discussed in section 8.4. The result concerning disorder is important because it shows that the double-exchange mechanism for ferromagnetism does not depend on having mobile carriers. Localized states contribute to the one-electron energy just as well as extended ones, as long as the localization length is more than a few lattice constants. This presumably explains why T_C varies continuously through the FM-FI phase boundaries in figure 2. At low carrier density ($x \lesssim 0.2$) the occupied states are below a mobility edge, making the system an insulator, but double exchange still operates to give ferromagnetism.

We have laid considerable stress on D_0 as the most important, typically metallic, part of D. However in some systems the value of D is subject to enormous cancellation between D_0 and the second 'superexchange' term. Thus in a very weak itinerant ferromagnet such as $ZrZn_2$, with very small magnetization M, the bracket in equation (3.7) is proportional to M^2, so that $D \propto M$. In a rare-earth metal like Gd, or in an Anderson lattice model of a ferromagnetic heavy fermion system, it is a delicate matter in this formalism to derive the correct RKKY-like result [51]. The situation would be similar in a calculation of D based on the electronic structure picture of $t_{2g}^3 e_g^1$ ($S = 2$) spins coupled via p holes. Zhao [52] criticizes the standard DE picture with $S = 3/2$ spins coupled by e_g carriers. His criticism is based on a two-band estimate of D with finite J, which comes out very small or negative. His model is exactly that of Quijada et. al. [50] who estimate values of D in good agreement with experiment. Zhao does not estimate D in the alternative p-hole picture which he favours. It would be very surprising if the RKKY-like exchange of that picture were larger than that of the itinerant electron DE picture. It would be interesting to carry out proper calculations of D in the multi-band tight-binding formalism starting from a LSDA band structure (compatible with the DE picture) and from LSDA+U or Hartee-Fock band structure (the p-hole case). It was pointed out earlier that Solovyev and Terakura [46] obtained a reasonable value for D for a $x = 0.3$ manganite by means of the LSDA. They calculated the energies of static spin spirals of different wave-vectors $\boldsymbol{q}$ and fitted them to a Heisenberg expression for the magnon energy with exchange extending over many neighbours (see e.g. [53]). For small q this is equivalent to calculating the Bloch wall stiffness constant A which is exactly related to D. However there is no reason to place much reliance on the dispersion curve for larger q. Solovyev and Terakura had difficulty

reconciling their work with the observed doping dependence of D; experimentally in LSMO [54] D increases with x for $0.175 < x < 0.3$, just as T_C does (see figure 2). It is clear, from their analysis of a simplified two-band model, that their opposite conclusion is due to the double-exchange being largest at $x = 0$ since the e_g band is then half-full. At $x = 0$ the system should be a Mott insulator. Probably the best calculational method would be LDSA+U with a U large enough to split the $\uparrow$ spin e_g band but not large enough to reverse the ordering of p and d states. A picture like this is sketched in figure 12 of reference [25]. This does not change the general picture of the electronic structure we presented in section 2.

3.3 Spin-waves in the DE model

The spin-wave stiffness constant D in the one-band DE model (equation (3.1)) is easily deduced from the general multi-band formulation of section 3.1. The only role of the local spins is to provide an exchange splitting between $\uparrow$ and $\downarrow$ spin bands and to contribute $2SN$ to the local moment $N_\uparrow - N_\downarrow$. We can therefore use equation (3.7) and need an approximation to $\chi_J(0,\omega)$. A reasonable approach is to make a local approximation in which the electron self-energy Σ is assumed to be a function of energy only, with no dependence on wave-vector $\boldsymbol{k}$. This is formally exact in infinite dimensions [47] and is the basis of the coherent potential approximation (CPA) and dynamical mean field theory (DMFT). In this case the vertex correction in the spin current response function $\chi_J(0,\omega)$ makes no contribution and χ_J can be evaluated using a simple bubble diagram which involves the product of two one-electron Green functions. This result is well-known from the more familiar charge current response function used to calculate electrical and optical conductivity [55, 48]. Then equation (3.7) becomes [56, 57, 58]

$$D = \frac{1}{3(N_\uparrow - N_\downarrow)} \left(\frac{1}{2} \sum_{\boldsymbol{k}} \langle n_{\boldsymbol{k}\uparrow} + n_{\boldsymbol{k}\downarrow} \rangle \nabla^2 \epsilon_{\boldsymbol{k}} - \frac{1}{\pi} \mathrm{Im} \int \mathrm{d}\epsilon f(\epsilon) \sum_{\boldsymbol{k}} G_{\boldsymbol{k}\uparrow}(\epsilon) G_{\boldsymbol{k}\downarrow}(\epsilon) |\nabla \epsilon_{\boldsymbol{k}}|^2 \right) , \tag{3.12}$$

where $\epsilon_{\boldsymbol{k}} = \sum_j t_{ij} \exp[\mathrm{i}\boldsymbol{k} \cdot (\boldsymbol{R}_i - \boldsymbol{R}_j)]$ is the band energy, $\boldsymbol{R}_i$ being the position of site i, $f(\epsilon)$ is the Fermi function and the one-electron retarded Green function $G_{\boldsymbol{k}\sigma}$ for spin σ is given by

$$G_{\boldsymbol{k}\sigma}(\epsilon) = [\epsilon - \epsilon_{\boldsymbol{k}} - \Sigma_\sigma(\epsilon)]^{-1} \ . \tag{3.13}$$

The occupation number $\langle n_{\boldsymbol{k}\sigma} \rangle$ is determined by

$$\langle n_{\boldsymbol{k}\sigma} \rangle = -\frac{1}{\pi} \int \mathrm{Im}\ G_{\boldsymbol{k}\sigma}(\epsilon) f(\epsilon) \mathrm{d}\epsilon \, . \tag{3.14}$$

On substituting this into equation (3.12), and applying Green's theorem to the sum over $\boldsymbol{k}$ in the first term, we find

$$D = [6\pi(N_\uparrow - N_\downarrow)]^{-1} \mathrm{Im} \int \mathrm{d}\epsilon f(\epsilon) \sum_{\boldsymbol{k}} [G_{\boldsymbol{k}\uparrow}(\epsilon) - G_{\boldsymbol{k}\downarrow}(\epsilon)]^2 |\nabla \epsilon_{\boldsymbol{k}}|^2 \, . \tag{3.15}$$

This compact expression was previously obtained [57, 58] within the framework of a CPA-RPA calculation for ferromagnetic alloys. However it is clearly exact within any local approximation, for example DMFT, and can be used in the presence of coupling to local phonons. It shows how the cancellation between the two terms of equation (3.12) takes place as $N_\uparrow - N_\downarrow \to 0$. An equivalent result has been given by Lichtenstein and Katsnelson [53]. A convenient form of this result is obtained by introducing the function $M(E)$ [59] defined by the integral

$$M(E) = \left(\Omega/8\pi^3\right) \int |\nabla \epsilon_{\boldsymbol{k}}| \mathrm{d}S \tag{3.16}$$

over the surface $\epsilon_{\boldsymbol{k}} = E$ in $\boldsymbol{k}$ space. Here Ω is the volume of the unit cell. Then at $T = 0$

$$D = [6\pi(2S + n_\uparrow - n_\downarrow)]^{-1} \int_{-\infty}^{E_\mathrm{F}} \mathrm{d}\epsilon \int \mathrm{d}E M(E) \mathrm{Im}\ \left[G_{E\uparrow}(\epsilon) - G_{E\downarrow}(\epsilon)\right]^2 \tag{3.17}$$

where $G_{E\sigma}(\epsilon)$ is defined by equation (3.13) with $\epsilon_{\boldsymbol{k}}$ replaced by E and n_σ is the number of σ spin electrons per atom in the band in the ferromagnetic ground state. Normally, we consider J large enough such that $n_\downarrow = 0$, so that $n_\uparrow = n = 1 - x$.

If we make the Hartree-Fock approximation (HFA) to $G_{\boldsymbol{k}\sigma}$ we have $\Sigma_\uparrow = -JS/2$, $\Sigma_\downarrow = JS/2$ and it is easy to show that equation (3.12) yields the RPA result of Wang [60] and Furukawa [61] for D. The second term involves a factor Δ^{-1} where $\Delta = JS$ is the exchange splitting in the conduction band. If a Hubbard on-site Coulomb term $U \sum_i n_{i\uparrow} n_{i\downarrow}$ is added to the Hamiltonian of equation (3.1) the only effect on D, assuming the spins are already aligned completely, is that Δ is increased to $JS + Un$. If we then set $S = 0$ we recover the well-known RPA result for D in the Hubbard model (see e.g. [62]). If $J \to \infty$ in the DE model the RPA result for D reduces to the first term, which is called D_0 in the previous section. If we go beyond the HFA for $G_{\boldsymbol{k}\downarrow}$, in the state of complete spin alignment, we find that even for $J \to \infty$ (but finite S) there is always some $\downarrow$ spin spectral weight near the Fermi level which may even cause the totally spin-aligned state to be unstable, at least for $S = 1/2$ [63, 64, 65]. Thus half-metallicity may be destroyed and, even if not, the Fermi level lies at the top of the half-metallic gap. This effect was known long ago in the Hubbard model and is due to processes in the self-energy $\Sigma_\downarrow$ in which a $\downarrow$ spin electron flips its spin and appears as a $\uparrow$ spin electron near E_F plus a magnon [66, 67, 68, 69]. The $\uparrow$ spin electron and the magnon may bind to form low-lying $\downarrow$ spin quasi-particle states. The magnon dispersion curve necessarily runs into a continuum involving these states for wave-vector $\boldsymbol{q}$ close to an $\uparrow$ spin Fermi wave-vector [69]. Kaplan et. al. [70] have carried out some numerical studies of this effect in one dimension but seem unaware of the earlier analytical work. When the self-energy $\Sigma_\downarrow$ discussed above is introduced into $G_{\boldsymbol{k}\downarrow}$ in equation (3.15), the effect on D is to add a negative term to D_0 (the RPA value for $J \to \infty$) which is attributed to magnon-electron scattering [71, 68, 69]. The magnon excites $\uparrow$ spin electron-hole pairs. This has been investigated diagrammatically from the point of view of a $1/S$ expansion by Golosov [72] and the effect can reduce D in the two-dimensional DE model by a factor of 2. Golosov also discusses magnon damping due to magnon-electron

scattering; he finds that the inverse magnon lifetime is proportional to the sixth power of the wave-vector $\boldsymbol{q}$, as expected for a three-dimensional itinerant electron ferromagnet with complete spin alignment in the ground state [73].

Another approach to this problem is a variational one similar to the ones of references [64, 65]. An obvious ansatz for the state with one spin-wave excited from the ferromagnetic state of complete spin alignment is

$$(S^-_{\boldsymbol{q}} + \sum_{\boldsymbol{kp}} A_{\boldsymbol{kp}} S^-_{\boldsymbol{q+p-k}} c^\dagger_{\boldsymbol{k}\uparrow} c_{\boldsymbol{p}\uparrow}) \, |F\rangle \tag{3.18}$$

where $S^-_{\boldsymbol{q}}$ is the total spin-flipping operator for local and itinerant spins. It is difficult to choose the coefficients $A_{\boldsymbol{kp}}$ optimally, but a convenient choice is

$$A_{\boldsymbol{kp}} = [N(n+2S)]^{-1}(\epsilon_{\boldsymbol{p}} - \epsilon_{\boldsymbol{p+q}})(\epsilon_{\boldsymbol{k}} - \epsilon_{\boldsymbol{p}} + \hbar\omega^{\mathrm{RPA}}_{\boldsymbol{q+p-k}})^{-1} \, , \tag{3.19}$$

where

$$\hbar\omega^{\mathrm{RPA}}_{\boldsymbol{q}} = [N(n+2S)]^{-1} \sum_{\boldsymbol{l}} \langle n_{\boldsymbol{l}\uparrow}\rangle (\epsilon_{\boldsymbol{l+q}} - \epsilon_{\boldsymbol{l}}) \tag{3.20}$$

is the RPA spin-wave energy for $J \to \infty$. Then we find an upper bound on D, for $J \to \infty$, in the form

$$\begin{aligned} D = D_0 &- \frac{1}{3[N(n+2S)]^2} \sum_{\boldsymbol{kp}} \frac{|\nabla\epsilon_{\boldsymbol{p}}|^2}{\epsilon_{\boldsymbol{k}} - \epsilon_{\boldsymbol{p}} + \hbar\omega^{\mathrm{RPA}}_{\boldsymbol{p-k}}} \\ &- \frac{1}{3[N(n+2S)]^3} \sum_{\boldsymbol{k}} \sum_{\boldsymbol{pp'}} \frac{(\nabla\epsilon_{\boldsymbol{p}} \cdot \nabla\epsilon_{\boldsymbol{p'}}) \, (\epsilon_{\boldsymbol{p'+p-k}} - \epsilon_{\boldsymbol{p'}} - \epsilon_{\boldsymbol{p}} + \epsilon_{\boldsymbol{k}})}{\left(\epsilon_{\boldsymbol{k}} - \epsilon_{\boldsymbol{p}} + \hbar\omega^{\mathrm{RPA}}_{\boldsymbol{p-k}}\right) \left(\epsilon_{\boldsymbol{k}} - \epsilon_{\boldsymbol{p'}} + \hbar\omega^{\mathrm{RPA}}_{\boldsymbol{p'-k}}\right)} \, . \end{aligned} \tag{3.21}$$

Here the sums over $\boldsymbol{p}$, $\boldsymbol{p'}$ are restricted to occupied states in the $\uparrow$ spin band and the sum over $\boldsymbol{k}$ is restricted to unoccupied ones. This result agrees with that of Golosov [72] to order $1/S^2$. The last term in equation (3.21), involving $\nabla\epsilon_{\boldsymbol{p}} \cdot \nabla\epsilon_{\boldsymbol{p'}}$ with $\boldsymbol{p} \neq \boldsymbol{p'}$ in general, does not fit into the exact form of D in the local approximation (equation (3.12). This is not unexpected because the $\downarrow$ spin self-energy including electron-magnon scattering depends on wave-vector $\boldsymbol{k}$, not only on energy. The last term in equation (3.21) corresponds to a vertex correction first discussed by Edwards [71].

4 Magnetism and transport in the DE model

In the last section we saw that much is known about the low-lying excitations of the DE model. Recent work on the properties of the model over the whole temperature range often deals with the limit of classical local spins ($S \to \infty$). The most complete work along these lines is that of Furukawa [61], using dynamical mean field theory (DMFT) which is the best local approximation. No analytical progress can be made within DMFT for the quantum-spin DE model and numerical calculations have not yet appeared. However there

is no doubt that quantum spins introduce effects which do not exist for classical spins. For example the low-lying $\downarrow$ spin spectral weight discussed in the last section has total weight $(1-n)/(2S+1)$ for large J (see section 4.2) and therefore does not appear for $S \to \infty$. In this section we shall therefore concentrate on another local approximation, the many-body dynamical CPA [74, 75] in which quantum spins can be treated analytically and which agrees with DMFT in the classical limit. Like much current research on the DE model (see section 3.3) the method has its roots in work done on the Hubbard model in the sixties, in this case by Hubbard himself [76]. Since such work is no longer common knowledge we start with an introduction to CPA in the Hubbard model.

4.1 CPA for the Hubbard model

To introduce the many-body CPA we consider the Hubbard model, which is a simpler model for strongly correlated electrons than the DE model with quantum spins. The Hamiltonian for this model is

$$H_{\rm H} = \sum_{ij\sigma} t_{ij} c^\dagger_{i\sigma} c_{j\sigma} + U \sum_i n_{i\uparrow} n_{i\downarrow} \tag{4.1}$$

and Hubbard [76] set out to find an approximation to the one-electron retarded Green function $G_{\boldsymbol{k}\sigma}(\epsilon)$ which is exact in the atomic limit $t_{ij} = 0$. He used the equation of motion method and the idea of the alloy analogy described below. It turns out that Hubbard's approach, without the minor "resonance broadening correction", is equivalent to the CPA which was developed later [77]. The CPA derivation of Hubbard's result is much simpler than the original equation of motion method. However we had to resort to an extension of the original method to derive the many-body CPA for the DE model, with and without phonons, in the general form needed to discuss magnetic properties. In this paper we restrict the derivation to the paramagnetic state in zero magnetic field, although we summarize some more general results.

The alloy analogy consists in considering the $\uparrow$-spin electrons, say, to move in the potential due to static $\downarrow$-spin electrons, frozen in a random configuration which must be averaged over. Thus a one-electron Hamiltonian for $\uparrow$-spin is obtained from (4.1) by taking the last term to be $U \sum_i n_{i\uparrow} \langle n_{i\downarrow} \rangle$ where $\langle n_{i\downarrow} \rangle$ takes the value 1 with probability $n_\downarrow$ and 0 with probability $1-n_\downarrow$. Here n_σ is the number of σ-spin electrons per atom. It is important to note that the alloy analogy is quite distinct from the Hartree-Fock approximation in which $\langle n_{i\sigma} \rangle = n_\sigma$ for all i. In the alloy analogy a σ-spin electron moves in a random potential given by U on $n_{\bar\sigma}$ sites and 0 on $1 - n_{\bar\sigma}$ sites. In the CPA the random potential is replaced by a uniform, but energy-dependent, effective potential $\Sigma_\sigma(\epsilon)$ for an "effective medium". This effective potential, in general complex, is called the coherent potential and is in fact the electron self-energy. The procedure for determining Σ_σ is to insist on a zero average t-matrix for scattering by a central atom, with potential U or 0, set in the effective medium. Equivalently the average of the site-diagonal element $G_\sigma(\epsilon)$ of the Green function, for each type of central atom, is put equal to the site-diagonal element of the

Green function for the effective medium. Thus

$$G_\sigma = n_{\bar{\sigma}} \frac{G_\sigma}{1-(U-\Sigma_\sigma)\,G_\sigma} + (1-n_{\bar{\sigma}})\,\frac{G_\sigma}{1+\Sigma_\sigma G_\sigma} \tag{4.2}$$

and

$$G_\sigma(\epsilon) = \frac{1}{N}\sum_{\boldsymbol{k}} \frac{1}{\epsilon - \epsilon_{\boldsymbol{k}} - \Sigma_\sigma(\epsilon)} = G_0\left(\epsilon - \Sigma_\sigma(\epsilon)\right) \tag{4.3}$$

where the bare band Green function is given by

$$G_0(\epsilon) = \int \mathrm{d}\epsilon' \frac{N_0(\epsilon')}{\epsilon - \epsilon'}\,. \tag{4.4}$$

Here $\epsilon_{\boldsymbol{k}} = \sum_j t_{ij} \exp[\mathrm{i}\boldsymbol{k}\cdot(\boldsymbol{R}_i - \boldsymbol{R}_j)]$ is the band energy, where $\boldsymbol{R}_i$ is the position of site i, $N_0(\epsilon)$ is the corresponding density of states per atom and N is the number of lattice sites. Equations (4.2) and (4.3) are to be solved self-consistently for $\Sigma_\sigma(\epsilon)$ and hence for the local Green function $G_\sigma(\epsilon)$. Equation (4.2) may be written as

$$G_\sigma = \frac{n_{\bar{\sigma}}}{\Sigma_\sigma + G_\sigma^{-1} - U} + \frac{1-n_{\bar{\sigma}}}{\Sigma_\sigma + G_\sigma^{-1}}\,. \tag{4.5}$$

This may be compared with the exact Green function for the atomic limit ($t_{ij} = 0$) which is given by [76]

$$G_\sigma^{\mathrm{AL}}(\epsilon) = \frac{n_{\bar{\sigma}}}{\epsilon - U} + \frac{1-n_{\bar{\sigma}}}{\epsilon}\,, \tag{4.6}$$

where in this retarded Green function ϵ has a small positive imaginary part as usual. Hence

$$G_\sigma(\epsilon) = G_\sigma^{\mathrm{AL}}\left(\Sigma_\sigma + G_\sigma^{-1}\right)\,. \tag{4.7}$$

Clearly this CPA equation is exact in the atomic limit, when $N_0(\epsilon) = \delta(\epsilon)$ and it follows from equation (4.3) that $\Sigma_\sigma + G_\sigma^{-1} = \epsilon$. Solution of the CPA equation becomes simple if the density of states $N_0(\epsilon)$ is taken to be of the elliptic form

$$N_0(\epsilon) = \frac{2}{\pi W^2}\left(W^2 - \epsilon^2\right)^{1/2} \tag{4.8}$$

where $2W$ is the bandwidth. Then from equation (4.4)

$$G_0(\epsilon) = \frac{2}{W^2}\left[\epsilon - \left(\epsilon^2 - W^2\right)^{1/2}\right]\,. \tag{4.9}$$

Introducing this expression for G_σ in equation (4.3), and solving for $\epsilon - \Sigma_\sigma(\epsilon)$, we find

$$\Sigma_\sigma + G_\sigma^{-1} = \epsilon - W^2 G_\sigma/4\,. \tag{4.10}$$

Hence equations (4.6) and (4.7) give an algebraic equation for G_σ.

Solving this type of equation for G_σ, Hubbard [76] calculated the density of states $N_\sigma(\epsilon) = -\pi^{-1}\mathrm{Im}\ G_\sigma(\epsilon)$, considering particularly the paramagnetic state $n_\uparrow = n_\downarrow = n/2$ and concentrating on the half-filled band case $n = 1$. He showed that for U/W greater than a critical value, equal to 1 in the present approximation, a gap opens in $N(\epsilon)$ at the Fermi level so that the system becomes an insulator as envisaged by Mott. For $U \gg W$ the density of states consists of two peaks centred on $\epsilon = 0$ and $\epsilon = U$, these being broadened versions of the δ-functions at these energies in the atomic limit. Furthermore, for general band-filling n, the spectral weights in the two peaks are the same as in the atomic limit.

The CPA for the Hubbard model has some serious defects. There are no self-consistent solutions with magnetic order. Furthermore in the paramagnetic metallic state, for $n < 1$ or for $n = 1$ with U/W less than the critical value, the system is never a Fermi liquid. There is never a sharp Fermi surface at $T = 0$ with a Migdal discontinuity in the Bloch state occupation number, as pointed out by Edwards and Hewson [78]. This is due to the absence of states with infinite lifetime at the Fermi level, since within the alloy analogy all states are scattered by disorder. A modification of the CPA to remedy this defect, retaining the analytic simplicity of the method, had some limited success [79, 80, 81]. However the most satisfactory approach is DMFT which involves numerical solution of an associated self-consistent impurity problem [47, 82]. DMFT may be regarded as the best local approximation, in which the self-energy is a function of energy only, and is exact in infinite dimension.

The many-body CPA is considerably more satisfactory for the DE model than it is for the Hubbard model, as discussed in the next section. There is one limit, the case of classical spins ($S = \infty$), in which the CPA is identical to DMFT. This is because classical spins are static and an alloy analogy of frozen disordered spins is completely justified. DMFT for the DE model has only been implemented fully for classical spins [83, 84] and the many-body CPA discussed in the next section provides an approximate analytic extension of DMFT to quantum spins. The system orders ferromagnetically below a Curie temperature T_C, as it should, and the disordered spin state above T_C should be well described. However, the accuracy of the ground state at $T = 0$ for finite S is unclear. The saturated state with all itinerant and local spins completely aligned, which is the ground state for $S = \infty$ (we are always considering large J in the DE model), is never a self-consistent CPA solution for finite S [74]. This is due to low-lying $\downarrow$ spin states of the type discussed in section 3.3. In the treatment described there involving magnon emission the local approximation corresponds to neglecting the magnon energy, in which case $\downarrow$ spin quasi-particle states always appear below the Fermi level and the saturated state is unstable. In their approximate treatments of DMFT Meyer et. al. [85] also find $\downarrow$ spin states below the Fermi level for any finite S. Possibly this is a general result of the local approximation. The true parameter range of stability of the saturated ground state is unknown. It has been shown rigorously that for $J = \infty$ it is unstable for $S = 1/2$ and $0.12 < n < 0.45$, with a simple cubic nearest-neighbour tight-binding band [63]. Wurth and Müller-Hartmann [65] find no instability with respect to a single spin-flip for any n when $J = \infty$ and $S = 3/2$. If the true ground state is not saturated it seems unlikely to be

a uniform (spatially homogeneous) ferromagnet, with partially ordered local and itinerant spins, as in the uniform CPA ground state for finite S. Such a state would probably not be a Fermi liquid, just as in CPA, unless the electrons making up the spin S became partially delocalised with spectral weight at the Fermi level. Numerical DMFT results for quantum spins are urgently required to throw light on the matter.

4.2 The many-body CPA for the DE model

Edwards et. al. [74] developed the many-body CPA for the DE model using an extension of Hubbard's equation of motion method. Hubbard's "scattering correction" becomes more complicated owing to the form of the interaction term in the DE model whereby electrons can flip their spin via exchange of angular momentum with the local spins. This dynamical effect couples the equations for $G_\uparrow$ and $G_\downarrow$ and was first treated by Kubo [86] in a one-electron dynamical CPA. The main feature of the many-body CPA is that we recover Kubo's one-electron CPA as $n \to 0$ and the correct atomic limit for general band-filling n as $t_{ij} \to 0$. A second paper [75] showed the equivalence to DMFT in the limit $S \to \infty$, $J \to \infty$. The full equation of motion derivation of the many-body CPA is required to obtain general results in the presence of a magnetic field and/or magnetic order [75]. However it turns out that in the zero-field paramagnetic state we can deduce the CPA equation from the atomic limit Green function $G_\sigma^{\rm AL}$ and equation (4.7), just as in the Hubbard model. We shall therefore not repeat the full derivation in this paper although we shall discuss results on magnetic properties in section 4.4.

The atomic limit Green function, $G_\uparrow^{\rm AL}$, say, is easily obtained by the equation of motion method using the Hamiltonian (3.1) with $t_{ij} = 0$ [74]. The result for zero field ($h = 0$) is

$$G_\uparrow^{\rm AL}(\epsilon) = \frac{1}{2S+1}\left[\frac{\langle (S+S^z)\,n_\downarrow - S^-\sigma^+\rangle}{\epsilon + J(S+1)/2} + \frac{\langle (S-S^z)\,(1-n_\downarrow) - S^-\sigma^+\rangle}{\epsilon - J(S+1)/2}\right.$$
$$\left. + \frac{\langle (S+1+S^z)\,(1-n_\downarrow) + S^-\sigma^+\rangle}{\epsilon + JS/2} + \frac{\langle (S+1-S^z)\,n_\downarrow + S^-\sigma^+\rangle}{\epsilon - JS/2}\right] \tag{4.11}$$

and for $h \neq 0$ one merely has to replace ϵ by $\epsilon + h/2$. The angle brackets $\langle \ldots \rangle$ represent thermal averages and all operators within them correspond to the same site i, this suffix thus being omitted. This expression, with four poles, is considerably more complicated than the two-pole Hubbard model expression of equation (4.6). The poles at $\epsilon = \pm JS/2$, $\pm J(S+1)/2$ correspond to energies to add or remove an electron from the atom, that is to transitions between singly-occupied states and either unoccupied or doubly-occupied states. The singly-occupied states have total spin $S + \frac{1}{2}$ or $S - \frac{1}{2}$ with energies $-JS/2$ and $J(S+1)/2$ respectively; the unoccupied and doubly-occupied states have zero energy. In a state of complete spin alignment, with all local and itinerant spins $\uparrow$, $G_\uparrow^{\rm AL}$ has a single pole at $\epsilon = -JS/2$ and $G_\downarrow^{\rm AL}$ has three poles at $\epsilon = \pm JS/2$ and $J(S+1)/2$. The weight in the low-lying $\downarrow$ spin level at $-JS/2$ is $(1-n)/(2S+1)$.

In the zero-field paramagnetic case it turns out that the CPA equation for $G(\epsilon)$ with the redundant suffix σ omitted, is given by equation (4.7) as in the Hubbard model. Thus,

taking the band to have the elliptic form (4.8), the CPA equation for G is

$$G(\epsilon) = G^{\mathrm{AL}}\left(\epsilon - W^2 G/4\right) \tag{4.12}$$

with G^{AL} given by

$$\begin{aligned} G^{\mathrm{AL}}_{\uparrow}(\epsilon) = \frac{1}{2S+1}\Bigg[&\frac{nS/2 - \langle \boldsymbol{S}\cdot\boldsymbol{\sigma}\rangle}{\epsilon + J(S+1)/2} + \frac{S(1-n/2) - \langle \boldsymbol{S}\cdot\boldsymbol{\sigma}\rangle}{\epsilon - J(S+1)/2} \\ &+ \frac{(S+1)(1-n/2) + \langle \boldsymbol{S}\cdot\boldsymbol{\sigma}\rangle}{\epsilon + JS/2} + \frac{n(S+1)/2 + \langle \boldsymbol{S}\cdot\boldsymbol{\sigma}\rangle}{\epsilon - JS/2}\Bigg]. \end{aligned} \tag{4.13}$$

The spin symmetry of the paramagnetic state has been used to simplify the expectations in the previous form of G^{AL}, equation (4.11). It is easy to show that $\langle \boldsymbol{S}\cdot\boldsymbol{\sigma}\rangle \to nS/2$ as $J \to \infty$ and $\langle \boldsymbol{S}\cdot\boldsymbol{\sigma}\rangle$ will be very near this limit as long as $JS \gtrsim 2W$. We make this approximation in calculating $G(\epsilon)$, and hence the density of states, $N(\epsilon) = -\pi^{-1}\mathrm{Im}\, G(\epsilon)$ from equations (4.12) and (4.13). The results are shown in figure 11 for $S = 3/2$ and $J = 4W$ for various n. Clearly, from equation (4.13), the approximation to $\langle \boldsymbol{S}\cdot\boldsymbol{\sigma}\rangle$ has the effect of removing the weak band centred on $\epsilon = -J(S+1)/2$ but it does not affect the total weight or the distribution of weight between the two lower and two upper bands. It may be seen that as n increases from 0 the band near $\epsilon = J(S+1)/2$ is reduced in weight and a new band appears near $JS/2$, until at $n = 1$ no weight remains in the band near $J(S+1)/2$. The weight in the band near $-JS/2$ is $(S+1-n/2)/(2S+1)$ per spin so if JS is sufficiently large to separate the bands ($JS \gtrsim 2W$) this band will just be filled at $n = 1$ producing a Mott insulator as expected. This redistribution of weight between bands as they fill with electrons is characteristic of the many-body CPA and was missing from Kubo's one-electron CPA [86] which was restricted to $n = 0$.

In the strong-coupling limit $J \to \infty$, which is taken with a shift of energy origin $\epsilon \to \epsilon - JS/2$, equation (4.13) simplifies to

$$G^{\mathrm{AL}}(\epsilon) = \epsilon^{-1}(S+1-n/2)/(2S+1)\,. \tag{4.14}$$

Equation (4.12) then becomes a quadratic equation for G with solution

$$G(\epsilon) = \alpha^2 \frac{2}{D^2}\left[\epsilon - \sqrt{\epsilon^2 - D^2}\right] \tag{4.15}$$

where $\alpha^2 = (S+1-n/2)/(2S+1)$ and $D = \alpha W$. By comparing with equations (4.8) and (4.9) we see that the density of states is a single elliptical band of weight α^2 and bandwidth $2\alpha W$. As $S \to \infty$ the band-narrowing factor $\alpha \to 1/\sqrt{2} = 0.707$, which is close to the classical result of 2/3, obtained by averaging $\cos(\theta/2)$ over the solid angle.

In the classical spin limit $S \to \infty$ we rescale J, replacing it by J/S, and the CPA equation becomes

$$G = \frac{1}{2}\left[\frac{1}{\Sigma + G^{-1} + J/2} + \frac{1}{\Sigma + G^{-1} - J/2}\right]. \tag{4.16}$$

Here we have used the general equation (4.7), valid for arbitrary band-shape, rather than equation (4.12). Equation (4.16) is precisely the equation obtained by Furukawa [61] within DMFT.

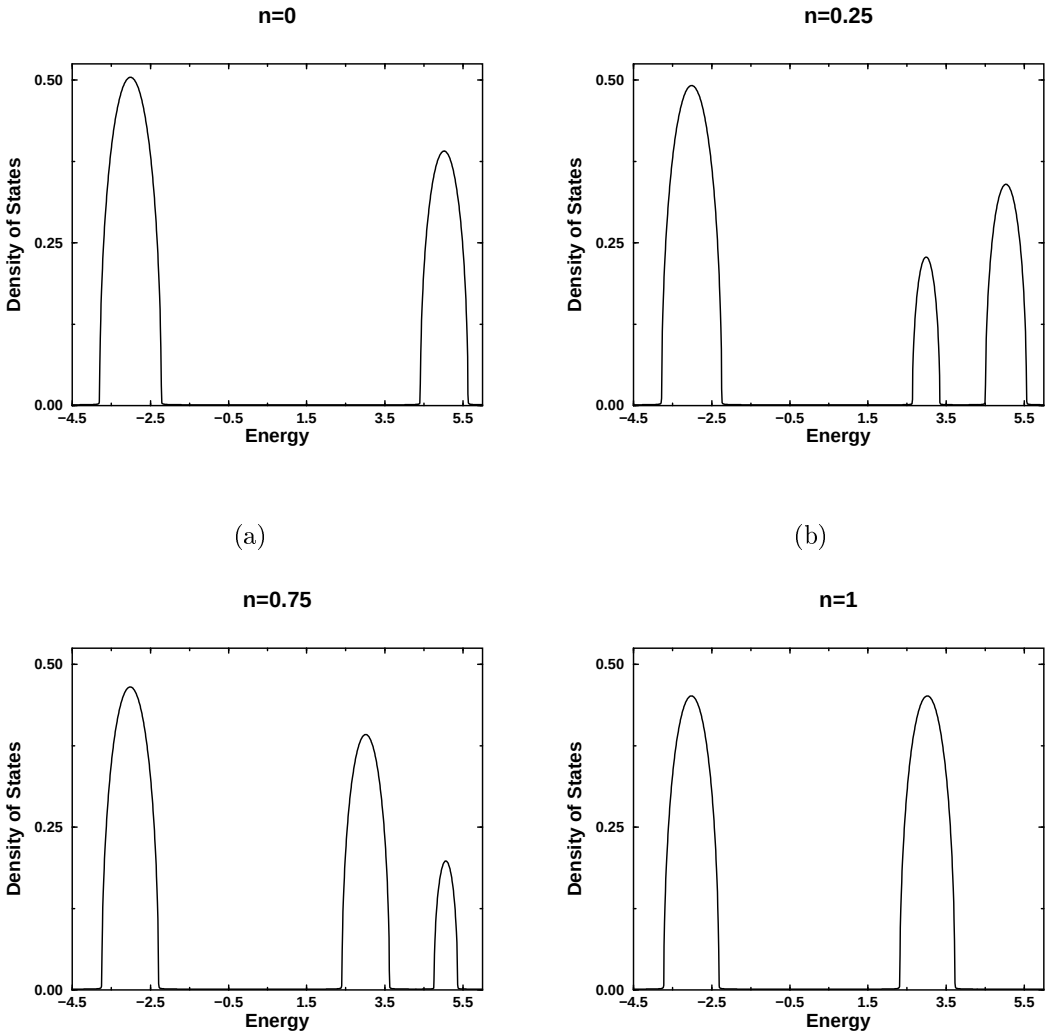

(a) (b)

(c) (d)

Figure 11: The density of states in the paramagnetic state of the double-exchange model for $S = 3/2$, $J = 4W$, and $n = 0$, 0.25, 0.75 and 1. The Fermi level is always within the lowest band until this is just filled for $n = 1$. Energy units of W are used. (from reference [74])

4.3 Resistivity in the paramagnetic state of the DE model

The Kubo formula for the conductivity σ involves the two-particle current-current response function. However in the local approximation of CPA or DMFT there is no vertex correction [55, 48] and σ may be expressed in terms of the one-particle spectral function

$$A_{\boldsymbol{k}}(\epsilon) = -\pi^{-1}\mathrm{Im}\ G_{\boldsymbol{k}}(\epsilon) = -\pi^{-1}\mathrm{Im}\ \left[\epsilon - \epsilon_{\boldsymbol{k}} - \Sigma(\epsilon)\right]^{-1}\ . \tag{4.17}$$

In the paramagnetic state G is T-independent if we assume $\langle \boldsymbol{S}\cdot\boldsymbol{\sigma}\rangle = nS/2$, and σ depends on temperature only weakly through the Fermi function. If we neglect this thermal smearing around the Fermi energy μ we may calculate at $T = 0$ but consider the results to apply to the actual paramagnetic state at $T > T_{\mathrm{C}}$. We find [74]

$$\sigma = \frac{2\pi \mathrm{e}^2}{3Na^3\hbar}\sum_{\boldsymbol{k}} \boldsymbol{v}_k^2\left[A_{\boldsymbol{k}}(\mu)\right]^2 \tag{4.18}$$

where $\boldsymbol{v}_{\boldsymbol{k}} = \nabla\epsilon_{\boldsymbol{k}}$ is the electron velocity and a^3 is the volume of the unit cell. Just as in section 3.3 we can introduce the function $M(E)$, defined by equation (3.16), and write

$$\sigma = \frac{2\pi e^2}{3a^3\hbar}\int \mathrm{d}E M(E)|A_E(\mu)|^2\,, \tag{4.19}$$

where $A_E(\mu)$ is defined by the right-hand expression in equation (4.17) with $\epsilon = \mu$, $\epsilon_{\boldsymbol{k}} = E$. For a simple cubic tight-binding band $\epsilon_{\boldsymbol{k}} = -2t\sum_\beta \cos k_\beta a$, with β summed over x, y, z, $\nabla^2\epsilon_{\boldsymbol{k}} = -a^2\epsilon_{\boldsymbol{k}}$. Then it is straight-forward to show that

$$M(E) = -a^2\int_{-\infty}^{E} E N_{\mathrm{c}}(E)\mathrm{d}E \tag{4.20}$$

where $N_{\mathrm{c}}(E)$ is the density of states for the simple cubic band. If $N_{\mathrm{c}}(E)$ is replaced by a suitably-scaled Gaussian $N_{\mathrm{g}}(E) = (3/\pi)^{1/2}W^{-1}\exp\left[-3(E/W)^2\right]$, corresponding to a hypercubic lattice in infinite dimensions, $M(E)$ becomes $M_{\mathrm{g}} = (a^2W^2/6)N_{\mathrm{g}}(E)$. However if $N_{\mathrm{c}}(E)$ is replaced by the elliptic density of states $N_0(E)$ it becomes $M_0(E) = [a^2(W^2 - E^2)/3]N_0(E)$. We refer to previous treatments of the $M(E)$ factor in σ when we discuss the optical conductivity in section 8.3.2.

Since it is convenient to use $N_0(\epsilon)$ to calculate the Green function and self-energy, as in the previous section, it is reasonable to evaluate σ using equation (4.19) with $M(E) = M_0(E)$. Edwards et. al. [74] took the strong-coupling limit $J \to \infty$ for simplicity and the results for the resistivity $\rho = \sigma^{-1}$ are plotted against band-filling n for various S in figure 12. The lattice constant was taken as $a = 5$ Å which is comparable with the Mn–Mn spacing in manganites. For $J = \infty$ the band-width W is the only energy-scale and, since the integral in equation (4.19) is dimensionless when a factor a^2 is taken out, ρ does not depend on W. In fact in the DE regime $JS \gtrsim 2W$ the resistivity is almost independent of both J and W. It is seen in figure 12 that ρ diverges correctly at $n = 0$, owing to the absence of carriers, and at $n = 1$ where the system becomes a Mott insulator. Well

away from these insulating limits ρ does not depend strongly on S, so that quantum spin effects are not very important. Furthermore $\rho \approx 1$ mΩcm over a wide range of band-filling, which is much smaller than observed in some manganites above $T_{\rm C}$, for example in LCMO (see figure 5). This agrees with the conclusion of Millis et. al. [87] that the DE model, with electrons scattered purely by disordered local spins, cannot describe the physics of the manganites completely. Early work by Furukawa [83] seemed to point to another conclusion, although the DMFT is equivalent to the CPA approach. Edwards et. al. [74] showed that the confusion arose from Furukawa's use of a convenient, but rather unreasonable, Lorentzian density of states. This makes the calculation of $A_E(\mu)$ very simple and Furukawa effectively took $M(E)$ in equation (4.19) to be Lorentzian also. In later work Furukawa [61] used the elliptic band. Results of such calculations for the limit $J \to \infty$ are shown in figure 13 and it is remarkable that ρ is at least an order of magnitude larger than one finds in figure 12 for the more reasonable elliptic band.

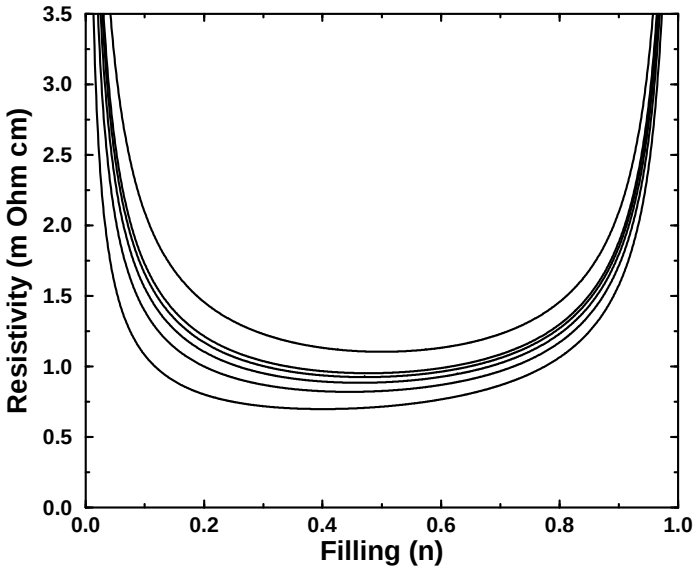

Figure 12: The zero field paramagnetic state resistivity $\rho = \sigma^{-1}$ versus band-filling n for the double-exchange model from reference [74]. Here $J = \infty$, $a = 5$ Å, and $S = 1/2$, 1, 3/2, 2, 5/2 and ∞, ρ increasing with S. The elliptical density of states and formula (4.19) with $M(E) \equiv M_0(E)$ are used (from reference [74]).

4.4 Magnetism in the DE model

As discussed at the beginning of section 4.2, the full equation of motion approach to many-body CPA is required to determine magnetic properties such as spin susceptibility χ and

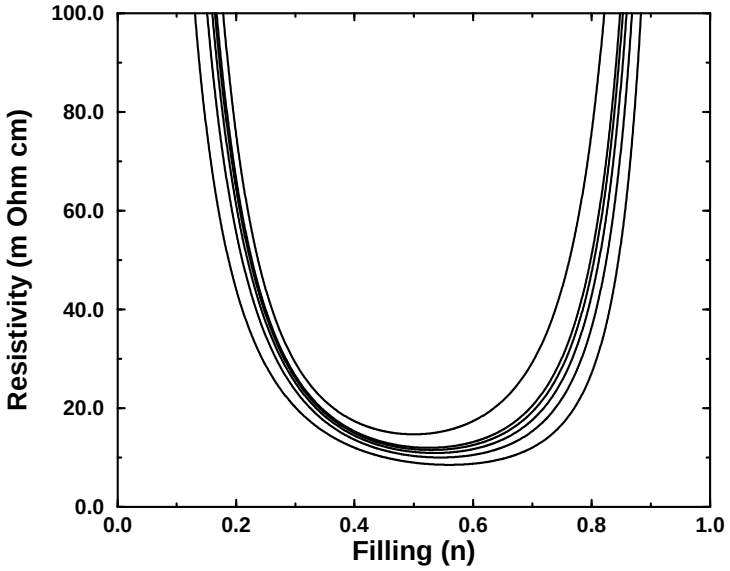

Figure 13: As in figure 12 but using a Lorentzian density of states and formula (4.19) with $M(E) = (W^2a^2/6\pi)(E^2 + W^2)^{-1}$. (from reference [74])

Curie temperature T_C. In reference [74] this involved a hierarchy of Green functions satisfying $4S+1$ coupled algebraic equations for local spin S; only the $S = 1/2$ case was briefly discussed. In reference [75] a major simplification was achieved by introducing generating Green functions which generate all the required Green functions by differentiation with respect to a parameter. The coupled equations are then replaced by a single first-order linear differential equation, the parameter being the independent variable, whose analytic solution yields the required CPA equations for the Green functions. The classical limit $S = \infty$ can then be taken and for $J = \infty$ the equations coincide with those of DMFT, which are only obtainable in the classical limit. The many-body CPA is therefore an analytic approximation to DMFT for arbitrary quantum spin S which becomes exact for $S = \infty$. The many-body CPA also coincides with Kubo's [86] one-electron CPA in the limit $n \to 0$ where that is valid.

To determine the magnetic properties one problem remains; the CPA and DMFT equations contain one set of correlation functions $\langle (S^z)^m \rangle$ which cannot be obtained directly from the Green functions. There is an indirect procedure for determining these correlation functions within CPA but it proves to be unsatisfactory, never yielding ferromagnetic solutions. However, for $S = \infty$, DMFT provides a way to calculate the probability distribution function $P(S^z)$, and hence $\langle (S^z)^m \rangle$, and Green and Edwards [75] used an empirical extension of this for finite S. This extension guarantees that the spin susceptibility exhibits the correct Curie laws for band occupations $n = 0$ and $n = 1$. Thus for $n = 0$ we have a Curie law over the whole temperature range, corresponding to N independent spins S.

For $n = 1$, with $J = \infty$, we have independent spins $S + \frac{1}{2}$. For $0 < n < 1$ we find a finite Curie temperature $T_{\rm C}$ and some results [75] are shown in figure 14. In figure 14(a) $T_{\rm C}$ is plotted as a function of n for various S with $J = \infty$, using the elliptic band. Clearly for finite S ferromagnetism is more stable for $n > 0.5$ than for $n < 0.5$, in agreement with the findings of Brunton and Edwards [63]. For $S = \infty$ the result agrees closely with that of Furukawa [61]. In figure 14(b) we see the effect on $T_{\rm C}$ for $S = 1/2$ of changing the bare band-shape from elliptic to simple cubic tight-binding. A dip in $T_{\rm C}$ occurs around $n = 0.3$ which is the region where the ground state of the simple cubic DE model with $S = 1/2$ is rigorously not one of complete spin alignment [63].

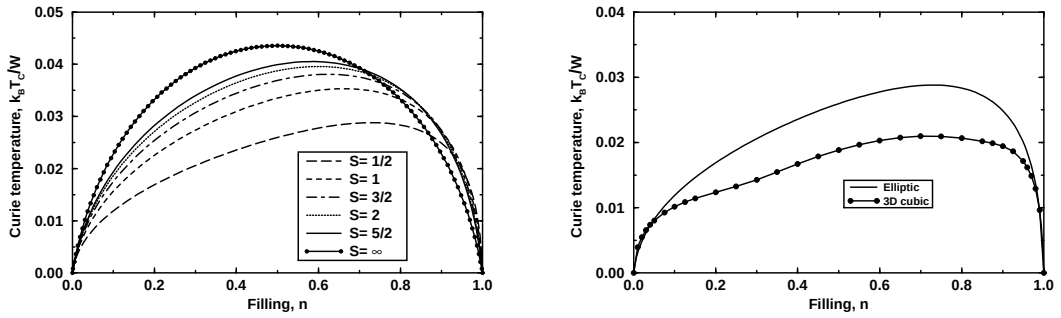

(a) (b)

Figure 14: The Curie temperature $k_{\rm B}T_{\rm C}/W$ of the double-exchange model versus band-filling n for various S, calculated with $J = \infty$ using the elliptic band (a); the effect on $T_{\rm C}$ for $S = 1/2$ of changing the elliptic band to the density of states for a simple cubic tight-binding band with nearest neighbour hopping (b). (from reference [75])

5 The metal-insulator transition

In section 1 we pointed out the wide range of behaviour in manganites. LSMO with $x \approx 0.3$ has a metal-poor metal transition at $T_{\rm C}$, whereas in LCMO the resistivity $\rho(T)$ decreases with rising temperature above $T_{\rm C}$ (see figure 5). Moreover the resistivity near $T_{\rm C}$ is an order of magnitude larger in LCMO than in LSMO. This behaviour of LCMO, and many other manganites, is characterized as a metal-insulator (MI) transition. Furukawa has pointed out that the contrasting behaviour of LSMO is quite well described by the DE model . Furukawa's $\rho(T)$ curve (figure 9 of reference [61]) is similar to that of figure 21 in this paper, which corresponds to weak electron-phonon coupling i.e. essentially to the pure DE model. A central problem in the theory of the manganites is to explain the origin of the MI transition in systems like LCMO and to explain why it does not occur in LSMO. Clearly the pure DE model is insufficient, as first emphasized by Millis et. al. [87]. However a common element of many theories of the MI transition is the narrowing of

the band in the paramagnetic state above T_C due to the DE mechanism. This narrowing of the band encourages any tendency to localize the electrons and produce insulating behaviour. However theories differ greatly as to what actually drives the localization. Millis et. al. [87, 88] and Röder et. al. [89] propose that the driving force is strong electron-phonon coupling associated with the dynamic Jahn-Teller effect. On the other hand Varma [90] and Müller-Hartmann and Dagotto [91] proposed that localization could occur due to a combination of magnetic disorder and non-magnetic A-site disorder. Nagaev's theory [8, 92] is also based on A-site disorder while Furukawa [61] argues in favour of phase separation models of LCMO with, for example, ferromagnetic and charge-ordered regions. We begin with a discussion of models based on disorder.

5.1 The role of disorder

Sheng et. al. [93] pursued a line similar to Varma's [90]. They studied localization due to both non-magnetic randomness and the off-diagonal disorder associated with the classical spin DE model. As mentioned in section 3.1, the effective hopping integral is $t_{ij}\cos(\theta_{ij}/2)$ where the angle θ_{ij} between neighbouring spins varies randomly in the paramagnetic state. Sheng et. al. showed using scaling theory that this off-diagonal disorder alone can only localize a small fraction of electron states close to the band edges but fails to cause localization of the electron states at the Fermi level for the ferromagnetic regime with $x = 0.2$–0.5. Li et. al. [94] came to a similar conclusion using a transfer-matrix method. This is an important result because local approximations such as DMFT and CPA are not able to detect localization. Both groups further showed that to obtain a MI transition between the ferromagnetic and paramagnetic state, by means of the mobility edge moving through the Fermi level on introducing the off-diagonal disorder of the paramagnetic state, one needs large diagonal disorder with random site energies in the range $(-W, W)$. Here $2W$ is the bandwidth in the ferromagnetic state and $W \sim 1$ eV typically. The random energies at Mn sites in $La_{1-x}Ca_xMnO_3$, say, arise from varying local environments of La^{3+} and Ca^{2+} ions. Neglecting metallic screening, the change in potential at a Mn site due to changing the charge on one of the neighbouring A sites by e is about 0.4 eV, assuming a local dielectric constant of 10. Pickett and Singh [35] deduce from a band calculation on ordered $La_{2/3}Ca_{1/3}MnO_3$ that in the disordered case Mn site energies have a Gaussian-like distribution with full width at half maximum equal to 0.6 eV. This is much less than $2W$ so the condition for a MI transition is not fulfilled. Smolyaninova et. al. [95] searched for scaling behaviour of their resistivity measurements on $La_{0.67}Ca_{0.33}MnO_3$ and $Nd_{0.7}Sr_{0.3}MnO_3$ thin films; they concluded their results were incompatible with an Anderson localization transition.

Nagaev's [8, 92] theory is rather different. He assumes the charge carriers are holes in the O p band so that DE does not apply. His idea relies on the fact that a charge disturbance in a metallic ferromagnet produces a magnetic response extending over a magnetic correlation length ξ. In a state of complete spin alignment at $T = 0$, ξ is essentially the lattice spacing but ξ diverges at T_C. Nagaev therefore proposes that A-site disorder leads to extensive static variation in the exchange potential which could localize carriers, particularly for

$T \approx T_C$. An applied magnetic field reduces ξ and will lower the resistance as required for the CMR effect. Unfortunately, no quantitative work seems to have been done on the model which makes it difficult to asses.

Diagonal disorder in the DE model with classical or Ising local spins has also been treated using CPA [96] or DMFT [97, 98]. Within these local approximations localization does not occur and the only possibility of a MI transition is for a gap to open in the density of states at the Fermi level. A random site potential is considered, within a one-band model, which takes the value $\Delta/2$ on a fraction x of the sites, and $-\Delta/2$ on the others. The idea is that for a suitable Δ a gap will open as the band narrows in the paramagnetic state. These models are faced with several problems. A more Gaussian-like distribution of site energies, as appropriate on Mn sites due to A-site disorder, would not produce a gap and, even with the binary distribution, one requires $\Delta \approx W$, the half band-width, which is unrealistically large. Another difficulty is the position of the gap relative to the Fermi level. The band which should be split by disorder is the lowest one in the density of states shown in figure 11. In the case of classical or Ising local spins the total weight in this band is one state per site (including both spins) and, when split by disorder, the weight below the gap is $1-x$. The gap is therefore positioned at the Fermi level as required for $n = 1-x$. However for quantum spins S it is clear from section 4.2 that the corresponding weight is $(1-x)(2S+2-n)/(2S+1)$; thus the electron density n would have to be assigned arbitrarily a strange dependence on x, $n = 5(1-x)/(5-x)$ for $S = 3/2$, to place the Fermi level in the gap.

The conclusion of this section is that disorder alone cannot account for the MI transition in manganites with $x \approx 0.3$. The effect of A-site disorder is sufficiently weak for a virtual crystal approximation to be a reasonable starting-point for considering the effects of electron-phonon coupling. Of course if this coupling is so strong that narrow polaron bands appear then disorder will become important [94]. We discuss this in section 7.

5.2 Electron-phonon coupling

For sufficiently strong coupling to local phonon modes an electron produces a strong distortion of the lattice in its immediate neighbourhood. This distortion moves with the electron and the whole structure is called a small polaron. At low temperatures the small polaron occupies a narrow band of coherent Bloch-like states which narrows even further as the temperature rises. At high temperatures, typically larger than that corresponding to half the phonon energy, the polaron moves diffusively with an activation energy (see e.g. [99]). A condition for small polarons to exist is $E_p > Wz^{-1/2}$ [100], where E_p is the polaron binding energy, W is the half-width of the bare electron band and z is the coordination number of the lattice. The idea proposed by Millis et. al. [87] is that as the band narrows on passing into the paramagnetic state, by the DE effect, this criterion just becomes satisfied. Thus in the low-temperature ferromagnetic state, where the criterion is not satisfied, the system is metallic and electron-phonon interaction merely produces a small enhancement of the quasi-particle mass; the quasi-particles in this Fermi-liquid are sometimes called large polarons. As T_C is approached small polarons are formed and their motion is governed

by an activation energy related to $E_{\rm p}$. This picture of the MI transition was developed in different ways by Millis et. al. [88] and Röder et. al. [89]. Millis et. al. used DMFT and treated the phonons classically, whereas Röder et. al. used the quantum-mechanical approach of small-polaron theory. This approach is discussed further in section 7.

The electrons may couple to different local phonon modes, which may have the Q_1, Q_2, Q_3 symmetries shown in figure 1. The breathing mode Q_1 is the simplest but the Q_2 JT mode is usually regarded as the most important and was emphasized by Millis et. al. [87]. To describe the JT coupling properly one should consider a two-band model with the correct e_g symmetry. This was done by Millis et. al. [88] and Zang et. al. [101]. Röder et. al. [89] and Zang et. al. [101] treat DE in a simple mean-field way, by means of a band-narrowing, but avoid double occupation of sites by effectively using spinless electrons. Millis et. al. [88] treat the Hund's rule coupling J but in a two-band model large J no longer produces a Mott insulator for $n = 1$, as it does in the one-band model. It is therefore necessary to introduce on-site Coulomb interaction [102, 103]. Millis et. al. [88] do not do this so that for $n = 1$, which should correspond to the undoped insulator, they have a metal. Also, for weak electron-phonon interaction, they find $T_{\rm C}$ is largest for this value of n. This contrasts strongly with figure 14 where, in the one-band DE model, $T_{\rm C} = 0$ at $n = 0$ and 1 and has a maximum in between. Held and Vollhardt [103], using DMFT, obtain very similar results to those of figure 14 for $S = \infty$ in a two-band model with strong on-site Coulomb interaction included. However the values for $T_{\rm C}$ are about twice those in figure 14. Nevertheless, if on-site Coulomb interaction is neglected for simplicity, it is sensible to use a one-band model to describe the manganites. In fact Green [42] developed the theory of such a model (the Holstein-DE model) in which electrons couple to quantum spins and quantum phonons. He used the many-body CPA method [74, 75] which was discussed in section 4. In the limit of classical spins and phonons this method is equivalent to the DMFT of Millis et. al. [88]. Green's work therefore bridges the gap between this classical phonon treatment and the polaron theories. We therefore describe it in some detail in the next section. Comparison between theory and experiment indicates that electron-phonon coupling in the manganites is just in the intermediate regime where small-polarons are on the verge of forming. At present the many-body CPA is the only theoretical method which can deal satisfactory with this cross-over regime and in section 8 we show how it can be used to tie together experimental data using many different techniques.

6 The many-body CPA for the Holstein-DE model

This section is based on Green's [42] recent study of the Holstein-DE model in which the electrons of the DE model couple to local phonons as in the Holstein treatment of small

polarons [104, 105]. The Hamiltonian is

$$H = \sum_{ij\sigma} t_{ij} c^\dagger_{i\sigma} c_{j\sigma} - J \sum_i \boldsymbol{S}_i \cdot \boldsymbol{\sigma}_i - h \sum_i (S^z_i + \sigma^z_i) \\ - g \sum_i n_i \left(b^\dagger_i + b_i \right) + \omega \sum_i b^\dagger_i b_i \,. \tag{6.1}$$

The first three terms constitute the DE Hamiltonian of equation (3.1) while the first, fourth and fifth terms form the Holstein model. Einstein phonons on site i, with energy ω and creation operator $b^\dagger_i$, couple to the electron occupation number $n_i = \sum_\sigma n_{i\sigma}$ with coupling strength g. The electron-phonon coupling is of the form $-g' \sum_i n_i x_i$, where x_i is the displacement of a shell of atoms surrounding site i, and in application to the manganites it may be regarded as an effective Jahn-Teller coupling. Previous studies of this model have either concentrated on coherent polaron bands, like Röder et. al. [89], or have treated the phonons classically [88] so that there are no polaron bands at all. The many-body CPA approach is able to encompass both aspects and to describe the crossover from quantum polarons to the classical picture as temperature and/or model parameters are varied. The relationship to previous theoretical work and to experimental studies of the manganites is discussed fully in section 8. However we mention briefly below some related work on the pure Holstein model, without coupling to local spins.

Sumi considered the Holstein model with one electron in the band, first treating the phonons classically [106] and later quantum mechanically [107]. The classical case, with frozen displacements x_i, corresponds to a multicomponent alloy for which CPA is the best local approximation. In his dynamical CPA treatment of quantum phonons, Sumi [107] treated the one-site dynamics correctly and his work is completely equivalent to the more recent DMFT treatment of Ciuchi et. al. [108]. As a general rule dynamical CPA and DMFT are the same for one-electron problems. DMFT is the correct extension of CPA to the many-body problem of finite electron density but for the Holstein model, as for the DE model, it cannot be carried through analytically in the quantum case. Numerical work [109] applying DMFT to the Holstein model has been aimed mostly at understanding superconducting transition temperatures and charge-density-wave instabilities rather than the polaron physics with which we are mainly concerned. An unfortunate feature of the Holstein model for spin 1/2 electrons is that in a quantum treatment the true ground state for strong electron-phonon coupling consists of unphysical singlet bipolarons with two electrons bound on the same site. This problem does not occur in the one-band Holstein-DE model since strong coupling J to local spins prevents double occupation of sites, as pointed out earlier. It is also bypassed if the phonons are treated classically, as in the work of Millis et. al. [110] on the Holstein model. The Holstein model is more complicated than the DE model and it turns out that Green's many-body CPA no longer reduces to the correct one-electron dynamical CPA/DMFT [107, 108] as band-filling $n \to 0$. Although correct in the atomic limit $t_{ij} = 0$, the theory is clearly cruder for the Holstein and Holstein-DE model than for the pure DE model.

We start by deriving the Green function for the Holstein-DE model in the atomic limit. The Hamiltonian $H_{\rm AL}$ in this limit is given by equation (6.1) with the first term omitted

and with site indices and summation suppressed. We remove the electron-phonon coupling by the standard canonical transformation [99] $\tilde{H} = \mathrm{e}^{s} H_{\mathrm{AL}} \mathrm{e}^{-s}$ where $s = -(g/\omega) n (b^{\dagger} - b)$. Under this transformation $b \rightarrow b + (g/\omega) n$ and the Hamiltonian separates into a fermionic and bosonic component:

$$\tilde{H} = H_{\mathrm{f}} + H_{\mathrm{b}} \tag{6.2}$$

$$H_{\mathrm{f}} = -J \boldsymbol{S} \cdot \boldsymbol{\sigma} - h \left(S^{z} + \sigma^{z} \right) - \left(g^{2}/\omega \right) n^{2} \, , \; H_{\mathrm{b}} = \omega b^{\dagger} b \, . \tag{6.3}$$

The transformation corresponds to a displacement of the equilibrium position of the phonon harmonic oscillator in the presence of an electron and the downward energy shift g^{2}/ω is a polaron binding energy which we write as $\lambda\omega$, where $\lambda = g^{2}/\omega^{2}$. If two electrons occupy the site ($n = 2$), which will not occur for large J, the energy shift becomes $4g^{2}/\omega^{2}$ corresponding to an on-site bipolaron. Writing out explicitly the thermal average in the definition of the one-particle retarded Green function we have

$$\begin{aligned} G_{\sigma}^{\mathrm{AL}}(t) &= -\mathrm{i}\theta(t) \left\langle \left[c_{\sigma}(t), c_{\sigma}^{\dagger} \right]_{+} \right\rangle \\ &= -\mathrm{i}\theta(t) \frac{\mathrm{Tr} \left\{ \mathrm{e}^{-\beta H_{\mathrm{AL}}} \left[c_{\sigma}(t), c_{\sigma}^{\dagger} \right]_{+} \right\}}{\mathrm{Tr} \left\{ \mathrm{e}^{-\beta H_{\mathrm{AL}}} \right\}} \end{aligned} \tag{6.4}$$

and the canonical transformation introduced above can be carried out within the traces, using the property of cyclic invariance. Thus $H_{\mathrm{AL}} \rightarrow \tilde{H}$, $c_{\sigma}^{\dagger} \rightarrow X^{\dagger} c_{\sigma}^{\dagger}$ and $c_{\sigma}(t)$ becomes

$$\mathrm{e}^{\mathrm{i}\tilde{H}t} X c_{\sigma} \mathrm{e}^{-\mathrm{i}\tilde{H}t} \tag{6.5}$$

where $X = \exp\left[g(b^{\dagger} - b)/\omega \right]$. Using equation (6.2), we can write the traces in equation (6.4) as products of fermionic and bosonic traces. Hence we find

$$G_{\sigma}^{\mathrm{AL}}(t) = -\mathrm{i}\theta(t) \left\{ \left\langle c_{\sigma}(t) c_{\sigma}^{\dagger} \right\rangle_{\mathrm{f}} F(t) + \left\langle c_{\sigma}^{\dagger} c_{\sigma}(t) \right\rangle_{\mathrm{f}} F^{*}(t) \right\} \tag{6.6}$$

where $F(t) = \langle X(t) X^{\dagger} \rangle_{\mathrm{b}}$ and the thermal averages $\langle \; \rangle_{\mathrm{f}}$, $\langle \; \rangle_{\mathrm{b}}$ correspond to the systems with Hamiltonians H_{f} and H_{b} respectively. It may be shown [99] that

$$F(t) = \mathrm{e}^{-\lambda(2b+1)} \exp\left\{ 2\lambda \left[b(b+1) \right]^{1/2} \cos\left[\omega(t + i\beta/2) \right] \right\} \tag{6.7}$$

where $b = b(\omega) = \left(\mathrm{e}^{\beta\omega} - 1 \right)^{-1}$ is the Bose function with $\beta = (k_{\mathrm{B}} T)^{-1}$. The last factor is of the form $\exp(z \cos\phi)$ which generates the modified Bessel functions $\mathrm{I}_{r}(z)$:

$$\exp(z \cos\phi) = \sum_{r=-\infty}^{\infty} \mathrm{I}_{r}(z) \mathrm{e}^{\mathrm{i}r\phi} \, . \tag{6.8}$$

To evaluate the fermionic averages we consider for simplicity the limit $J \rightarrow \infty$ in zero field

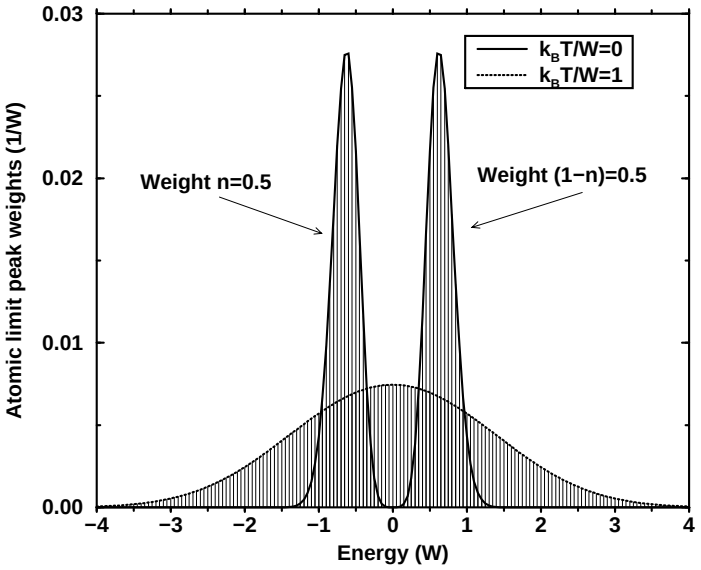

Figure 15: One-electron spectra of the Holstein-DE model in the atomic limit at zero and very high temperature. They consist of delta-functions, with energy spacing ω, whose strength is indicated by the envelope curves. The plots are for the paramagnetic state with $S = J = \infty$, $h = 0$, $n = 0.5$, $\omega/W = 0.05$ and $g/W = 0.18$, where W is a unit of energy later to be identified with the half-width of the electron band in the full Hamiltonian [42].

($h = 0$). Then the last term in $H_{\rm f}$ may be written $-(g^2/\omega)n$, since $n = 0$ or 1 only, and this may be absorbed into the chemical potential which is finally determined to give the correct number of electrons n per atom. Thus $H_{\rm f}$ is just the DE Hamiltonian in the atomic limit and the sum of the two fermionic averages corresponds to the function $G^{\rm AL}(t)$ whose Fourier transform is given by equation (4.14). It is easy to see that the first and second thermal averages in equation (6.6) take constant values $(1-n)(S+1)/(2S+1)$ and $n/2$ respectively. Hence, from equations (6.6)-(6.8), we obtain the Fourier transform of $G^{\rm AL}$, with $J \to \infty$ and $h = 0$, in the form

$$G^{\rm AL}(\epsilon) = \sum_{r=-\infty}^{\infty} \frac{{\rm I}_r\{2\lambda\,[b(\omega)(b(\omega)+1)]^{1/2}\}}{(2S+1)\exp\{\lambda\,[2b(\omega)+1]\}} \frac{(2S+1)\frac{n}{2}{\rm e}^{r\beta\omega/2} + (S+1)(1-n){\rm e}^{-r\beta\omega/2}}{\epsilon + r\omega}\,. \tag{6.9}$$

The density of states $-\pi^{-1}{\rm Im}\ G^{\rm AL}(\epsilon)$ is shown in figure 15 for the classical spin limit $S \to \infty$ at quarter-filling $n = 0.5$. It consists of delta-function peaks separated in energy by ω and the envelope curves show the weight distribution at low and high temperature. W is an energy unit which, when we go beyond the atomic limit, will be the half-width of the itinerant electron band, as usual. The values adopted for the parameters ω/W and g/W relate to the manganites, as discussed in section 8. The symmetry of the spectrum about zero energy is due to the choice of filling $n = 0.5$; in general at $T = 0$ the lower and upper 'bands' have weights n and $1-n$ respectively. By counting weights it may be seen that for any n the chemical potential lies in the peak at $\epsilon = 0$, which has very small weight ${\rm e}^{-\lambda}/2$ per spin. The shape of the envelope function at $T = 0$, with two maxima and very small values at the centre of the pseudogap between them, may be understood physically as follows. The delta-function at $\epsilon = r\omega$ ($r \geq 0$) corresponds to an excitation from the ground state, with no electron and the undisplaced oscillator in its ground state, to a state with one electron and the displaced oscillator in its $r^{\rm th}$ excited state. The strength of the delta-function depends on the square of the overlap integral between the displaced and undisplaced oscillator wave functions. Clearly this is very small for $r = 0$ and goes through a maximum with increasing r as the normalized displaced wave function spreads out. At $T = 0$ it is easily seen from equation (6.9), using ${\rm I}_r(z) \sim (z/2)^{|r|}/|r|!$ for small z, that the weight of the delta-functions at $\epsilon = \pm r\omega$ is proportional to $\lambda^r/r!$. Hence the maxima in the envelope curve occur at $\epsilon \approx \pm\lambda\omega$, which is the polaron binding energy.

We now turn to the Holstein-DE model with finite band-width. As for the DE model it is necessary to use the full equation of motion method to derive the many-body CPA in the presence of a magnetic field and/or magnetic order [42]. In the present case it is very difficult to determine self-consistently all the expectation values which appear. Green therefore approximated them by their values in the atomic limit. It then turns out that in the zero field paramagnetic state, for $J = \infty$ and with the elliptic band, the CPA Green function G again satisfies equation (4.12), with $G^{\rm AL}$ now given by equation (6.9).

The densities of states calculated for $T = 0$ using equations (6.9) and (4.12) with $S = \infty$, $n = 0.5$, $\omega/W = 0.05$ and various values of g/W are shown in figure 16. Apart from lacking the perfect symmetry about the chemical potential $\mu = 0$ the results are

qualitatively similar for other values of n not too close to 0 or 1. For $g = 0$ we recover the elliptic band with half-width $W/\sqrt{2}$ as for the DE model with $J = \infty$, $S = \infty$. As g increases the density of states broadens and small subbands are split off from the band edges. As g increases further a pseudogap develops near the chemical potential. At a critical value $g = g_c$ a gap appears which contains a small polaron band around the chemical potential. Increasing g further causes more bands to be formed in the gap, with weights similar to those of the relevant atomic limit. It should be pointed out that the paramagnetic state considered here at $T = 0$ is not the actual ground state, which is ferromagnetic. We discuss the magnetic state later. The effect of increasing temperature on the density of states in the gap region is shown in figure 17 for $g = 0.18W > g_c$. With increasing T the polaron bands grow rapidly and eventually merge to fill the gap.

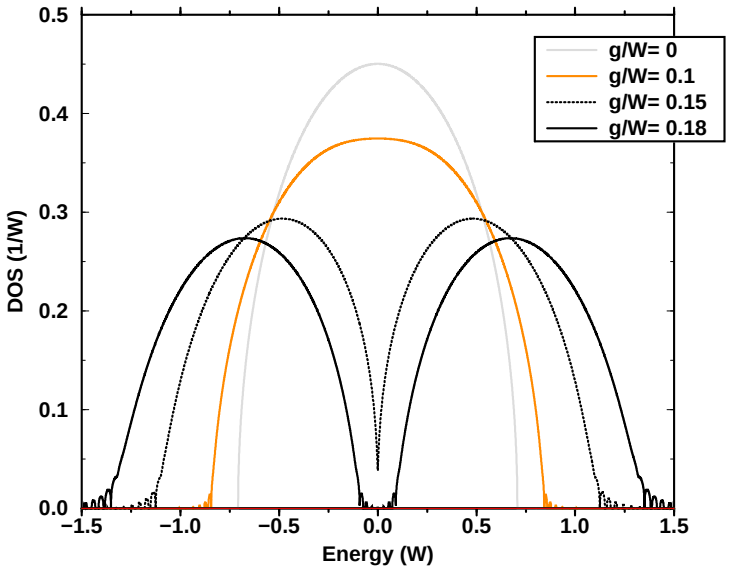

Figure 16: The one-electron density of states (DOS) for the Holstein-DE model with half-bandwidth W, for the hypothetical paramagnetic state at $T = 0$, with various strengths of electron-phonon coupling g/W. Other parameters as in figure 15 [42].

It is important to compare these results with the standard small polaron theory developed by Holstein [104, 105]. Holstein distinguished between 'diagonal transitions', in which the number of phonons is unchanged as the electron moves from site to site, and 'nondiagonal transitions' in which phonon occupation numbers change. The former give rise to a coherent Bloch-like polaron band of half-width $We^{-\lambda(2b+1)}$ which decreases with increasing temperature. The nondiagonal transitions are inelastic processes which destroy phase coherence and the polaron moves by diffusive hopping. The hopping probability increases with temperature so that polaron motion crosses over from coherent Bloch-like at $T = 0$ to diffusive hopping as $k_B T$ approaches the phonon energy ω. The paramagnetic

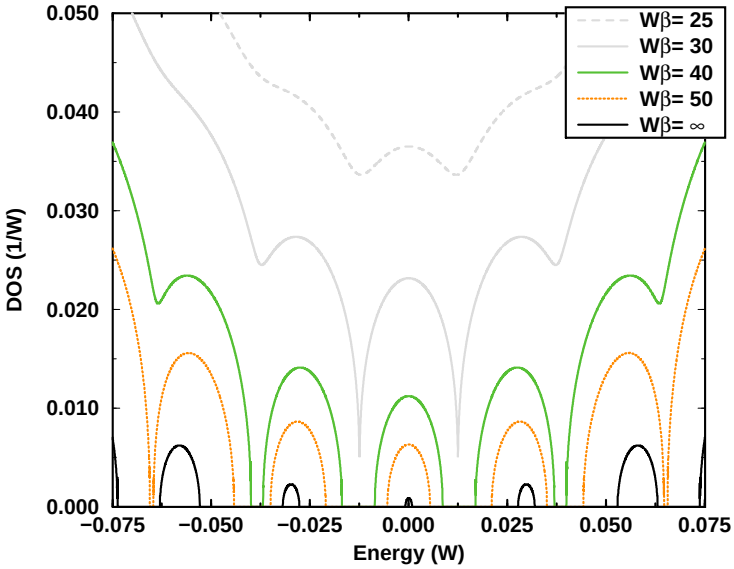

Figure 17: Evolution with temperature $\beta = (k_{\rm B}T)^{-1}$ of the polaron subbands in the pseudogap around the chemical potential $\mu = 0$ for $g/W = 0.18$. These subbands at $T = 0$ can just be seen in figure 16 [42]. All parameters as in figure 15.

state of the Holstein-DE model differs from this standard picture in one important respect. There are no well-defined Bloch states, owing to strong scattering by the disordered local spins, so no coherent polaron band will form. This is fortunate because the CPA treatment of electron-phonon scattering will never lead to coherent states of infinite lifetime at the Fermi surface at $T = 0$. However in the presence of strong spin disorder it should be satisfactory. We interpret the central band around the chemical potential in figure 17 as an incoherent polaron band whose increasing width as the temperature rises is due to life-time broadening of the atomic level. The life-time decreases as the hopping probability increases with rising temperature.

To substantiate this picture we study the central polaron band in the limit of very strong electron-phonon coupling. In this limit it can be shown that we need retain only the $r = 0$ term in equation (6.9) and it is then easy to solve equation (4.12) for G. The result is of the same form as equation (4.15) but with

$$D^2 = \frac{1}{2}W^2 \mathrm{e}^{-\lambda(2b+1)} \mathrm{I}_0 \left(2\lambda \left[b(b+1)\right]^{1/2}\right) \tag{6.10}$$

and $\alpha^2 = D^2/W^2$ in the case $S = \infty$. The central band is thus elliptical with half-width D and weight D^2/W^2. It is now easy to calculate the conductivity σ from equation (4.18)

and, using $D^2 \ll W^2$, we find

$$\sigma = \frac{\pi e^2}{6\hbar a}\frac{D^2}{W^2} \approx \frac{\pi e^2}{12\hbar a}\left(\frac{\beta\omega}{4\pi\lambda}\right)^{1/2} e^{-\beta\lambda\omega/4}\,. \tag{6.11}$$

The last step follows by using the asymptotic forms for strong coupling and high temperature $I_0(z) \sim (2\pi z)^{-1/2}\exp z$ and $b \sim (\beta\omega)^{-1}$. This form of σ is similar to that for small polaron hopping conduction in the adiabatic limit ($W \gg \omega$) [111] but with activation energy $\lambda\omega/4$ equal to one quarter, instead of one half, of the polaron binding energy. Nevertheless this establishes the link between the many-body CPA and standard small polaron theory in the strong coupling limit. However the results shown in figure 17, with parameters relevant to typical manganites, are far from this limit. They correspond to intermediate coupling and in the actual paramagnetic state above the Curie temperature the polaron bands are largely washed out. In this regime, with increasing temperature, there is a crossover from polaronic behaviour to a situation where the phonons behave classically, the case considered by Millis et. al. [88]. For electron-phonon coupling greater than a critical value these authors find a gap in the density of states which gradually fills with increasing temperature. However in their classical treatment there are no polaron bands in the gap so that the link with standard polaron physics is not established.

Apart from the symmetry about $\epsilon = 0$ the above results for $n = 0.5$ are not untypical of the general case. For general n the main lower and upper bands, separated by a gap for $g > g_c$, have approximate weights n and $1 - n$ respectively. The chemical potential at $T = 0$ is always confined to the polaron band arising from the $r = 0$ term of equation (6.9), and moves from the bottom at $n = 0$ to the top at $n = 1$, so that we correctly have an insulator in these limits.

To calculate the Curie temperature T_C we need the full CPA theory combined with an exact result of DMFT for $S = \infty$ [42]. Results on T_C for the same parameters as before are plotted as functions of electron-phonon coupling g in figure 18. The suppression of T_C with increasing g was first noted by Röder et. al. [89] and the CPA results are quite similar to those of Millis et. al. [88]. In CPA there is no reliable means of calculating the probability distribution function $P(S^z)$, so to go below T_C Green [42] used the mean-field approximation for the ferromagnetic Heisenberg model with classical spins and nearest neighbour exchange. The exchange constant is determined by T_C. We plot the up- and down-spin density of states for $T = 0.005W/k_B \ll T_C$ and $g = 0.16W > g_c$ in figure 19, also showing curves for the saturated ferromagnetic state and paramagnetic state at $T = 0$ for comparison. The value $g = 0.16W$ is closer to g_c than the value of $0.18W$ used in figures 16 and 17 and we discuss these results in relation to the manganites in section 8. In figure 20 the resistivity ρ is plotted as a function of temperature, for the same parameter set, with different applied fields h. The resistivity peaks sharply at T_C, and for comparison we show results for weaker electron-phonon coupling $g/W = 0.10$ in figure 21. The curve in figure 21 is almost indistinguishable from that of figure 7 in reference [42] for $g/W = 0.01$. This is not surprising since we see from figures 16 and 18 of this paper that the density of states and T_C change very little between $g/W = 0$ and $g/W = 0.1$. These results are all discussed further in section 8.

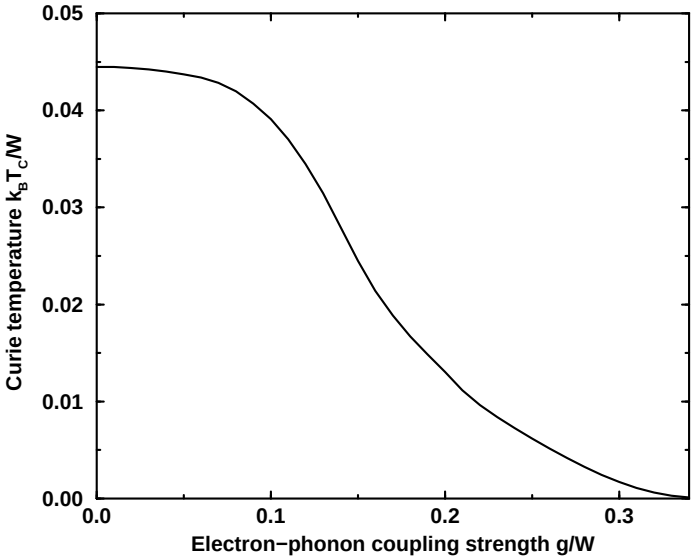

Figure 18: Suppression of the Curie temperature of the Holstein-DE model with increasing electron-phonon coupling g/W. The plot is for $S = J = \infty$, $h = 0$, $n = 0.5$ and $\omega/W = 0.05$ [42].

7 Polarons and bipolarons

Much experimental data on the manganites in both the paramagnetic and ferromagnetic state is interpreted in terms of the standard Holstein small-polaron theory [104, 105, 99]. However there are usually difficulties in finding parameters which are both plausible and capable of explaining data from more than one type of measurement. This is not surprising in view of the conclusions of the last section, namely that many manganites are only just at the threshold of small-polaron formation even in the paramagnetic state. This means that one is still far from the strong coupling limit where standard theory applies. Let us review some of the problems in applying the standard theory, starting with the low temperature state.

The width of the coherent polaron band at $T = 0$ is reduced from the bare band-width by a factor $\mathrm{e}^{-E_\mathrm{p}/\omega}$, where E_p is the polaron binding energy (g^2/ω in the notation of the last section) and ω is the phonon energy. For the typical values $E_\mathrm{p} = 0.5$ eV, $\omega = 0.05$ eV this factor is less than 10^{-4}. The polaron band is so narrow that any disorder in the system will produce Anderson localization and a metallic state is impossible. To avoid this problem, by reducing the narrowing factor to 10^{-1} say, one requires $E_\mathrm{p}/\omega \approx 2$ so that $E_\mathrm{p} \approx 0.1$ eV. But then the condition for small-polaron formation $E_\mathrm{p} > W z^{-\frac{1}{2}}$, where W is half the bare band-width and z is the number of nearest neighbours [100], is far from being met. Even a band-narrowing factor of 0.1 is too much to be compatible with heat capacity measurements

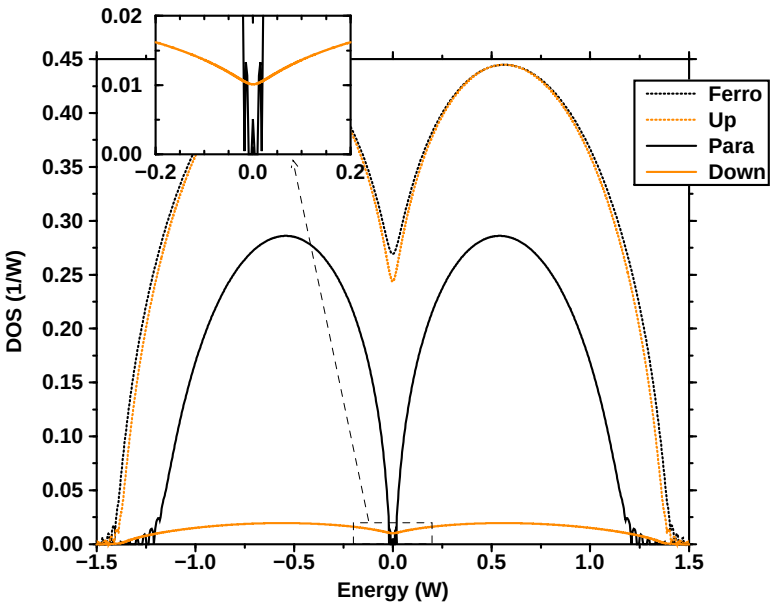

Figure 19: The up- and down-spin density of states of the Holstein-DE model with $g/W = 0.16$ for $k_{\rm B}T = 0.005W \ll k_{\rm B}T_{\rm C}$ where $\langle S^z \rangle = 0.915$. Also shown are the DOS for the saturated ferromagnetic state at $T = 0$ and for the hypothetical paramagnetic state at $T = 0$. All plots are for $S = J = \infty$, $h = 0$, $n = 0.5$, $\omega/W = 0.05$ and $g/W = 0.16$ [42].

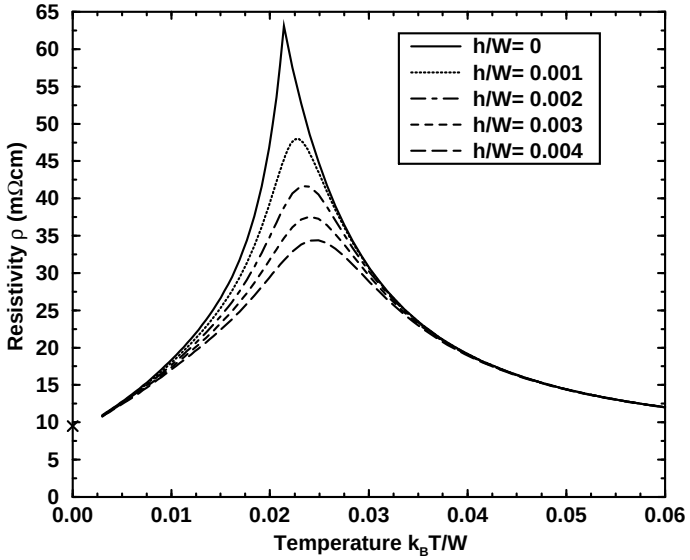

Figure 20: Resistivity ρ versus temperature for the Holstein-DE model with $S = J = \infty$, $n = 0.5$, $\omega/W = 0.05$, intermediate coupling $g/W = 0.16$ and various applied fields h. The lattice constant is taken as $a = 5$ Å, slightly larger than the Mn–Mn spacing in the manganites [42].

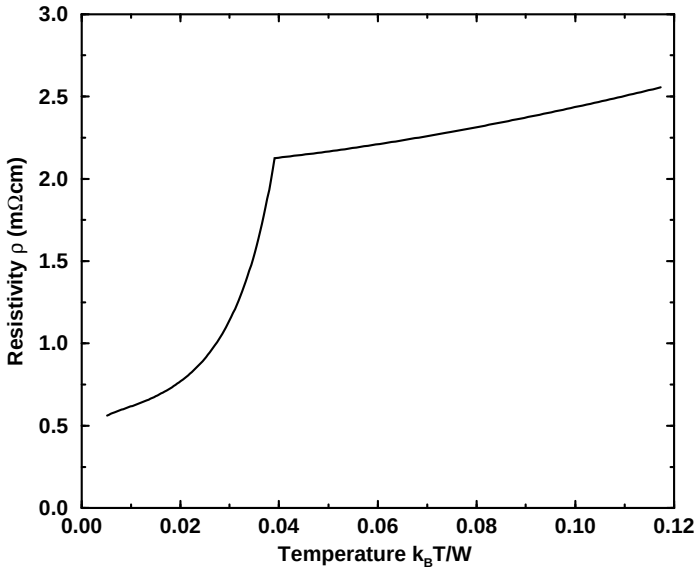

Figure 21: The same plot as figure 20 but for weak electron-phonon coupling $g/W = 0.10$.

[1]; the term linear in T at low temperatures indicates a quasi-particle density of states not much larger than that given by band calculations.

To examine the high temperature state one must consider the adiabatic limit (hopping integral > phonon energy). Worledge et. al. [112] used the result of Emin and Holstein [111] for the conductivity in this limit, $\sigma = (A/T)\exp(-E_{\rm a}/k_{\rm B}T)$, to obtain excellent fits to their data on $La_{1-x}Ca_xMnO_3$ films for $T = 300$–1200 K over the whole range of x. However for $x = 0.3$ the activation energy $E_{\rm a} \approx 0.08$ eV which is the same as in $Nd_{0.7}Sr_{0.3}MnO_3$ films [113]; according to the theory this should be about $E_{\rm p}/2$ which makes $E_{\rm p}$ too small for consistency with small-polaron formation. Also according to small-polaron theory [99] the optical conductivity peaks at phonon energy $2E_{\rm p} \approx 4E_{\rm a}$; almost universally this peak in the paramagnetic state of pseudo-cubic manganites is observed at about 1 eV [50] which is therefore inconsistent with $E_{\rm a} \approx 0.08$ eV. This problem does not occur in the many-body CPA calculations where $E_{\rm a}$ and the optical conductivity peak are both given correctly for one set of parameters [43] (see section 8.3.2).

Alexandrov and Bratkovsky (AB) [114, 115, 116] have recently proposed a new polaronic theory of the manganites, including CMR. It is based on an extended Holstein model [117] in an attempt to avoid some of the difficulties discussed above. AB assume the O p-hole model of the manganite electronic structure so that DE does not come into play. The antiferromagnetic interaction between the local Mn spins $S = 2$ and the carriers is then assumed weak enough to treat within mean field theory. It is supposed that small polarons are the carriers in the ferromagnetic state, but near $T_{\rm C}$ they mostly combine to form immobile singlet, and possibly triplet, bipolarons. This leads to the rapid rise in resistivity near $T_{\rm C}$; it falls slowly above $T_{\rm C}$ as the bipolarons dissociate thermally. It is necessary to assume that it is not favourable for polarons in the ferromagnetic state to combine as triplet bipolarons. AB propose that this is because the immobility of the bipolarons suppresses their exchange interaction with the local spins. The two holes in the bipolarons are supposed to reside on nearest neighbour oxygen sites. An applied magnetic field tends to split up the immobile bipolarons and reduce the resistivity; this is the CMR effect.

To avoid the problem of very narrow polaron bands at $T = 0$ Alexandrov and Kornilovich [117] introduced an extended Holstein model (EHM) in which the interaction between an electron on site i and a local phonon at site j is long range, corresponding to the effect of unscreened Coulomb interactions. This may also be regarded as an extension of the Fröhlich dielectric continuum model [118] to a discrete lattice. The model has also been studied by Fehske et. al. [119]. They stress that the EHM polaron is a large polaron in the whole electron-phonon coupling range. That is the lattice distortion is spread over large distances even if the coupling is strong, a regime where a small polaron is formed in the Holstein model. Alexandrov and Kornilovich describe a 'small' Fröhlich polaron, with a large size lattice distortion but an electronic wave function of small radius. It is unclear how these two length scales can be distinguished [119] unless the electron is tightly bound to a defect. The main point is that the EHM polaron band is much less narrow than the small Holstein polaron band with the same binding energy. This is because the lattice distortion undergoes smaller relative changes as the electron moves from site to site. AB [116] also find that the peak energy in optical conductivity is $2\gamma E_{\rm p}$, with $\gamma \approx 0.2$–0.4,

and $E_a = \gamma E_p/2$. The low observed activation energy discussed above can therefore be accommodated but, in a theory involving single polarons only, the inconsistency with the energy of the peak in optical conductivity above T_C would persist. However, according to AB, this peak above T_C is associated with splitting up a bipolaron, which requires a larger energy than $2\gamma E_p$. The theory is therefore consistent with the observed shift of optical conductivity towards higher energy on going from the ferromagnetic to the paramagnetic state. This is discussed again in section 8.3.2.

AB's theory presents certain problems. First, the model based on O p-hole conduction is open to considerable doubt, as discussed in section 2. Secondly, it is unclear why, in a $x = 0.3$ metallic manganite with residual resistivity less than 0.1 mΩcm , the long-range Fröhlich interaction is not screened. Chakraverty et. al. [120, 121] argue that it will be reduced to a local Holstein interaction. Also the small enhancement of the quasi-particle density of states at the Fermi level, as deduced from the specific heat, is hardly compatible with a polaronic band at $T = 0$. Zhao et. al. [122] argue for small-polaron metallic conduction in the ferromagnetic state of LCMO on the basis of fitting their measured resistivity $\rho(T)$ below 100 K to the theoretical predictions. From other data they infer mass enhancements of 9 and 35 in $La_{0.7}Ca_{0.3}MnO_3$ and $Nd_{0.7}Sr_{0.3}MnO_3$ which, although small for small polarons, seem too large to be compatible with specific heat measurements. Another consideration is that AB's 'small' Fröhlich polaron is really a large polaron. If a bipolaron can form it will be an extended object in which the two carriers are only confined within the large region of lattice distortion. Nagaev argues strongly against AB's theory and we refer again to the public correspondence [123, 116] between him and AB in section 8.1.

Röder et. al. [89] adopted a different method of avoiding the extreme polaronic band-narrowing effect. They used a variational Lang-Firsov transformation which contains parameters γ and Δ whose role is to quench part of the dynamical polaron effect as a static distortion. Thus the operator s, introduced just before equation (6.2), becomes $-(g/\omega)(\gamma n + \Delta)(b^\dagger - b)$ and the transformation is applied to every site in the lattice. The band-narrowing factor is then modified from $e^{-E_p/\omega}$ to $e^{-\gamma^2 E_p/\omega}$ and $0 < \gamma < 1$. The main result is that the T_C of the pure DE model is reduced by this factor due to electron-phonon coupling; the resistivity was not calculated. The most recent work along similar lines is that of Perroni et. al. [124, 125]. The DE effect is treated by a simple band-narrowing but these authors go much further than Röder et. al. In particular they calculate a one-electron Green function which is quite similar to Green's [42] and, like his, yields the correct atomic limit (equation (6.9)) for the classical spin case considered. However instead of a smooth evolution of a pseudogap with increasing temperature, they find phase separation above $0.65T_C$ with ferromagnetic regions of low electron density (large polaron behaviour) and paramagnetic insulating regions of high electron density (localized small polarons). However the effect of the nanoscale structure of such regions, enforced by Coulomb interaction, is not considered.

8 Theory and experiment

The experimental evidence and theoretical arguments reviewed in previous sections point to the Holstein-DE model as a plausible model of the manganites $A_{1-x}A'_xMnO_3$, at least for $x \approx 0.33$. For this degree of doping with the divalent element A′ one is normally in the middle of the ferromagnetic regime and inhomogeneity due to charge and orbital ordering is least likely. In order to confront theory with experiment effectively it is essential to keep the number of adjustable parameters to a minimum. Ideally one would like to understand the difference between materials, as reflected in the results of many different types of experiments, by changes in one crucial parameter. The many-body CPA approach to the Holstein-DE model gives us the opportunity to attempt this and from section 6 it is clear that the crucial parameter is the electron-phonon coupling g/W. In this section we take fixed reasonable values of the parameters ω and W. Band calculations [17, 18] suggest $W = 1$ eV as an appropriate half-bandwidth for the e_g band. Then it is reasonable to take $\omega/W = 0.05$ to correspond to the observed transverse optic phonons with $\omega \approx 40$–70 meV which couple strongly to the electrons in LCMO [126]. It is also reasonable to take the DE limit $J \to \infty$ [127]. Furthermore we see from figures 14(a) and 12 that for the DE model neither T_C nor the resistivity ρ vary enormously with S so that $S = \infty$ is a convenient approximation to the $S = 3/2$ Mn spins. These are the parameters which have been used in figures 16– 21. The band-filling is also restricted to $n = 1 - x = 0.5$ rather than $n = 0.6$–0.7. This is very convenient because the chemical potential remains fixed for all T by electron-hole symmetry in the case $S = \infty$. This will change the critical value of g/W for small polaron formation somewhat but the correct general picture should emerge. Since we consider a homogeneous state we are not concerned with the existence of charge ordering for $x = 0.5$. We now compare the theory with different types of experiment.

8.1 Transport properties and Curie temperature

Perhaps the most striking feature of the manganites is the very different behaviour observed in apparently similar materials such as LSMO and LCMO. For LSMO, with $x \approx 0.33$, $T_C \approx 370$ K whereas for LCMO, with a similar x, $T_C \approx 240$ K. The difference in behaviour of the resistivity ρ above T_C is much more striking (see figures 4 and 5). For LSMO $\rho \approx 4\,\mathrm{m\Omega\,cm}$ and increases slowly with temperature as in a poor metal [15]. The $\rho(T)$ curve is very similar to that of figure 21 for $g/W = 0.1$ except for a much larger resistivity at low temperature in the calculations. Since this feature persists even for $g/W = 0.01$ (figure 7 in reference [42]) it presumably arises from overestimated spin disorder scattering at low temperatures due to use of the classical spin Heisenberg model to determine $P(S^z)$. In LCMO the resistivity rises to a maximum at T_C of about 40 mΩcm and then falls with increasing temperature above T_C. In contrast to LSMO there is thus a transition from metallic to insulating behaviour. Also the resistivity peak is strongly reduced and shifted to higher temperature with increasing applied magnetic field (figure 5). This is the CMR effect. This type of behaviour is seen in figure 20 for $g/W = 0.16$. The decrease of ρ with increasing temperature above T_C is associated with the increasing density of states at the

Fermi level, as seen in figure 17. The main differences between theory and experiment are a more rapid observed drop in ρ with decreasing temperature below $T_{\rm C}$ and a more sensitive observed CMR effect. $h/W = 0.004$ corresponds to a field of about 20 T for $W = 1$ eV and the corresponding reduction in ρ in figure 20 is achieved with a field of about 5 T experimentally. Millis et. al. [88] noted a similar problem in their work using classical phonons. Both of the discrepancies mentioned might be remedied by introducing a dependence of g on ρ, corresponding to more efficient screening of the electron-phonon interaction with increasing density of states. The huge reduction in resistivity peak on reducing g/W from 0.16 to 0.10 shows the extreme sensitivity of ρ to changes in g. The main point to notice is that we can understand the enormous difference between LCMO and LSMO within the Holstein-DE model by assuming the electron-phonon coupling changes from $g/W = 0.16$ in LCMO to $g/W = 0.10$, or slightly greater, in LSMO. The observed ratio of the Curie temperatures, slightly less than 2, is then in accord with figure 18. As discussed in section 6 the critical coupling $g_{\rm c}$ for the formation of a polaron band is $g_{\rm c}/W \approx 0.15$, with phonon energy $\omega/W = 0.05$, and to obtain the right order of magnitude for ρ above $T_{\rm C}$ in LCMO, g/W is pinned down closely to 0.16. A larger value for g leads to too high a resistivity and too low a Curie temperature. It is interesting that neither $\rho(T)$ nor $T_{\rm C}$ change when g/W is varied between 0.1 and 0. This means that the resistivity of LSMO can be described quite well by the pure DE model, as stressed by Furukawa [61], but electron-phonon coupling is not negligible and shows up in the optical conductivity, for example, which we discuss in section 8.3.2. However, from the results of Millis et. al. [88] for classical phonons, one can understand why a coupling small enough to give a LSMO-like $\rho(T)$ curve does not lead to a change in slope of the rms oxygen displacements, as a function of temperature, at $T_{\rm C}$. No such change is found in LSMO [6], in contrast to the case of LCMO [128]. It is more difficult to understand the observation [129] of static local Jahn-Teller distortions in LSMO at room temperature, apparently associated with localized carriers in the presence of metallic conduction.

From figure 16 we see that for $g/W = 0.1$, appropriate to LSMO, there is no sign of a pseudogap in the density of states. An actual gap in the hypothetical paramagnetic state at $T = 0$ appears at $g = g_{\rm c}$ with $g_{\rm c}/W$ between 0.15 and 0.16. From figure 19 we see that for $g/W = 0.16$, appropriate to LCMO, a few polaron subbands have appeared in the gap. These are seen much more clearly in figure 17 for $g/W = 0.18$ when there is a larger gap. However the subband structure is washed out completely for $\beta W = 25$, corresponding to $T = 464$ K for $W = 1$ eV, and this effect will occur at a much lower temperature for $g/W = 0.16$. Thus in the actual paramagnetic state of LCMO above $T_{\rm C}$ we do not expect the quantum nature of phonons to manifest itself, so we are essentially in the classical regime of Millis et. al. [88]. The same is true in the saturated ferromagnetic state at $T = 0$ where only a pseudogap appears in figure 19. As the temperature rises towards $T_{\rm C}$ a minority spin band grows, also with a pseudogap, while the majority spin band loses weight. The width of the ferromagnetic bands decreases with increasing temperature, corresponding to the DE effect, but the narrowing in the paramagnetic state is not so marked as in the pure DE model. Thus double exchange is not so effective in the presence of strong electron-phonon coupling, which is consistent with the reduction in $T_{\rm C}$ shown in

figure 18. We discuss this again in section 8.4 in connection with spin-waves.

Clearly the picture of the manganites which emerges here is close in spirit to that of Millis et. al. [88], although the relationship to polaron physics is not so clear in their classical approximation. We have described earlier how some other authors adopt completely different viewpoints. In particular Nagaev [130] argues against any polaronic effects, while Alexandrov and Bratkovsky [115, 116] assume strong electron-phonon coupling with small polarons even in the ferromagnetic state and with immobile bipolarons forming near $T_{\rm C}$. The public correspondence [123, 116] between Nagaev and Alexandrov and Bratkovsky (AB) centres on estimating the magnitude of the polaron binding energy $E_{\rm p}$ and the criterion for small polaron formation [114]. Since the picture of LCMO presented here lies between their extreme views it is interesting to compare our estimates with theirs. For LCMO we find $E_{\rm p} = g^2/\omega \approx 0.5$ eV for $W = 1$ eV whereas, for manganites in general, Nagaev estimates $E_{\rm p} \approx 0.1$–0.3 eV and AB estimate $E_{\rm p} \approx 1$ eV. Our condition for small-polaron formation in a paramagnetic state at $T = 0$ is $g > g_{\rm c} \approx 0.15W$ which corresponds to $E_{\rm p} > 0.45W$. Nagaev adopts the criterion $E_{\rm p} > W$, remembering that W is the half-bandwidth in our notation, while AB [114] propose $E_{\rm p} > 2W(8z)^{-1/2} = 0.29W$ with number of nearest neighbours z taken as 6. AB's condition is less stringent than Eagle's [100] condition for 'nearly small polarons' $E_{\rm p} > Wz^{-1/2} = 0.41W$ which is close to ours. Both as regards this criterion and the value of $E_{\rm p}$ for LCMO, the results of the Holstein-DE model are intermediate between Nagaev's and AB's, as expected. For LSMO, on the other hand, our estimate of $E_{\rm p}$ is 0.2 eV. In this case we agree with Nagaev and Furukawa [61] that electron-phonon coupling is not so important. AB's work is reviewed in section 7.

8.2 Isotope and pressure effects

There is an excellent review of oxygen isotope effects in manganites by Zhao et. al. [131]. The most striking effects are a decrease in $T_{\rm C}$ and an increase in resistivity ρ, particularly near $T_{\rm C}$, when ^{16}O is replaced by ^{18}O. However other important effects are an induced metal-insulator transition, a shift of the charge-ordering transition and effects on the thermal-expansion coefficient and electron paramagnetic resonance (EPR) measurements. Although Zhao et. al. attempt to understand these effects using the concepts of small-polarons and bipolarons, they point out clearly the difficulties in such a theory. We believe that most of these difficulties can be resolved within the many-body CPA approach to the Holstein-DE model, which frees us from the strong coupling regime of standard small-polaron theory.

The oxygen isotope exponent is defined as $\alpha_0 = -(\Delta T_{\rm C}/T_{\rm C})/(\Delta M/M)$, where $T_{\rm C}$ and M are the Curie temperature and oxygen mass for the ^{16}O sample. α_0 ranges from 0.07 with $T_{\rm C} = 367$ K in $La_{0.67}Sr_{0.33}MnO_3$ to 0.85 in $La_{0.8}Ca_{0.2}MnO_{3+y}$ ($T_{\rm C} = 206$ K) and up to 4 in $(La_{0.25}Nd_{0.75})_{0.7}Ca_{0.3}MnO_3$ ($T_{\rm C} \approx 110$ K). Zhao et. al. [131] point out that all available data (for $x \approx 0.2$–0.35) can be fitted by an equation

$$\alpha_0 = 21.9 \exp(-0.016 T_{\rm C}) \,. \tag{8.1}$$

According to the DE model and small-polaron theory $T_C \propto \exp(-\gamma^2 E_p/\omega)$, which is the usual band-narrowing factor (see section 7) with $0 \leq \gamma^2 \leq 1$ [89]. When the mass M changes, ω varies as $M^{-1/2}$ but the polaron binding energy E_p is independent of M since it corresponds to a static response of neighbouring oxygen atoms to an e_g electron on a Mn site. Hence T_C decreases rapidly with increasing M and it is easy to show that $T_C \propto \exp(-2\alpha_0)$ [131]. Zhao et. al. [131] point out that this is incompatible with the experimental relation (8.1). They go on to make the very important observation that the effect of pressure on T_C, again over a wide range of manganites, is summarized accurately by the equation

$$d \ln T_C / dP = 4.4 \exp(-0.016 T_C) . \tag{8.2}$$

Combining equations (8.1) and (8.2) one has $\alpha_0 = 5(d \ln T_C/dP)$. Zhao et. al. deduce from this simple proportionality between the isotope exponent and the pressure-effect coefficient that the major effect of pressure is to increase the phonon frequency. We come to a completely different conclusion from the following analysis using the many-body CPA approach to the Holstein-DE model.

In discussing the pressure effect, Green [42] observed that the increase in T_C, and decrease in ρ, stems mainly from a decrease in the effective coupling constant $g^2/(\omega W) = E_p/W$. As pointed out in section 1 (see figure 3), the effect of pressure is equivalent to an increase in $\langle r_A \rangle$ and broadens the e_g band, that is W increases. Green [42] therefore modelled the strong suppression of the resistivity peak and the increase in Curie temperature in LCMO by increasing the bandwidth, and assuming other terms in the Hamiltonian are constant. Calculated results are shown in figure 22. A simple estimate, using the known compressibility and dependence of W on lattice constant, shows that the theoretical pressure for a given effect is about four times larger than that required experimentally. This is the same factor that was found in the case of the magnetic field required for a given CMR effect, so both discrepancies could possibly be removed with the same dependence of g on ρ, due to screening, postulated in section 8.1. We return to this point later. In fact near T_C the CMR effect (figure 20) and the pressure effect (figure 22) are both driven by a change of bandwidth. In the first case the magnetic field produces a substantial magnetization for $T \approx T_C$ and this increases W by the DE effect.

To investigate the isotope effect in our model, assuming only an effect via ω, some care is needed. It was pointed out that in equation (6.1) the electron-phonon coupling term corresponds to a term $-g' \sum_i n_i x_i$ where x_i is to be associated with oxygen displacement around a Mn atom. Here g' should be independent of the oxygen mass M. In the second-quantized form of equation (6.1) one finds $g = g' (2M\omega)^{-1/2}$ so that the polaron binding energy $E_p = g^2/\omega = g'^2/(2M\omega^2)$. Since for an oscillator $\omega \propto M^{-1/2}$ the polaron binding energy g^2/ω is independent of M as expected. However g varies as $M^{-1/4}$. We therefore recalculated the resistivity $\rho(T)$ with the same parameters as used in figure 20 for ^{16}O but with g and ω scaled appropriately for ^{18}O. The results are compared in figure 23. The almost complete absence of an isotope effect in both T_C and ρ confirms Green's observation that $\rho(T)$ depends almost exclusively on the parameter E_p/W. Since E_p should not depend

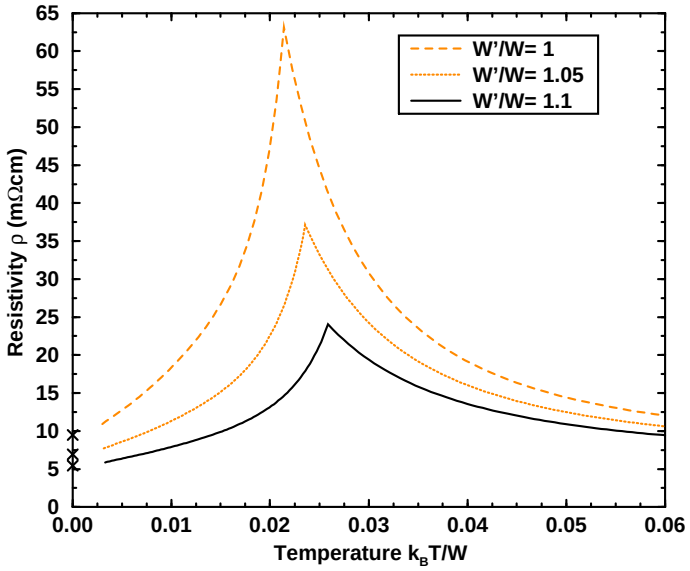

Figure 22: The effect of pressure on the resistivity and Curie temperature in LCMO by increasing the half-bandwidth W to $W' = 1.05W$ and $1.1W$ [42].

on M we have to conclude that the isotope effect is due to a decrease of bandwidth $2W$ when M is increased.

Thus we make the hypothesis that the isotope effect occurs via the e_g bandwidth $2W$ rather than the phonon energy ω, whose undoubted change has no effect. We must stress that $2W$ is the bare band-structure bandwidth. Clearly a sort of scaling theory, linking CMR, pressure effect and isotope effect, can be constructed but this will be done elsewhere. The change in the $\rho(T)$ curve is typically quite similar for $^{18}O \rightarrow ^{16}O$ back-substitution to an applied field of 5–10 T or a pressure of 5–10 kbar. Babushkina et. al. [132] have already suggested that a metal-insulator transition induced by oxygen isotope substitution in $(La_{1-y}Pr_y)_{0.7}Ca_{0.3}MnO_3$ may proceed by a change of bandwidth. They point out that the mean-square displacement of an ion from its nominal position depends on the ionic mass M, even at $T = 0$, due to zero-point vibrations. Such displacements could affect the Mn–O–Mn bond angle on which the bandwidth critically depends. Similar effects were observed earlier in $(La_{0.5}Nd_{0.5})_{0.67}Ca_{0.33}MnO_3$ [133]. Babushkina et. al. also see large shifts of the $\rho(T)$ curves with applied magnetic field, as one would expect from the above discussion. Clearly similar ideas can be applied to shifts in charge-ordering transitions due to isotopic substitution and magnetic field. The isotope effect in the jump of the thermal expansion coefficient at T_C is easily understandable since it is related by thermodynamics to the pressure effect [131].

We now have to address the question of whether replacing ^{16}O by ^{18}O can produce the required decrease of W to account for the effect on $\rho(T)$. The change in $\rho(T)$ is typically

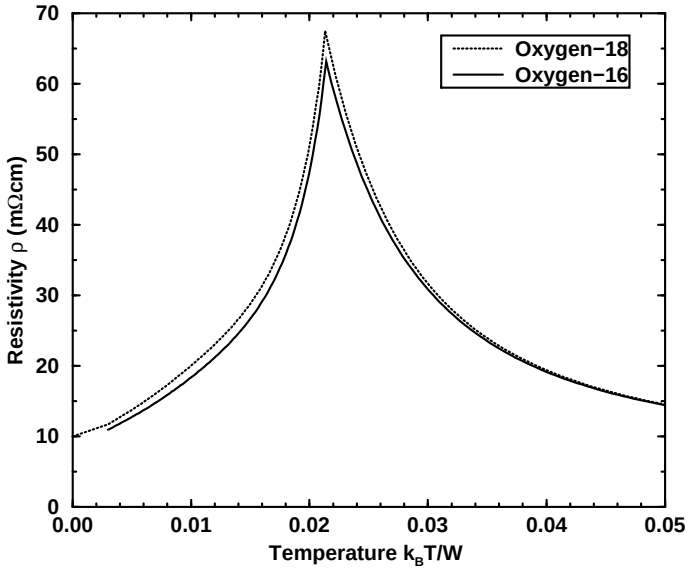

Figure 23: The absence of an isotope effect in LCMO due to a simple mass scaling $\left(\propto M^{-1/2}\right)$ of the phonon frequency.

like that calculated for a 5–10% decrease in W (cf. figure 22). If we allow for the factor of 4 proposed earlier, due to improved screening of the electron-phonon coupling as the system becomes more metallic this is reduced to 1–2%. According to Zhao et. al. [134] the volumes of the unit cells of ^{16}O and ^{18}O samples of $La_{0.67}Ca_{0.33}MnO_3$ at room temperature are the same within the accuracy of the x-ray determination. Singh and Pickett [23] have investigated the change in band structure of a $La_{2/3}Ba_{1/3}MnO_3$ virtual crystal on going from a cubic perovskite structure to a Pnma structure consistent with the neutron refinement of Dai et. al. [128] for $La_{0.65}Ca_{0.35}MnO_3$, the two structures having the same unit cell volume. Large band-narrowings occur owing to bending of the Mn–O–Mn bonds; in particular a gap of a few tenths of an eV opens between the majority spin e_g and t_{2g} bands. The distortion from the cubic structure has no static JT components, consisting essentially of rotations of O octahedra. It is not inconceivable that isotopic substitution could modify these rotations sufficiently to give a 1–2% reduction in the e_g bandwidth. Further theoretical and experimental investigation of this possibility is highly desirable. Finally we come back to the enhancement factor of 4 postulated above. It means that a 1% increase in W corresponds to a 4% decrease in E_p/W, the large relative change in E_p being assumed to arise from increased screening with increased metallization. This is not unreasonable since it is known from optical conductivity measurements, discussed in section 8.3.2, that the polaron binding energy E_p decreases from 1.2 eV in $Nd_{0.7}Sr_{0.3}MnO_3$ to about 0.6 eV in LSMO. The change in e_g bandwidth between these two materials is certainly much less than a factor 2 so that in general a much larger relative change in

$E_{\rm p}/W$ than in W is a reasonable hypothesis.

In summary our picture of the isotope effect due to ^{16}O $\rightarrow^{18}$O substitution is as follows. The change in phonon frequency plays no part. The effect is driven by a 1–2% reduction in the e_g bandwidth $2W$ associated with small changes in the rotations of O octahedra probably arising from modified vibrational amplitude of the O ions due to their mass change. This primary effect is strongly enhanced by an increased polaron binding energy $E_{\rm p}$ arising from reduced metallic screening. The scaling parameter $E_{\rm p}/W$ links CMR, pressure-effect and the various isotope effects.

We should mention that Nagaev [130, 135] has taken a completely different line on the isotope effect in which electron-phonon coupling has no role. He considered several possibilities, all based on the isotope dependence of the number of excess or deficient oxygen atoms in thermodynamic equilibrium. Since he quoted experimental evidence for this [136] his arguments were quite persuasive. However Zhao et. al. [137] have criticized the experimental work of Franck et. al. [136] and they refute Nagaev's model in which the isotope effect is not intrinsic.

8.3 Pseudogaps

According to theory we expect pseudogaps at the Fermi level to be observable in the density of states of LCMO both below and above $T_{\rm C}$. These should appear in experiments such as scanning tunnelling spectroscopy, photoemission and optical conductivity measurements. No pseudo-gap is expected in LSMO below $T_{\rm C}$ and the effect should be much less than in LCMO above $T_{\rm C}$. The pseudogap is a feature of the atomic limit, typified by the envelope function in figure 15 for $T = 0$ with maxima determined by the polaron binding energy g^2/ω, and is completely washed out when $g^2/(\omega W) < 0.2$ (see figure 16). Early results of scanning tunnelling spectroscopy on LCMO [138] with $x = 0.3$ seem unlikely to relate to the bulk. In the ferromagnetic state at 77 K there is a huge gap of about 1 eV. It is not clear why the authors interpret this as evidence for half-metallic ferromagnetism. A gap of this size associated with small-polaron formation in the bulk would imply an unrealistically large electron-phonon coupling, certainly incompatible with metallic conduction and a Curie temperature of reasonable magnitude for LCMO. More recently Biswas et. al. [139] reported a scanning tunnelling spectroscopy study of several manganites. The results are very much in accord with the theory. There is no gap in the low temperature ferromagnetic state but a small gap (pseudogap) appears for $T \approx T_{\rm C}$ in the low (high) $T_{\rm C}$ materials. As T increases above $T_{\rm C}$ the pseudogap or gap gets filled in as we would expect (see figure 17). The decrease in resistivity with increasing T is due to the gradual filling of the pseudogap.

8.3.1 Angle-resolved photoemission spectroscopy (ARPES)

In an extremely interesting paper on ARPES for the bilayer manganite $La_{1.2}Sr_{1.8}Mn_2O_7$, nominally with $n = 0.6$, Dessau et. al. [36] interpret their results very much in the spirit of the Holstein model. The low $T_{\rm C} = 126$ K in this bilayer manganite is partly due to quasi-two dimensional fluctuations, but the large resistivity $\rho \simeq 3$ mΩcm at low temperatures

indicates that small-polaron bands might exist even in the ferromagnetic state. Consequently the electron-phonon coupling should be stronger than in cubic manganites like LCMO and to model the system by the Holstein-DE model Hohenadler and Edwards [43] chose $g/W = 0.2$. The one-electron spectral function $A_{\boldsymbol{k}}(\epsilon)$ is given by equation (4.17) and the band is taken to be of the form $\epsilon_{\boldsymbol{k}} = -W \cos \pi y$ for $\boldsymbol{k} = \pi(1, y)$, $0 \leq y \leq 1$ with $W = 1$ eV as usual. This roughly models a band, calculated by Dessau et. al. [36], which crosses the Fermi level $E_{\rm F}$ at $\boldsymbol{k} = \pi(1, \frac{1}{2})$. The calculated results [43] for $A_{\boldsymbol{k}}$ are shown in figure 24. Well away from the Fermi level, a well-defined peak exists which broadens as $\boldsymbol{k}$ approaches the Fermi momentum at $y = 0.5$. For larger y the weight below the Fermi level is strongly reduced. The peaks never approach the Fermi level closely which is an important feature of the observed spectra [36] reproduced in figure 25. The theoretical curves in figure 24 resemble quite closely the data of figure 25(c). There is a pseudogap in the calculated spectra extending about 0.1 eV on each side of the Fermi level. In fact this pseudogap contains polaron bands like those shown in figure 17. However, their amplitude is too small to show up in figure 24 and in the experimental data. Nevertheless, it is the central polaron band around the Fermi level which is presumably responsible for the low but finite conductivity of the system. This comparison between theory and experiment supports the conclusion of Dessau et. al. [36] that, in the manganites with a layered structure, strong electron-phonon coupling (with the appearance of a pseudogap) is already important below $T_{\rm C}$. This contrasts with the usual pseudocubic manganites where the pseudogap only appears above $T_{\rm C}$. It should be mentioned that Moreo et. al. [140] interpret the observed pseudogap not as an intrinsic property but in terms of phase separation.

8.3.2 Optical conductivity

Using the notation of section 4.3 we can write the optical conductivity $\sigma(\nu)$, corresponding to the elliptic density of states in equation (4.8), in the form [141, 142, 43]

$$\sigma(\nu) = \frac{2\pi e^2}{3a^3\hbar} \int \mathrm{d}\epsilon \int \mathrm{d}E M_0(E) A_E(\epsilon) A_E(\epsilon + \nu) \frac{f(\epsilon) - f(\epsilon + \nu)}{\nu} \,. \tag{8.3}$$

This expression satisfies the correct one-band sum rule [142, 50] that $(2/\pi) \int_0^\infty \sigma(\nu) \mathrm{d}\nu = -Ke^2/(3a\hbar)$, where the 'kinetic energy' K is the thermal average per lattice site of the first term in the Hamiltonian (6.1). The energy K appeared previously in equation (3.11) for the spin-wave stiffness constant. For $\nu = 0$, equation (8.3) yields the dc conductivity given by equation (4.19). In the ferromagnetic state of the pure DE model ($g/W = 0$) at $T = 0$ the spectral function $A_E(\epsilon) = \delta(\epsilon - E)$ so that, from equation (8.3), $\sigma(\nu) \propto \delta(\nu)$. However, in LSMO with $x = 0.3$ the observed intraband transitions spread up to 1 eV [143] which suggests that phonons are important for producing broadened spectral functions. A sharp Drude peak below 0.04 eV, arising from δ-like parts of $A_E(\epsilon)$ for E near the Fermi level, accounts only for half of the total intraband spectral weight [143]. An alternative interpretation is that orbital degrees of freedom in the doubly-degenerate $\mathrm{e_g}$ band, combined with strong correlation (no doubly-occupied sites), lead to incoherent motion of carriers [144, 145]. Here we pursue the comparison of results of the many-body CPA treatment of

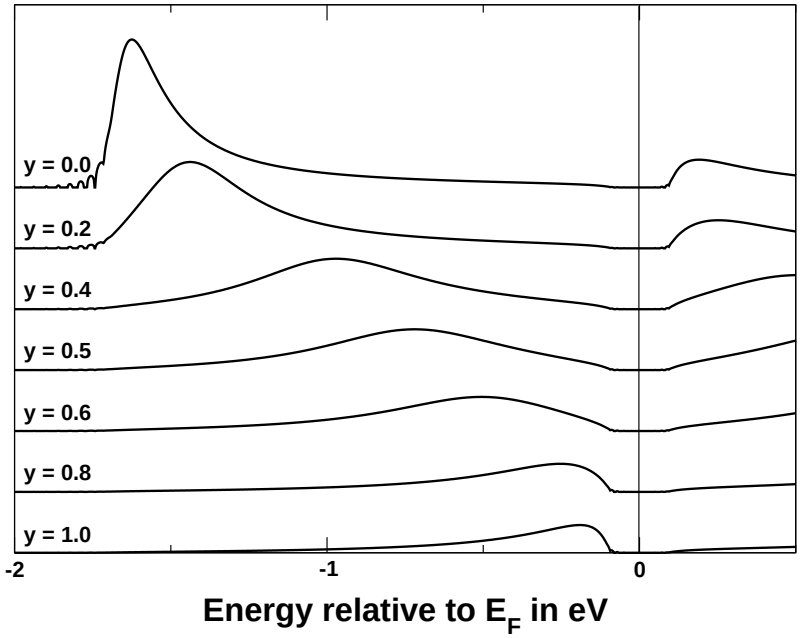

Figure 24: The spectral function $A_{\boldsymbol{k}}(\epsilon)$ in the ferromagnetic state at $T = 0$ for the Holstein-DE model with $J = S = \infty$, $n = 0.5$ and strong electron-phonon coupling $g/W = 0.20$, and $\boldsymbol{k} = \pi(1, y)$ [43].

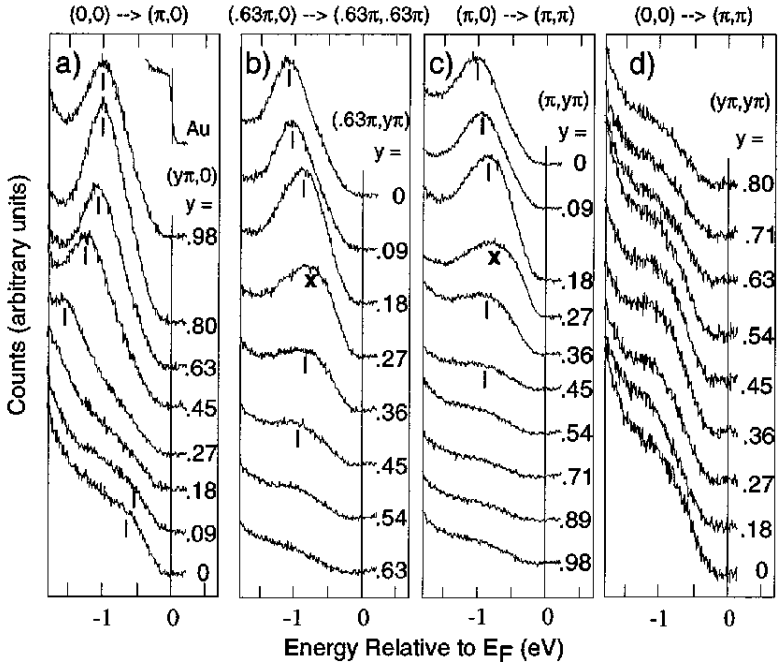

Figure 25: ARPES spectra of $La_{1.2}Sr_{1.8}Mn_2O_7$ ($T_C = 126\,K$) in the ferromagnetic state at $T = 10\,K$, reproduced from Dessau et. al. [36].

the Holstein-DE model with experiment. A defect of Green's [42] CPA treatment is that the sharp quasi-particle peak in the spectral function, which should exist in the ferromagnetic state at $T = 0$, is missing. This is due to incoherent scattering by the phonons which gives a spurious residual resistivity. Thus the Drude peak in $\sigma(\nu)$ is absent, as in the classical phonon treatment of Millis et. al. [88]. Also in the one-band model with $J = \infty$ interband transitions between Hund's rule split bands, and p→d charge transfer transitions do not feature. These are observed at photon energy $\nu > 3$ eV and $\sigma(\nu)$ calculated in the one-band model is only non-zero in the region $\nu < 2.5$ eV with in general only one peak. Hohenadler and Edwards [43] calculated $\sigma(\nu)$ in the Holstein-DE model with $g/W = 0.16$ and compared with experimental data on an unannealed film of $Nd_{0.7}Sr_{0.3}MnO_3$ (NSMO) [146]. The comparison is shown in figure 26. This data was chosen because the low temperature incoherent scattering in the sample matches closely the incoherent scattering introduced by CPA. In annealed NSMO films [50], and in single crystals [147], $\sigma(\nu)$ in the low temperature ferromagnetic state continues to rise with decreasing ν down to much lower photon energy, and $\sigma(0) \approx 3$ $(\mathrm{m\Omega cm})^{-1}$. Clearly in our calculation, and those of Millis et. al. [88], the shift of the peak to lower energy is held up due to spurious incoherent scattering in the ground state, which limits the low-temperature dc conductivity. There seems little doubt that a more correct treatment of the Holstein-DE model at low temperatures would lead to something more like the shift observed in good samples. Very recently Perroni et. al. [124] seem to have achieved this together with a Drude peak at low temperatures in their variational Lang-Firsov treatment. It is to be hoped that these features survive even if their predicted phase separation is suppressed by Coulomb interaction. In any case one does not need to invoke a change from unbinding bipolarons to unbinding polarons to explain the shift, as is done by Alexandrov and Bratkovsky [114]. It is also not clear why in the bipolaron regime these authors find a Gaussian form for $\sigma(\nu)$ without a threshold photon energy. In the bipolaron regime there should be a gap in the single-particle spectrum, analogous to that in a superconductor, but with magnitude of the order of the bipolaron binding energy. There is no such gap in the metallic 'unpaired' single polaron regime.

In the paramagnetic state above T_C, $\sigma(\nu)$ is much less sample dependent and the CPA calculations are much more reliable. Many authors [88, 50, 146, 43] agree on the following interpretation of the peak at about 1 eV. During the absorption process an electron moves from one site to a neighbouring one which was previously unoccupied. The electron motion is accompanied by a lattice distortion, of Jahn-Teller type, which corresponds to a displacement of the local phonon oscillator coordinate in the Holstein-DE model. When an electron enters (leaves) a site the final displaced (undisplaced) oscillator is generally in an excited state with typical excitation energy g^2/ω. This is the atomic-limit polaron binding energy and for the parameters assumed here is about 0.5 eV. Thus the peak in $\sigma(\nu)$ (figure 26(a)) occurs at about twice the polaron binding energy just as in the standard small-polaron theory [99]. However for the present intermediate electron-phonon coupling $g/W = 0.16$ polaron bands near the Fermi level are largely washed out above T_C [42], so standard small-polaron theory is not expected to apply to $\sigma(\nu)$ for low photon energies. This is certainly the case because small-polaron theory would predict an activation energy in the dc conductivity $\sigma(0)$ of 0.25 eV, half the polaron binding energy.

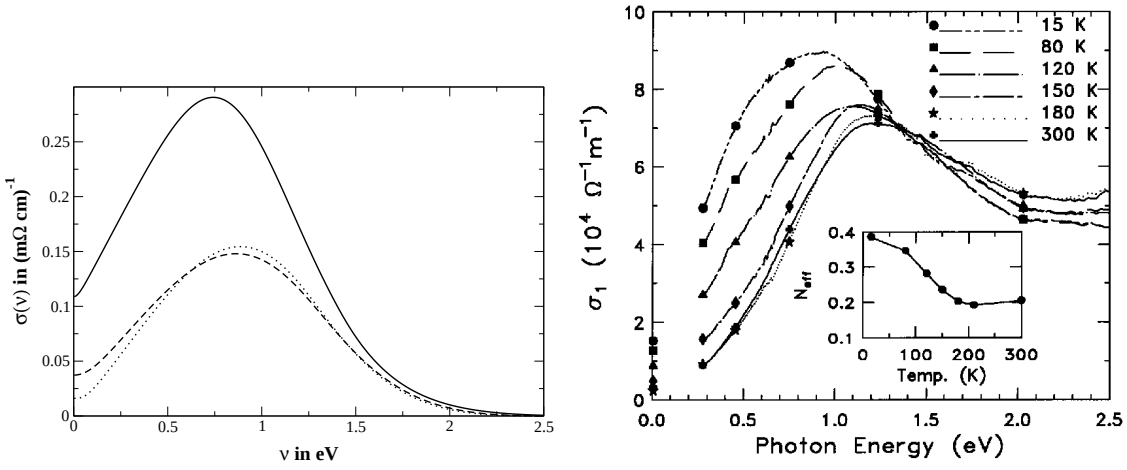

(a) (b)

Figure 26: (a) Calculated optical conductivity for strong electron-phonon coupling $g/W = 0.16$ in the ferromagnetic state at $T = 0$ (full line), the paramagnetic state at $T = T_C$ (dotted line) and the paramagnetic state at $T = 1.5T_C$ (dashed line). The plot is for $J = S = \infty$, $n = 0.5$ and $a = 5$ Å [43]. (b) optical conductivity of $Nd_{0.7}Sr_{0.3}MnO_3$ at different temperatures, reproduced from Kaplan et. al. [146].

However in NSMO the activation energy is observed to be about 0.08 eV [113] and Green's [42] calculations (see figure 20) are in good agreement with this.

We conclude that the energy of the peak in $\sigma(\nu)$ for $T > T_C$ is a reliable measure of twice the polaron binding energy, but that the activation energy for dc conductivity gives no such direct information. The most extreme illustration of this is LSMO with $x = 0.3$. There is no activation energy for $\sigma(0) = \rho^{-1}$ which slowly decreases with temperature above T_C (see figure 4). But the temperature-dependent part of $\sigma(\nu)$ has a clear peak at about 0.6 eV for $T > T_C$ [143]. This indicates a polaron binding energy of 0.3 eV, which corresponds to $g/W \approx 0.12$ for the other parameters assumed in this section. The estimate of $g/W \simeq 0.1$ we have sometimes suggested for this material is probably too low. However the difference between $g/W = 0.16$ for LCMO and NSMO and $g/W = 0.12$ for LSMO, all with $x = 0.3$, is sufficient to explain their very different behaviour.

8.4 Spin waves

In section 3.2 we pointed out that the simple result of equation (3.11) for the spin-wave stiffness constant D applies even when local electron-phonon coupling is included. In particular it applies to the Holstein-DE model and a simple variational argument shows that is is an upper bound to the true value of D [43]. The complete spin-wave dispersion curve takes the form of that for a simple nearest-neighbour Heisenberg model [84, 43], as

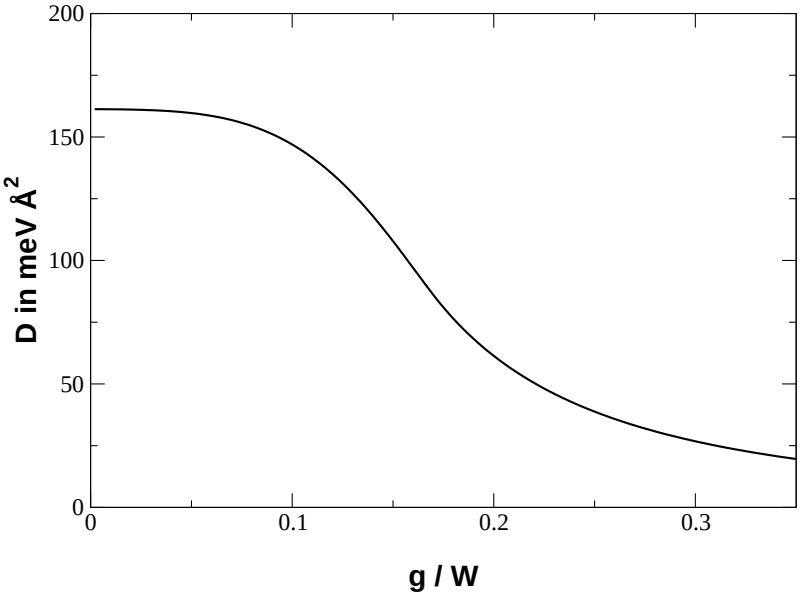

Figure 27: The spin-wave stiffness D versus electron-phonon coupling g in the saturated ferromagnetic state at $T = 0$. The plot is for $S = J = \infty$, $W = 1$ eV, $n = 0.5$ and $a = 4$ Å [43].

observed in $La_{0.7}Pb_{0.3}MnO_3$ [148]. Deviations from this simple result are found near the zone boundary in manganites with lower T_C than the Pb doped material [149, 150, 151]. Hohenadler and Edwards [43] calculated D as a function of the electron-phonon coupling g/W and the result is shown in figure 27. This behaviour of D in the Holstein-DE model is very similar to that of T_C, as calculated by Green [42] (see figure 18). The main difference is in the extreme strong-coupling limit where T_C becomes very small at $g/W \approx 0.35$ whereas D is decreasing quite slowly. The slow decrease of D is exactly what one expects from equation (3.11) and small-polaron theory, where the kinetic energy $K \sim g^{-2}$ [152, 153]. T_C seems to be determined more by the width of the narrow polaron band around the Fermi level, which decreases exponentially with g. This is the result found by Röder et. al. [89] which is essentially $T_C \propto D(g = 0)\exp(-\gamma E_p/\omega)$, in the notation of section 7. Here $D(g = 0)$ is given by equation (3.11) for the pure DE model. For manganites with higher T_C, where the spin-wave dispersion curve is Heisenberg-like, one expects that the ratio $\delta = D/(k_B T_C a^2)$, where a is the lattice constant, should be approximately 0.286 which is the value for the $S = 3/2$ Heisenberg model. In fact Hohenadler and Edwards [43] find, combining their results with those of Green for T_C (see figure 18), that $\delta \approx 0.24$ for $g/W = 0.1$ which is appropriate to a high T_C manganite like LSMO ($x \approx 0.3$). Clearly, from figures 18 and 27, δ increases as g/W becomes larger, that is as T_C becomes smaller. This agrees with experiment; for example in $Nd_{0.7}Sr_{0.3}MnO_3$ ($T_C = 197.9$ K), $\delta \approx 0.64$ [149]. In this system, and in LCMO [154], the spin-wave stiffness constant does not collapse to zero at $T = T_C$ so the behaviour is certainly not Heisenberg-like. The properties of the Holstein-DE model in this parameter regime need further investigation. The phase

separation for $T > 0.65T_C$ predicted by Perroni et. al. [124] should be examined in the presence of Coulomb interaction.

9 Conclusions

A brief review inevitably involves a personal choice of topic and emphasis, Here we have concentrated on the physics of manganites such as $La_{1-x}Ca_xMnO_3$ in the ferromagnetic regime with $x \sim$ 0.2–0.4. We have not discussed interesting phenomena such as charge and orbital ordering which occur elsewhere in the phase diagram.

The main conclusion is that the Holstein-DE model is capable of describing semi-quantitatively a wide range of experimental data on these materials. The model combines Zener's double exchange mechanism for ferromagnetism with the possibility of polaronic effects associated with strong electron-phonon coupling. These are the essential ingredients proposed by Millis et. al. [87, 88]. The double-exchange mechanism relies on the mobile carriers in doped systems being Mn e_g electrons rather than O p holes. The theoretical and experimental evidence that this is indeed the case is reviewed in section 2. In section 3 the concept of double exchange is set within the general scheme of itinerant electron magnetism. One ingredient omitted in the Holstein-DE model is A-site disorder and the discussion of section 5.1 shows that this omission is not serious for systems with $x \sim 0.3$.

The most complete theory of the Holstein-DE model, capable of dealing with quantum spins and phonons, is that of Green [42]; it is developed in a concise way in section 6. The theory makes use of the many-body CPA method introduced earlier [74, 75] for treating the pure double-exchange model, as described in section 4. For the pure DE model this method is equivalent to Furukawa's dynamical mean-field theory in his limit of classical spins. Theoretical results for the Holstein-DE model are compared with experiment in section 8. One striking conclusion is that the manganites fall in the regime of intermediate electron-phonon coupling, just on the verge of small-polaron formation. Thus in general the standard results of small-polaron theory do not apply. However even in the intermediate-coupling regime the atomic-limit polaron binding energy E_p is still a significant parameter and a peak in the optical conductivity $\sigma(\nu)$ occurs at photon energy $2E_p$, just as in standard small-polaron theory. But the activation energy for electrical conduction above T_C turns out to be much smaller than that predicted by small-polaron theory, in agreement with experiment. The key parameter in the theory is E_p/W, the ratio of the polaron binding energy to the half-width of the e_g band. This determines the Curie temperature T_C and the form of the resistivity $\rho(T)$; there is essentially no explicit dependence on the phonon frequency ω in the intermediate-coupling regime. Thus the oxygen isotope effect in T_C and $\rho(T)$ is not a consequence of the change in ω associated with a change of isotopic mass. The observed proportionality between the isotope exponent and the pressure-coefficient indicates that the shift of T_C arises from a change of E_p/W in both cases. The primary effect may be regarded as a change in W due to a change in Mn–O–Mn bond angle, and this effect is strongly enhanced by a change in E_p due to modified screening of the electron-phonon coupling arising from a changed density of states at the Fermi level. It

is proposed, following Babushkina et. al. [132], that a change in Mn–O–Mn bond angle arising from isotopic substitution is due to a modified vibrational amplitude of the O ions owing to the mass change. This proposal, and that concerning the screening of the electron-phonon coupling, requires further theoretical and experimental investigation. The large isotope effect, pressure effect, colossal magnetoresistance and the striking difference between $La_{0.7}Sr_{0.3}MnO_3$ and $La_{0.7}Ca_{0.3}MnO_3$ are all due to extreme sensitivity to the parameter E_p/W in the intermediate coupling regime ($E_p/W \sim 0.5$).

Another point which requires investigation is the nature of the ferromagnetic transition at T_C. It is found, both theoretically and experimentally, that in manganites with low T_C the ratio of spin-wave stiffness constant D to T_C is much larger than the Heisenberg-like value occurring in those with high T_C. Experimentally, in the low T_C systems, D does not collapse to zero at T_C. Nanoscale phase separation near and above T_C is a possible explanation [154] and further theoretical work along these lines is required.

The physics of the manganites involves a subtle interplay between magnetism and electron-phonon coupling. The same might be said, with less certainty, of high temperature superconductivity in the cuprates. It seems clear from this review that a firm theoretical understanding of the manganites is within reach. Methods of handling electron-phonon coupling in the intermediate coupling regime have been developed. An intriguing prospect is that this experience gained with the manganites may lead to important advances in our understanding of the cuprates.

Acknowledgments

This review began life as a conference paper (*cond-mat/0109266*) which was rejected on grounds of length. That paper had a coauthor, Alex Green, and section 6 draws extensively on his published work. However the critical opinions expressed in this much-expanded review are my own and it was decided, with Alex Green's agreement, that I should take the responsibility of sole authorship. I am grateful to him for providing two previously unpublished figures (figures 21 and 23) and for several years of fruitful collaboration. More recently I have enjoyed collaborating with Martin Hohenadler who has also given invaluable assistance in preparing this review for publication. I am also grateful to Kenn Kubo for inspiring our work on double-exchange in the early stages. I also thank Lesley Cohen, D. M. Eagles, J. K. Freericks, N. Furukawa, K. Kamenev, D. Meyer and K. A. Müller for helpful discussion. I am also grateful to the UK Engineering and Physical Sciences Research Council (EPSRC) for financial support. The EPSRC Magnetic Oxide Network, coordinated by Gillian Gehring, has also been a stimulating influence.

References

[1] Coey, J. M. D., Viret, M., and von Molnár, S., 1999, *Advances in Physics*, 48, 167

[2] Zaanen, J., Sawatzky, G. A., and Allen, J. W., 1985, *Phys. Rev. Lett.*, 55, 418

[3] Zener, C., 1951, *Phys. Rev.*, 82, 403

[4] Satpathy, S., Popović, Z. S., and Vukajlovič, F. R., 1996, *Phys. Rev. Lett.*, 76, 960

[5] Murakami, Y., Hill, J. P., Gibbs, D., Blume, M., Koyama, I., Tanaka, M., Kawata, H., Arima, T., Tokura, Y., Hirota, K., and Endoh, Y., 1998, *Phys. Rev. Lett.*, 81, 582

[6] Martin, M. C., Shirane, G., Endoh, Y., Hirota, K., Moritomo, Y., and Tokura, Y., 1996, *Phys. Rev. B*, 53, 14285

[7] Moreo, A., Yunoki, S., and Dagotto, E., 1999, *Science*, 283, 2034

[8] Nagaev, E. L., 1996, *Phys. Uspekhi*, 39, 781

[9] Tomioka, Y., Asamitsu, A., Kuwuhara, H., Moritomo, Y., and Tokura, Y., 1996, *Phys. Rev. B*, 53, R1689

[10] Schiffer, P., Ramirez, A. P., Bao, W., and Cheong, S.-W., 1995, *Phys. Rev. Lett.*, 75, 3336

[11] Rodriguez-Martinez, L. M. and Attfield, J. P., 1996, *Phys. Rev. B*, 54, 15622

[12] Hwang, H. Y., Cheong, S.-W., Ong, N. P., and Batlogg, B., 1996, *Phys. Rev. Lett.*, 77, 2041

[13] Mathur, N. D., Burnell, G., Isaac, S. P., Jackson, T. J., Teo, B.-S., MacManus-Driscoll, J. L., Cohen, L. F., Evetts, J. E., and Blamire, M. G., 1997, *Nature*, 387, 266

[14] Hwang, H. Y., Palstra, T. T. M., Cheong, S.-W., and Batlogg, B., 1995, *Phys. Rev. B*, 52, 15046

[15] Urushibara, A., Moritomo, Y., Arima, T., Asamitsu, A., Kido, G., and Tokura, Y., 1995, *Phys. Rev. B*, 51, 14103

[16] McIlroy, D. N., Waldfried, C., Zhang, J., Choi, J.-W., Foong, F., Liou, S. H., and Dowben, P. A., 1996, *Phys. Rev. B*, 54, 17438

[17] Pickett, W. E. and Singh, D. J., 1996, *Phys. Rev. B*, 53, 1146

[18] Sarma, D. D., Shanti, N., Barman, S. R., Hamada, N., Sawada, H., and Terakura, K., 1995, *Phys. Rev. Lett.*, 75, 1126

[19] Zaanen, J., Sawatzky, G. A., and Allen, J. W., 1986, *J. Magn. Magn. Mat.*, 54, 607

[20] Terakura, K., Williams, A. R., Oguchi, T., and Kübler, J., 1984, *Phys. Rev. Lett.*, 52, 1830

[21] Su, Y.-S., Kaplan, T. A., Mahanti, S. D., and Harrison, J. F., 2000, *Phys. Rev. B*, 61, 1324

[22] Barman, S. R., Chainani, A., and Sarma, D. D., 1994, *Phys. Rev. B*, 49, 8475

[23] Singh, D. J. and Pickett, W. E., 1998, *Phys. Rev. B*, 57, 88

[24] Chainani, A., Mathew, M., and Sarma, D. D., 1993, *Phys. Rev. B*, 47, 15397

[25] Saitoh, T., Bocquet, A. E., Mizokawa, T., Namatame, H., Fujimori, A., Abbata, M., Takeda, Y., and Takano, M., 1995, *Phys. Rev. B*, 51, 13942

[26] Park, J.-H., Chen, C. T., Cheong, S. W., Bao, W., Meigs, G., Chakarian, V., and Idzerda, Y. U., 1996, *Phys. Rev. Lett.*, 76, 4215

[27] Park, J.-H., Vescovo, E., Kim, H.-J., Kwon, C., Ramesh, R., and Venkatesan, T., 1998, *Phys. Rev. Lett.*, 81, 1953

[28] Soulen Jr., R. J., Byers, J. M., Osofsky, M. S., Nadgorny, B., Ambrose, T., Cheong, S. F., Broussard, P. R., Tanaka, C. T., Nowak, J., Moodera, J. S., Barry, A., and Coey, J. M. D., 1998, *Science*, 282, 85

[29] Osofsky, M. S., Nadgorny, B., Soulen Jr., R. J., Broussard, P., Rubinstein, M., Byers, J., Laprade, G., Mukovskii, Y. M., Shulyatev, D., and Arsenov, A., 1999, *J. Appl. Phys.*, 85, 5567

[30] Lu, Y., Li, X. W., Gong, G. Q., Xiao, G., Gupta, A., Lecoeur, P., Sun, J. Z., Wang, Y. Y., and Dravid, V. P., 1996, *Phys. Rev. B*, 54, R8357

[31] Sun, J. L., Krusin-Elbaum, L., Duncombe, P. R., Gupta, A., and Laibowwitz, R. B., 1997, *App. Phys. Lett.*, 70, 1769

[32] Park, J.-H., Vescovo, E., Kim, H.-J., Kwon, C., Ramesh, R., and Venkatesan, T., 1998, *Nature*, 392, 794

[33] Alvarado, S. F., Eib, W., Munz, P., Siegmann, H. C., Campagna, M., and Remeika, J. P., 1976, *Phys. Rev. Lett.*, 13, 4918

[34] Livesay, E. A., West, R. N., Dugdale, S. B., Santi, G., and Jarlborg, T., 1999, *J. Phys.: Condens. Matter*, 11, L279

[35] Pickett, W. E. and Singh, D. J., 1997, *Phys. Rev. B*, 55, R8642

[36] Dessau, D. S., Saitoh, T., Park, C.-H., Shen, Z.-X., Villella, P., Hamada, N., Moritomo, Y., and Tokura, Y., 1998, *Phys. Rev. Lett.*, 81, 192

[37] Ju, H. L., Sohn, H.-C., and Krishnan, K. M., 1997, *Phys. Rev. Lett.*, 79, 3230

[38] Hewson, A. C., 1993, *The Kondo problem to Heavy Fermions* (Cambridge University Press)

[39] Anderson, P. W. and Hasegawa, H., 1955, *Phys. Rev.*, 100, 675

[40] de Gennes, P. G., 1960, *Phys. Rev.*, 118, 141

[41] Kubo, K. and Ohata, N., 1972, *J. Phys. Soc. Jpn.*, 33, 21

[42] Green, A. C. M., 2001, *Phys. Rev. B*, 63, 205110

[43] Hohenadler, M. and Edwards, D. M., 2001, *cond-mat/0111175*, submitted to *J. Phys.: Condens. Matter*

[44] Edwards, D. M. and Muniz, R. B., 1985, *J. Phys. F: Met. Phys.*, 15, 2339

[45] Muniz, R. B., Cooke, J. F., and Edwards, D. M., 1985, *J. Phys. F: Met. Phys.*, 15, 2357

[46] Solovyev, I. V. and Terakura, K., 1999, *Phys. Rev. Lett.*, 82, 2959

[47] Georges, A., Kotliar, G., Krauth, W., and Rosenberg, M. J., 1996, *Rev. Mod. Phys.*, 68, 13

[48] Pruschke, T., Jarrell, M., and Freericks, J. K., 1995, *Advances in Physics*, 44, 187

[49] Edwards, D. M. and Fisher, B., 1971, *J. Physique Coll. C1*, 32, 697

[50] Quijada, M., Černe, J., Simpson, J. R., Drew, H. D., Ahn, K. H., Millis, A. J., Shreekala, R., Ramesh, R., Rajeswari, M., and Venkatesan, T., 1998, *Phys. Rev. B*, 58, 16093

[51] Edwards, D. M. and Rigby, A. M., unpublished, Rigby, A. M., 1992, Ph.D. thesis (University of London)

[52] Zhao, G.-m., 2000, *Phys. Rev. B*, 62, 11639

[53] Lichtenstein, A. I. and Katsnelson, M. I., 2001, *Band-ferromagnetism*, edited by K. Baberschke, M. Donath, and W. Nolting (Springer), p 75

[54] Endoh, Y. and Hirota, K., 1997, *J. Phys. Soc. Japan*, 66, 2264

[55] Velicky, B., 1969, *Phys. Rev.*, 184, 614

[56] Hill, D. J. and Edwards, D. M., 1973, *J. Phys. F: Met. Phys.*, 3, L162

[57] Fukuyama, H., 1973, *AIP Conf. Proc.*, 10, 1127

[58] Edwards, D. M. and Hill, D. J., 1976, *J. Phys. F: Met. Phys.*, 6, 607

[59] Wakoh, S., Edwards, D. M., and Wohlfarth, E. P., 1971, *J. Physique C1*, 32, 1073

[60] Wang, X., 1998, *Phys. Rev. B*, 57, 7427

[61] Furukawa, N., 1999, *Physics of Manganites*, edited by T. A. Kaplan and S. D. Mahanti (Kluwer, New York), p 1

[62] Izuyama, T., Kim, D. J., and Kubo, R., 1963, *J. Phys. Soc. Japan*, 18, 1025

[63] Brunton, R. E. and Edwards, D. M., 1998, *J. Phys.: Condens. Matter*, 10, 5421

[64] Okabe, T., 1997, *Prog. Theor. Phys.*, 97, 21

[65] Wurth, P. and Müller-Hartmann, E., 1998, *Eur. Phys. J. B*, 5, 403

[66] Edwards, D. M., 1968, *J. Appl. Phys.*, 39, 481

[67] Roth, L. M., 1969, *Phys. Rev.*, 186, 428

[68] Hertz, J. A. and Edwards, D. M., 1973, *J. Phys. F: met. Phys.*, 3, 2174

[69] Edwards, D. M. and Hertz, J. A., 1973, *J. Phys. F: Met. Phys.*, 3, 2191

[70] Kaplan, T. A., Mahanti, S. D., and Su, Y.-S., 2001, *Phys. Rev. Lett.*, 86, 3634

[71] Edwards, D. M., 1967, *Prog. Roy. Soc. A*, 300, 373

[72] Golosov, D. I., 2000, *Phys. Rev. Lett.*, 84, 3974

[73] Thompson, E. D., 1965, *J. Appl. Phys.*, 36, 1133

[74] Edwards, D. M., Green, A. C. M., and Kubo, K., 1999, *J. Phys.: Condens. Matter*, 11, 2791

[75] Green, A. C. M. and Edwards, D. M., 1999, *J. Phys.: Condens. Matter*, 11, 10511, *erratum*, 2000, 12, 9107

[76] Hubbard, J., 1964, *Proc. Roy. Soc.*, 281, 401

[77] Elliot, R. J., Krumhansl, J. A., and Leath, P. L., 1974, *Rev. Mod. Phys.*, 46, 465

[78] Edwards, D. M. and Hewson, A. C., 1968, *Rev. Mod. Phys.*, 40, 810

[79] Edwards, D. M. and Hertz, J. A., 1990, *Physica B*, 163, 527

[80] Luchini, M. U. and Edwards, D. M., 1995, *J. Low. Temp. Phys.*, 99, 305

[81] Potthoff, M., Herrmann, T., and Nolting, W., 1998, *Eur. Phys. J. B*, 4, 485

[82] Bulla, R., Hewson, A. C., and Pruschke, T., 1998, *J. Phys.: Condens. Matter*, 10, 8365

[83] Furukawa, N., 1994, *J. Phys. Soc. Jpn.*, 63, 3214

[84] Furukawa, N., 1996, *J. Phys. Soc. Jpn.*, 65, 1174

[85] Meyer, D., Santos, C., and Nolting, W., 2001, *J. Phys.: Condens. Matter*, 13, 2531

[86] Kubo, K., 1974, *J. Phys. Soc. Jpn.*, 36, 32

[87] Millis, A. J., Littlewood, P. B., and Shraiman, B. I., 1995, *Phys. Rev. Lett.*, 74, 5144

[88] Millis, A. J., Müller, R., and Shraiman, B. I., 1996, *Phys. Rev. B*, 54, 5405

[89] Röder, H., Zang, J., and Bishop, A. R., 1996, *Phys. Rev. Lett.*, 76, 1356

[90] Varma, C. M., 1996, *Phys. Rev. B*, 54, 7308

[91] Müller-Hartmann, E. and Dagotto, E., 1996, *Phys. Rev. B*, 54, R6819

[92] Nagaev, E. L., 1996, *Phys. Rev. B*, 54, 16608

[93] Sheng, L., Xing, D. Y., Sheng, D. N., and Ting, C. S., 1997, *Phys. Rev. B*, 56, R7053

[94] Li, Q., Zang, J., Bishop, A. R., and Soukoulis, C. M., 1997, *Phys. Rev. B*, 56, 4541

[95] Smolyaninova, V. N., Xie, X. C., Zhang, F. C., Rajeswari, M., Greene, R. L., and Das Sarma, S., 2000, *Phys. Rev. B*, 62, 3010

[96] Auslender, M. and Kogan, E., 2000, *cond-mat/0006184*

[97] Zhong, F., Dong, J., and Wang, Z. D., 1998, *Phys. Rev. B*, 58, 15310

[98] Letfulov, B. M. and Freericks, J. K., 2001, *cond-mat/0103471*

[99] Mahan, G. D., 1990, *Many-particle Physics* (Plenum Press), 2nd ed.

[100] Eagles, D. M., 1966, *Phys. Rev.*, 145, 645

[101] Zang, J., Bishop, A. R., and Röder, H., 1996, *Phys. Rev. B*, 53, R8840

[102] Benedetti, P. and Zeyher, R., 1999, *Phys. Rev. B*, 59, 9923

[103] Held, K. and Vollhardt, D., 2000, *Phys. Rev. Lett.*, 84, 5168

[104] Holstein, T., 1959, *Ann. Phys. (N.Y.)*, 8, 325

[105] Holstein, T., 1959, *Ann. Phys. (N.Y.)*, 8, 343

[106] Sumi, H., 1972, *J. Phys. Soc. Jpn.*, 33, 327

[107] Sumi, H., 1974, *J. Phys. Soc. Jpn.*, 36, 770

[108] Ciuchi, S., de Pasquale, F., Fratini, S., and Feinberg, D., 1997, *Phys. Rev. B*, 56, 4494

[109] Freericks, J. K., Jarrell, M., and Scalapino, D. J., 1993, *Phys. Rev. B*, 48, 6302

[110] Millis, A. J., Müller, R., and Shraiman, B. I., 1996, *Phys. Rev. B*, 54, 5389

[111] Emin, D. and Holstein, T., 1969, *Ann. Phys. (N.Y.)*, 53, 439

[112] Worledge, D. C., Miéville, L., and Geballe, T. H., 1998, *Phys. Rev. B*, 57, 15267

[113] Zhao, G.-m., Kang, D. J., Prellier, W., Rajeswari, M., and Keller, H., 1999, *cond-mat/9912355*

[114] Alexandrov, A. S. and Bratkovsky, A. M., 1999, *J. Phys.: Condens. Matter*, 11, L531

[115] Alexandrov, A. S. and Bratkovsky, A. M., 1999, *Phys. Rev. Lett.*, 82, 141

[116] Alexandrov, A. S. and Bratkovsky, A. M., 1999, *J. Phys.: Condens. Matter*, 11, 1989

[117] Alexandrov, A. S. and Kornilovich, P. E., 1999, *Phys. Rev. Lett.*, 82, 807

[118] Fröhlich, H., 1954, *Adv. Phys.*, 3, 325

[119] Fehske, H., Loos, J., and Wellein, G., 1999, *cond-mat/9911218*

[120] Chakraverty, B. K., Ranninger, J., and Feinberg, D., 1998, *Phys. Rev. Lett.*, 81, 433

[121] Chakraverty, B. K., Ranninger, J., and Feinberg, D., 1999, *Phys. Rev. Lett.*, 82, 2621

[122] Zhao, G.-m., Smolyaninova, V., Prellier, W., and Keller, H., 2000, *Phys. Rev. Lett.*, 84, 6086

[123] 2000, Comment and reply on ref. [115], *Phys. Rev. Lett.*, 84, 2042

[124] Perroni, C. A., De Filippis, G., Cataudella, V., and Iadonisi, G., 2001, *cond-mat/0106588*

[125] Cataudella, V., De Filippis, G., and Iadonisi, G., 2001, *Phys. Rev. B*, 63, 52406

[126] Kim, K. H., Gu, J. Y., Choi, H. S., Park, G. W., and Noh, T. W., 1996, *Phys. Rev. Lett.*, 77, 1877

[127] Sarma, D. D., Shanti, N., Krishnakumar, S. R., Saitoh, T., Mizokawa, T., Sekiyama, A., Kobayashi, K., Fujimori, A., Weschke, E., Meier, R., Kaindl, G., Takeda, Y., and Takano, M., 1996, *Phys. Rev. B*, 53, 6873

[128] Dai, P., Zhang, J., Mook, H. A., Liou, S.-H., Dowben, P. A., and Plummer, E. W., 1996, *Phys. Rev. B*, 54, R3694

[129] Louca, D., Egami, T., Brosha, E. L., Röder, H., and Bishop, A. R., 1997, *Phys. Rev. B*, 56, R8475

[130] Nagaev, E. L., 1999, *Phys. Lett. A*, 258, 65

[131] Zhao, G.-m., Keller, H., Greene, R. L., and Müller, K. A., 1999, *Physics of Manganites*, edited by T. A. Kaplan and S. D. Mahanti (Kluwer, New York), p 221

[132] Babushkina, N. A., Belova, L. M., Ozhogin, V. I., Gorbenko, O. Y., Kaul, A. R., Bosak, A. A., Khomskii, D. I., and Kugel, K. I., 1998, *J. Appl. Phys.*, 83, 7369

[133] Zhao, G.-m., Keller, H., Hofer, J., Shengelaya, A., and Müller, K. A., 1997, *Solid State Commun.*, 104, 57

[134] Zhao, G.-m., Hunt, M. B., and Keller, H., 1997, *Phys. Rev. Lett.*, 78, 955

[135] Nagaev, E. L., 1998, *Phys. Rev. B*, 58, 12242

[136] Franck, J. P., Isaac, I., Chen, W., Chrzanowski, J., and Irwin, J. C., 1998, *Phys. Rev. B*, 58, 5189

[137] Zhao, G.-m., Conder, K., Keller, H., and Müller, K. A., 2000, *Phys. Rev. B*, 62, 5334

[138] Wei, J. Y. T., Yeh, N.-C., and Vasquez, R. P., 1997, *Phys. Rev. Lett.*, 79, 5150

[139] Biswas, A., Elizabeth, S., Raychaudhuri, A. K., and Bhat, H. L., 1999, *Phys. Rev. B*, 59, 5368

[140] Moreo, A., Yunoki, S., and Dagotto, E., 1999, *Phys. Rev. Lett.*, 83, 2773

[141] Chung, W. and Freericks, J. K., 1998, *Phys. Rev. B*, 57, 11955

[142] Chattopadhyay, A., Millis, A. J., and Das Sarma, S., 2000, *Phys. Rev. B*, 61, 10738

[143] Okimoto, Y., Katsufuji, T., Ishikawa, T., Arima, T., and Tokura, Y., 1997, *Phys. Rev. B*, 55, 4206

[144] Ishihara, S., Yamanaka, M., and Nagaosa, N., 1997, *Phys. Rev. B*, 56, 686

[145] Mack, F. and Horsch, P., 1999, *Physics of Manganites*, edited by T. A. Kaplan and S. D. Mahanti (Kluwer, New York), p 103

[146] Kaplan, S. G., Quijada, M., Drew, H. D., Tanner, D. B., Xiong, G. C., Ramesh, R., Kwon, C., and Venkatesan, T., 1996, *Phys. Rev. Lett.*, 77, 2081

[147] Lee, H. J., Jung, J. H., Lee, Y. S., Ahn, J. S., Noh, T. W., Kim, K. H., and Cheong, S.-W., 1999, *Phys. Rev. B*, 60, 5251

[148] Perring, T. G., Aeppli, G., Hayden, S. M., Carter, S. A., Remeika, J. P., and Cheong, S.-W., 1996, *Phys. Rev. Lett.*, 77, 711

[149] Fernandez-Baca, J. A., Dai, P., Hwang, H. Y., Kloc, C., and Cheong, S.-W., 1998, *Phys. Rev. Lett.*, 80, 4012

[150] Hwang, H. Y., Dai, P., Cheong, S.-W., Aeppli, G., Tennant, D. A., and Mook, H. A., 1998, *Phys. Rev. Lett.*, 80, 1316

[151] Dai, P., Hwang, H. Y., Zhang, J., Fernandez-Baca, J. A., Cheong, S.-W., Kloc, C., Tomioka, Y., and Tokura, Y., 2000, *Phys. Rev. B*, 61, 9553

[152] Alexandrov, A. S. and Mott, N. F., 1994, *Rep. Prog. Phys.*, 57, 1197

[153] Firsov, Y. A., Kabanov, V. V., Kudinov, E. K., and Alexandrov, A. S., 1999, *Phys. Rev. B*, 59, 12132

[154] Lynn, J. W., Erwin, R. W., Borchers, J. A., Huang, Q., Santoro, A., Peng, J.-L., and Li, Z. Y., 1996, *Phys. Rev. Lett.*, 76, 4046

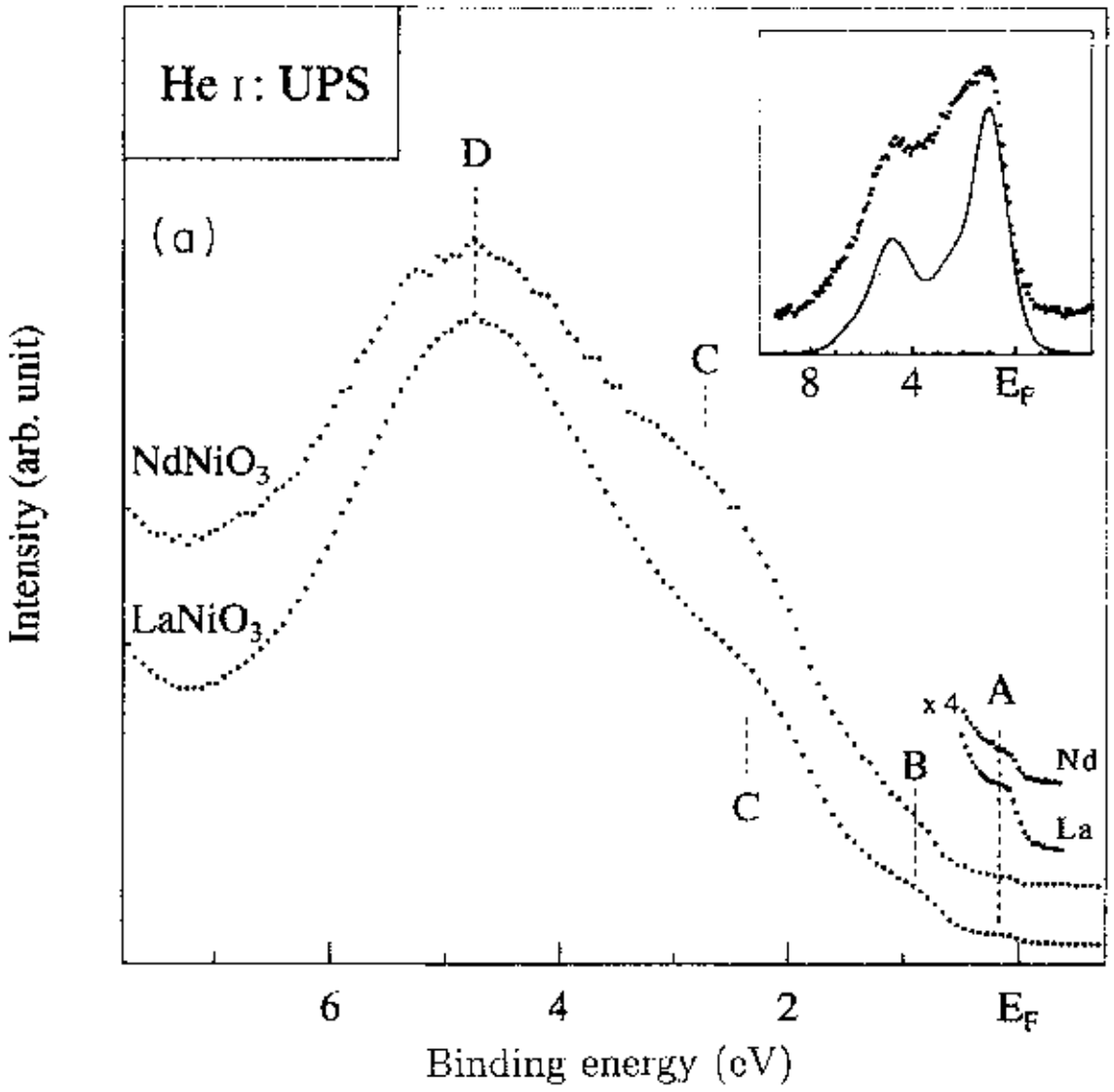
He I: UPS
(a)
D
C
C
B
A
x 4
Nd
La
NdNiO3
LaNiO3
Intensity (arb. unit)
8
4
EF
6
4
2
EF
Binding energy (eV)

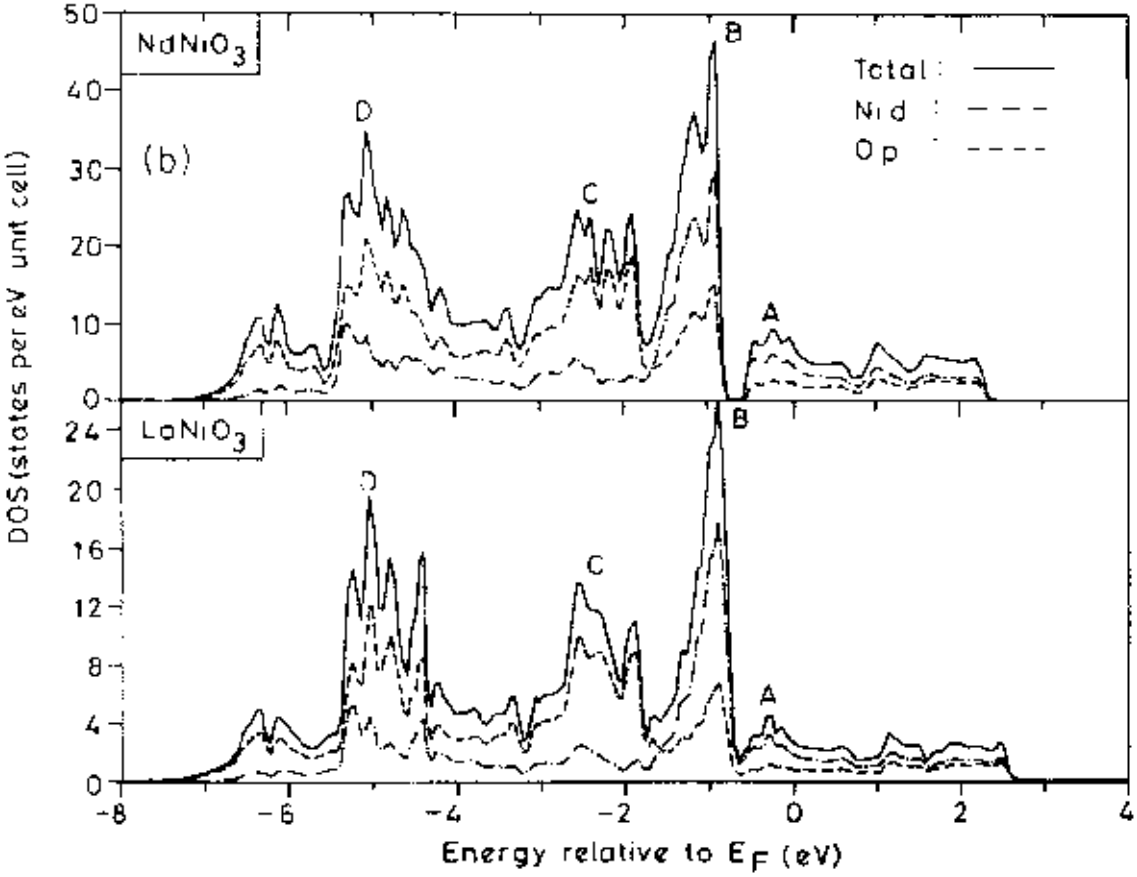
NdNiO3
(b)
Total
Ni d
O p
D
C
B
A
LaNiO3
DOS (states per eV unit cell)
Energy relative to EF (eV)

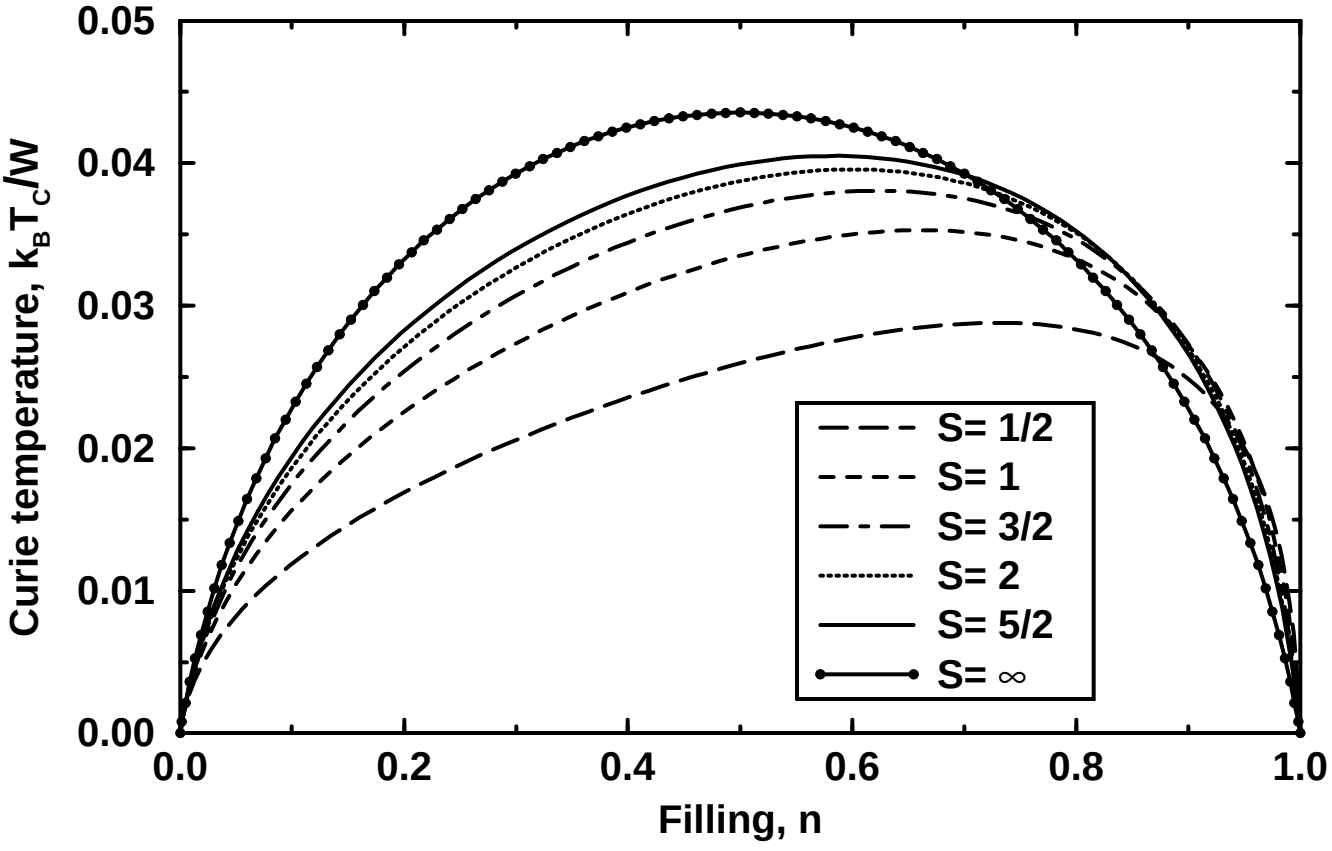
0.05
0.04
0.03
0.02
0.01
0.00
0.0
0.2
0.4
0.6
0.8
1.0
Curie temperature, $k_B T_C/W$
Filling, n
S= 1/2
S= 1
S= 3/2
S= 2
S= 5/2
S= ∞

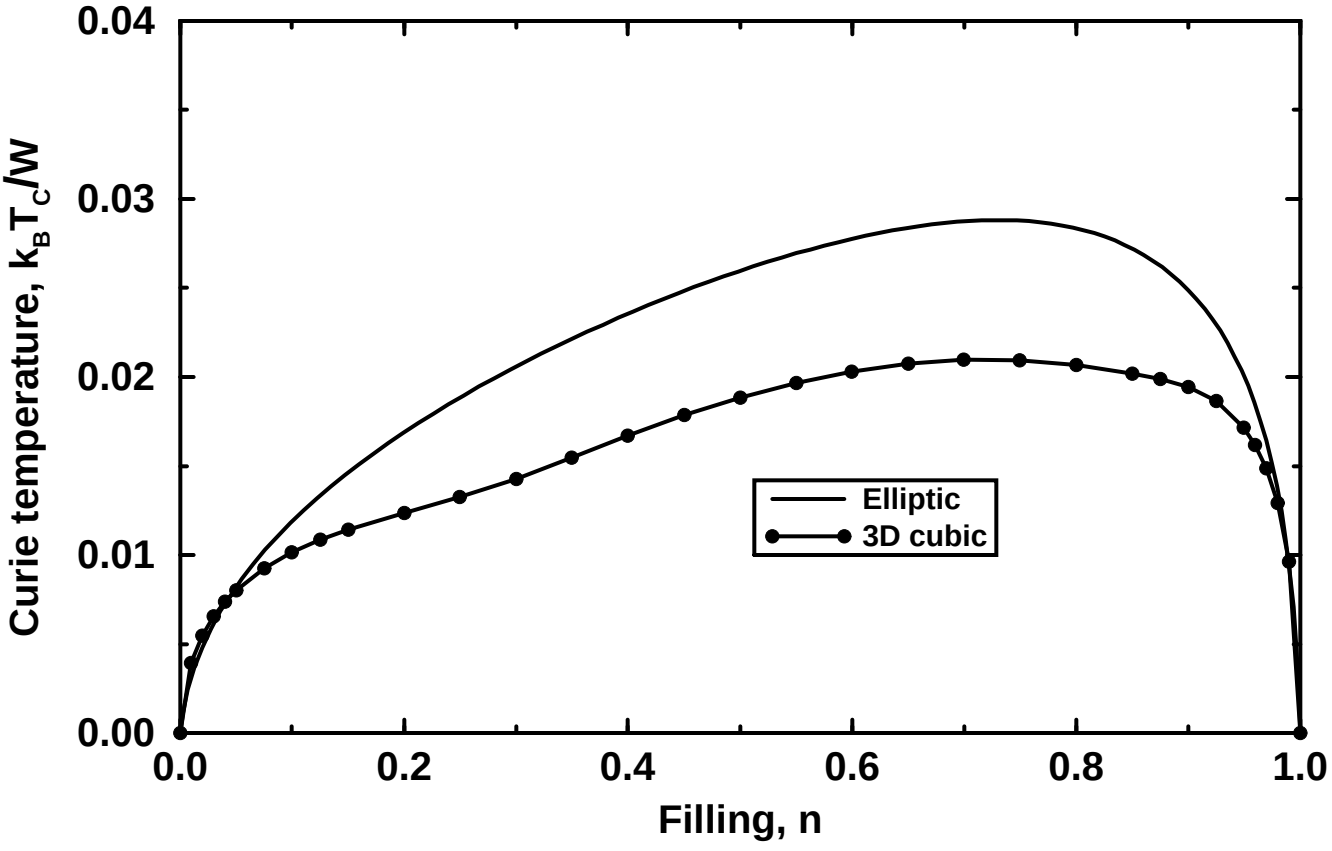
0.04
0.03
0.02
0.01
0.00
0.0
0.2
0.4
0.6
0.8
1.0
Curie temperature, $k_B T_C/W$
Filling, n
Elliptic
3D cubic